LATE HOLOCENE PALEOSEISMICITY AND ASSOCIATED LAND / SEA LEVEL CHANGE IN THE GREATER ANCHORAGE AREA

Ian Shennan, Sarah Hamilton & Antony Long

External grant award # 02HQGR0075

Investigators:
Ian Shennan, Sarah Hamilton, Ben Horton, Antony Long, John Mulholland, Catriona Noble and Yongqiang Zong
Sea Level Research Unit, Department of Geography, University of Durham, Durham, DH1 3LE, UK
and
Rod Combellick
Alaska Division of Geological & Geophysical Surveys, Fairbanks, Alaska, USA

Telephone +44 191 334 1934
Fax +44 191 334 1801
Email ian.shennan@durham.ac.uk
URL http://www.geography.dur.ac.uk

Start date: 1st March 2002
End date: 30th September 2003

Program Element II: Research on Earthquake Occurrence and Effects

Key Words: Paleoseismology; Surface Deformation; Neotectonics; Regional Seismic Hazards

Research supported by the U.S. Geological Survey (USGS), Department of the Interior, under USGS award number 02HQGR0075. The views and conclusions contained in this document are those of the authors and should not be interpreted as necessarily representing the official policies, either expressed or implied, of the U.S. Government.

LATE HOLOCENE PALEOSEISMICITY AND ASSOCIATED LAND / SEA LEVEL CHANGE IN THE GREATER ANCHORAGE AREA

Ian Shennan, Sarah Hamilton & Antony Long
Sea Level Research Unit, Department of Geography, University of Durham, Durham, DH1 3LE, UK
Telephone +44 191 334 1934
Fax +44 191 334 1801
Email ian.shennan@durham.ac.uk
URL http://www.geography.dur.ac.uk

TECHNICAL ABSTRACT

Field and laboratory analyses of tidal marsh sediment sequences provide evidence of multiple great earthquakes in the Greater Anchorage area: 1964 AD, ~850-950 years ago, ~1600 years ago and at least 3 earlier ones (the subject of study in our 2003-2004 USGS project). Records include those from a newly discovered site at Ocean View, close to downtown Anchorage.

Contemporary diatom assemblages from intertidal and supratidal environments at three sites around the Cook Inlet produce a quantitative diatom transfer function applicable to fossil assemblages from late Holocene sediment sequences. Use of a standardised water level index, based upon the difference between mean higher high water and mean sea level provides a method of allowing for differences in tidal range. Sample specific errors for elevation reconstructions from fossil sequences range from ~0.08 m in peat layers to ~0.35 m in tidal silt sequences.

Paired dating of samples using AMS dates on *in situ* plant macrofossils and bulk peat, from the top of each peat layer shows a significant older age for the bulk peat sample. While the source of this error remains unidentified it is very clear that no reliable chronology can be based on bulk peat dates, whether using AMS or conventional radiocarbon methods. A new chronology, including inter-site correlations and calculation of recurrence intervals, requires re-sampling of events from previously investigated sites using diatom analysis to exclude non-events and AMS dating methods on *in situ* macrofossils or rooted wood.

The penultimate great earthquake to cause extensive marsh submergence around the upper Cook Inlet occurred ~850-950 cal yr BP. Quantitative reconstructions from Girdwood indicate co-seismic submergence of +1.63 ± 0.39 m, similar to that experienced in 1964. Lack of modern analogues from the diatom samples studied from the same event at Ocean View, Anchorage prevents any quantitative estimate of co-seismic submergence there. Sequences at Girdwood, Ocean View and Kenai support an earthquake deformation cycle model with up to four main periods:

1. Rapid co-seismic submergence (sudden relative sea-level rise) during a large magnitude earthquake (magnitude>8)
2. Rapid post-seismic uplift (relative sea-level fall) immediately following the event on the timescale of decades
3. Slower inter-seismic uplift (relative sea-level fall) on the timescale of centuries
4. Pre-seismic relative sea-level rise immediately before the next co-seismic event

A sediment transplant experiment helps to differentiate the effects of sediment mixing and pre-seismic sea-level rise in the context of whether pre-seismic relative sea-level rise represents a precursor to a major earthquake.

LATE HOLOCENE PALEOSEISMICITY AND ASSOCIATED LAND / SEA LEVEL CHANGE IN THE GREATER ANCHORAGE AREA

Ian Shennan, Sarah Hamilton & Antony Long
Sea Level Research Unit, Department of Geography, University of Durham, DH1 3LE, UK

NON-TECHNICAL ABSTRACT

Field and laboratory analyses of tidal marsh sediment sequences provide evidence of multiple great earthquakes in the Greater Anchorage area: 1964, a previous one ~850-950 years ago, another ~1600 years ago. Microscopic fossils enable quantitative estimates of land movements relative to sea level, giving reconstructions at Girdwood of land subsidence over 1.5 m during the earthquake ~850-950 years ago. This is similar to those during the 1964 earthquake. We present methods for estimating the age and magnitude of land-level changes during and between earthquake events. Similar patterns prior to each event indicate a precursor sequence significant for earthquake hazard reduction.

Content

1. Context

1.1 Defining the earthquake deformation cycle in the greater Anchorage area
- **1.1.1** The vertical resolution of geologic estimates of relative land and sea-level changes from Holocene earthquakes
- **1.1.2** Isolation of local factors that may obscure the record
- **1.1.3** Evidence for pre-seismic relative sea-level change

2. Field Investigations

2.1 Contemporary samples
2.2 Late Holocene samples
2.3 Sediment mixing experiment

3. Methods

3.1 Microfossil analysis
3.2 Dating techniques
- **3.2.1** Radionuclide dating
- **3.2.2** Radiocarbon dating

3.3 Numerical techniques
- **3.3.1** Transfer function
- **3.3.2** Modern analogue technique

4. Results: Contemporary Samples & Transfer Function

4.1 Tide Levels
4.2 Diatom assemblages of contemporary training set
4.3 Quantitative techniques
- **4.3.1** Detrended Canonical Correspondence Analysis
- **4.3.2** Optimum conditions for diatom species
- **4.3.3** Transfer function – Regression of the contemporary data sets
- **4.3.4** Selection of regression models for the calibration of fossil data
- **4.3.5** The modern analogue technique

4.4 Winter samples 2002
- **4.4.1** Sediment mixing on tidal flats
- **4.4.2** Transport of ice blocks and sediment onto tidal marshes
- **4.4.3** Diatom analysis of ice and associated sediment

5. Results: Girdwood

5.1 The earthquake deformation cycle at Girdwood
5.2 Chrono-stratigraphy of Girdwood
5.3 Bio-stratigraphy of GW-1
5.4 Numerical analysis – calibration of GW-1
5.5 Relative sea- and land-level changes through GW-1
5.6 Summary of GW-1

6. Results: Ocean View

6.1 The earthquake deformation cycle at Ocean View
6.2 Litho-stratigraphy of Ocean View
6.3 Chrono-stratigraphy of Ocean View
6.4 Bio-stratigraphy of peats D and E
6.5 Numerical analysis – calibration of peats D and E
6.6 Relative sea- and land-level changes through peats D and E
6.7 Summary of Ocean View

7. Results: Kenai

7.1 The earthquake deformation cycle at Kenai
7.2 Litho-stratigraphy of Kenai
7.3 Chrono-stratigraphy of KE-7
7.4 Bio-stratigraphy of KE-7
7.5 Numerical analysis – calibration of KE-7
7.6 Relative sea- and land-level changes through KE-7
7.7 Summary of relative sea-level changes at Kenai

8. Results: Sediment Mixing Experiment

8.1 Introduction
8.2 Bio-stratigraphy
8.3 Possible sediment mixing
8.4 Summary

9. Synthesis & Discussion

9.1 Diatom transfer function for the Cook Inlet
9.2 Application to other data sets
9.3 Radiocarbon dating of events
9.4 Summary of events
9.5 Summary of the Earthquake Deformation Cycle
- **9.5.1** Pre-seismic relative sea-level rise as a precursor to a major earthquake
- **9.5.2** Other possible explanations for observed pre-seismic changes

1. Context

This project undertakes new field investigations and subsequent laboratory procedures to analyse evidence of late Holocene ground displacements in the greater Anchorage area associated with past subduction zone earthquakes. We completed two periods of fieldwork to collect surface samples and stratigraphic data from three tidal marshes in and around the greater Anchorage area: Girdwood, Ocean View (Anchorage) and Kenai (figure 1.1). We combine the results of this fieldwork with data collected and analysed by Hamilton (2003), Zong *et al*. (2003) and initial findings of our 2003-2004 NEHRP Project.

1.1 Defining the earthquake deformation cycle in the greater Anchorage area

Microfossil techniques can discriminate between marsh burial events caused by earthquakes and those caused by other, non-seismic processes. This work is important if we are to use marsh burial events to determine the frequency and spatial extent of late Holocene co-seismic ground displacements in the greater Anchorage area. Excellent observational data exist relating to the most recent (1964) great plate boundary earthquake in Alaska. These data show that, in the greater Anchorage area, co-seismic subsidence varied from <0.5 m to >1.5 m (Plafker, 1969). Girdwood experienced high (>1.5 m) subsidence in 1964, whereas Ocean View (Anchorage) lies within the intermediate zone ~0.7 to 1.5 m and Kenai <0.5 m.

In this location, the EDC model could contain up to four main periods (Shennan *et al*., 1999):

1. Rapid co-seismic submergence (sudden relative sea-level rise) during a large magnitude earthquake
2. Rapid post-seismic uplift (relative sea-level fall) immediately following the event on the timescale of decades
3. Slower inter-seismic uplift (relative sea-level fall) on the timescale of centuries
4. Pre-seismic relative sea-level rise immediately before the next co-seismic event

Identification of these four periods and assessment of five criteria (Nelson *et al*., 1996) are important when determining if a buried peat layer results from co-seismic submergence or non-seismic changes in relative sea level. The criteria are:

1. Suddenness of submergence
2. Amount of submergence
3. Lateral extent of peat-silt couplets with sharp upper contacts
4. Tsunami deposits
5. Synchroneity of submergence

We aim to discriminate between the seismic and non-seismic elements of relative sea-level change and marsh burial through the different stages of the earthquake deformation cycle (EDC). We achieve this by using a combination of microfossil data collected from i) contemporary intertidal and supratidal environments, ii) sediments associated with the penultimate earthquake and the 1964 event.

The project addresses three research questions:

1.1.1 The vertical resolution of geologic estimates of relative land and sea-level changes from Holocene earthquakes

Recent investigations in both seismic and non-seismic coastal environments show the potential of quantitative microfossil transfer functions in reconstructing the vertical resolution of relative land and sea-level changes (Edwards & Horton, 2000; Horton *et al*., 2000; Gehrels *et al*., 2001). Initial analyses at Kenai (Hamilton, 2003; Zong *et al*., 2003), Girdwood and Portage (Shennan *et al.*, 1999; Zong *et al.*, 2003) demonstrate good similarities between many of the fossil assemblages in late Holocene sediments and those collected from

transects taken across the present marshes. They also reveal numerous gaps in the contemporary data sets, leading to 'poor' modern analogues for critical sedimentary horizons, especially for the freshwater environments present immediately before the 1964 level and for the tidal flat environments immediately afterwards. Experience from these investigations help define a more extensive sampling design for the full range of contemporary marsh environments found around the Cook Inlet. Transfer functions lead to quantitative estimates with respect to contemporaneous tide levels for each sediment interval sampled through a complete Holocene EDC.

1.1.2 Isolation of local factors that may obscure the record

A critical element of the previous research in Cascadia was the definition of criteria to discriminate between local, site scale processes that contribute to marsh burial and those of seismic origin (e.g. Long & Shennan, 1994; Nelson *et al.,* 1996). These produced a theoretical framework and a series of essentially qualitative or at best semi-quantitative criteria. Transfer of the methods to Alaska raises further site-specific factors that must be considered. These include variable sediment discharge from glacier-fed rivers, frozen ground, El Nino Southern Oscillation (ENSO), differences in tidal range and sediment mixing that may lead to an ambiguous indication of seismic or non-seismic relative sea-level (RSL) control.

1.1.3 Evidence for pre-seismic relative sea-level change

Microfossil data collected from the Cascadia subduction zone (Shennan *et al.,* 1996, 1998; Long & Shennan, 1998) indicates that relative sea level may have risen in the years and decades immediately prior to several late Holocene earthquakes. Our initial work in Alaska (Shennan *et al.,* 1999; Hamilton, 2003; Zong *et al.,* 2003) indicates a similar phenomenon prior to the 1964 earthquake. These observations suggest that pre-seismic relative sea-level rise may be an early warning of an imminent plate boundary earthquake. We intend to test this hypothesis by collecting microfossil data from the sediments leading up to the 1964 deformation surface and the penultimate late Holocene event.

Identification of inter-seismic and pre-seismic relative sea-level change leading up to the 1964 and other late Holocene earthquakes can be applied to current and developing seismic models (e.g. Kato *et al*., 1997; Cohen & Freymueller, 1997: Wyss & Wiemer, 1999; Freymueller *et al*., 2000; Dragert *et al*., 2001). These models include elements such as seismic quiescence and aseismic slip and develop from theory but with observations over a limited timescale, typically a few years to a decade. Our evidence will provide an independent test of these models using a much longer timescale, decades to centuries.

2. Field Investigations

Field sampling at Ocean View (Anchorage) and Girdwood (figure 1.1) add to data from Kenai (Hamilton, 2003; Zong *et al*., 2003). In combination these sites cover a 110 km transect in the upper Cook Inlet region and experienced varying amounts of co-seismic displacement in 1964, <0.5 to >1.5 m.

Two field seasons took place during 2002 (April and summer). Observations of sedimentary processes and the collection of contemporary surface samples during late winter/early spring allowed a greater understanding of what conditions were like during the March 1964 Alaskan earthquake. We also retrieved the first set of sediment transplant experiments (see below) that we had set up in 2001. Field investigations during the summer involved the collection of contemporary surface samples together with their elevation (m) relative to mean higher high water (MHHW) from Girdwood, Ocean View and Kenai for the full range of modern day environments from tidal flat through salt marsh to raised bog communities. Data from all three sites form the modern training set, allowing quantification of the spatial variation of relative sea-level movements associated with post-seismic, inter-seismic, pre-seismic and

co-seismic periods for the 1964 and penultimate earthquake to affect the greater Anchorage area. They also allow understanding of other controls on relative sea level in the area including non-seismic processes, for example, eustatic and glacio- and hydro-isostatic changes. In addition we took tidal observations, sampled exposed sections and cored at Girdwood and Ocean View, retrieved further sediment transplant experiments and set up of an additional one to be retrieved in 2003.

2.1 Contemporary Samples

Contemporary diatom samples from Girdwood, Ocean View and Kenai together with their associated elevation (m MHHW) represent the full range of modern day environments from tidal flat through salt marsh to raised bog communities and form the modern training set. Scraping away of the surface and collection of the top 1 cm of sediment allowed for seasonal variations in diatom blooms and the effects of winter freezing. Samples were sealed in bags and the sampling site levelled to a temporary benchmark (TBM) using a standard level and staff. Their levelled elevation was then converted to m MHHW using data from NOAA (http://co-ops.nos.noaa.gov). Pugh (1996) defines MHHW as the average of the higher high water elevation of each tidal day, averaged over the United States National Tidal Datum Epoch. The alternative is to define elevation relative to mean lower low water (MLLW), which is chart datum. Elevation (m) relative to MLLW is not suitable as the reference tide level because at Kenai, the base flow of the river dampens out the effect of low tide, and the combination of large tidal range, extent of the intertidal zone and unstable sediments meant that low water could not be measured at Girdwood and Ocean View.

2.2 Late Holocene Samples

Investigation of exposed sections and/or coring (using a 25 mm diameter gouge) along transects at Girdwood, Ocean View and Kenai allowed the investigation of marsh litho-stratigraphy using the Troels Smith (1955) scheme of description. This characterises the large range of organic and inorganic sediment typical in most coastal lowlands. Plotting of marsh stratigraphy allowed the selection and sampling of suitable peat-silt sequences using a variety of monolith tins and coring devices.

At Girdwood, good exposures of two buried peat layers containing ghost forests are laterally extensive along the marsh front. Cleaning of a section allowed the description of stratigraphy and sampling of sediment using a variety of monolith tins and tubing. A transect of cores could not be taken across the marsh surface as the ground was too compact. Sealing of samples in plastic allowed transportation of sediment back to Durham for subsequent analyses.

At Ocean View, an upper buried peat layer, found approximately 15 to 25 cm below current marsh surface was sampled using a monolith tin. This method avoids contamination and enables the collection of a large volume of sediment. A deeper second buried peat layer was sampled using a Russian corer.

At Kenai, a monolith tin sampled the first peat-silt boundary, found approximately 5 cm below the surface. A gouge corer then sampled the sediment below. The removal of the upper peat layer using the monolith tin and the cleaning of cores using a knife helped reduce the risk of contamination and the collection of multiple cores from the same area checked consistency. As radiocarbon dating requires a greater volume of sediment, a Russian corer (50 mm diameter) sampled the second buried peat layer.

2.3 Sediment Mixing Experiment

Based upon the ecology of the distinct microfossil assemblages we have argued that the pre-seismic signals identified at Kenai and Girdwood are not caused by sediment mixing (Shennan *et al*., 1999; Hamilton, 2003; Zong *et al*., 2003). We test this hypothesis further by a field and laboratory experiment (figure 2.1). On May 23rd 2001 we transferred a series of

~30 x 30 x 15 cm samples of marsh sediment (taken from +0.8 ± 0.1 m MHHW) into shallow pits, of the same dimensions, at lower elevations (figure 2.1a & b) in the intertidal zone (~-0.35 ± 0.1m MHHW). This will simulate vertical displacement (figure 2.1d) comparable to the 1964 earthquake. By retrieving a small portion of the transferred sediment, together with new sediment accumulation on top (figure 2.1c), we simulate co-seismic submergence followed by immediate post-earthquake burial. This investigates the magnitude (or absence) of microfossil transfer down into the sediment by laboratory counting of the microfossil assemblages within the control and test blocks.

3. Methods

Laboratory work started in October 2002, concentrating on diatom analysis of both the contemporary and fossil sediment samples and the radiometric dating of sediment.

3.1 Microfossil analysis

Analysis of the full range of contemporary surface samples allows the development of a comprehensive contemporary data set, ranging from tidal flat through to raised bog environments. Sampling intervals of cores varied from 1 to 8 cm with smaller intervals taken around possible pre-seismic, co-seismic and post-seismic periods where greater resolution is required.

Preparation of diatom samples followed standard laboratory methods (Palmer & Abbott, 1986) with a minimum count of 250 diatom valves possible for most samples. Diatom identification used Van der Werff and Huls (1958-1974) together with supplementary texts of Denys (1991), Hartley *et al*. (1996), Hemphill-Haley (1993) and Patrick and Reimer (1966, 1975). TILIA (version 2.0 b5; Grimm, 1993) allows the plotting of results and the halobian classification system divides the diatom species into five categories of salt tolerance (table 3.1).

Table 3.1 The halobian classification scheme (Hemphill-Haley, 1993)

Classification	Salinity range (‰)	Description
Polyhalobous	> 30	Marine
Mesohalobous	0.2 to 30	Brackish
Oligohalobous - halophile	< 0.2	Freshwater – stimulated at low salinity
Oligohalobous - indifferent	< 0.2	Freshwater – tolerates low salinity
Halophobous	0	Salt-intolerant

In broad terms, the order of salinity classes should reflect the change from tidal flat through salt marsh, to freshwater marsh and bog. The marine (polyhalobous class) and brackish (mesohalobous class) groups usually dominate tidal flat environments and freshwater groups tolerant of different degrees of saline inundation (oligohalobous-halophile and oligohalobous-indifferent classes) become dominant through the transition from salt marsh to freshwater marsh (e.g. Zong *et al*., 2003). Salt-intolerant species (halophobous class) characterise the most landward communities, including acidic bog above the level of the highest tides. No attempt was made to separate out the allochthonous and autochthonous diatoms because we assume that processes acting today are the same as those acting in the past. According to Sawai (2001), the removal of dead diatoms by tidal currents may result in a residual assemblage for the surface tidal flat samples. However, this would also have occurred in the fossil tidal flat samples recorded by the silt units.

Microfossils help distinguish between seismic and non-seismic origins of peat-silt couplets (e.g. Long & Shennan, 1994; Nelson *et al*., 1996) and the tendency approach (e.g. Shennan, 1986) defines periods within the EDC model (e.g. Long & Shennan, 1994). A positive sea-level tendency represents an increase in marine influence and a negative sea-level tendency represents a decrease in marine influence.

3.2 Dating techniques

3.2.1 Radionuclide dating

The Well Detector in the Geography Department, University of Durham allows dating of sediment deposited over the past 100 to 150 years using Caesium-137 (^{137}Cs) and Lead-210 (^{210}Pb). Detectable levels of ^{137}Cs in the environment started in 1954 with maximum concentrations occurring in 1964, after which the Nuclear Test Ban Treaty stopped any further releases. At Ocean View, Girdwood and Kenai ^{137}Cs determines whether the burial of the uppermost peat layer together with any associated pre-seismic signal results from co-seismic submergence associated with the 1964 event.

The principle of ^{137}Cs determination is to establish the number of gamma emissions at 661.6 KeV over time. The same principle applies to ^{210}Pb that emits gamma radiation at 46.5 KeV (Lu, 1998). Determination of the concentration of ^{226}Ra allows the calculation of unsupported ^{210}Pb concentration by subtracting the ^{226}Ra concentration from the total ^{210}Pb amount. The results are in Becquerels (Bq), defined as one nuclear disintegration per second. The conversion to Bq per kilogram allows the calculation of concentration and permits comparisons between samples. The amount of error associated with the readings depends on the amount of time the detector has to measure the emissions from the sediment. Readings below 5 Bqkg^{-1} for ^{137}Cs and 20 Bqkg^{-1} for ^{210}Pb are insignificant.

3.2.2 Radiocarbon dating

In situ macrofossils were used for AMS radiocarbon dating. We use further results from Hamilton (2003) provided by the Natural Environment Research Council (NERC) allocation number 935 0901. CALIB 4.3 (Stuiver & Reimer, 1993) calibrates the radiocarbon results to calendar years before present using the atmospheric decadal data set (file INTCAL98.14C, Stuiver *at al*., 1998) and the 95% probability distribution method. Calibrated ages are reported as the range between the calculated minimum and maximum value, with the median age marked on figures.

3.3 Numerical techniques

Numerical techniques establish the relationship between contemporary diatom data and elevation (m) relative to MHHW and allow comparisons between the contemporary data set and every fossil sample analysed. These provide quantitative estimates of relative sea-level change throughout the entire profile, rather than just at stratigraphic boundaries.

3.3.1 Transfer function

Contemporary distribution of diatoms from tidal flat to freshwater environments allows development of a transfer function to reconstruct the magnitude of relative land and sea-level changes. Birks (1995) reviews the basic principles of quantitative environmental reconstruction. In this study, the primary aim of a transfer function (Imbrie & Kipp, 1971) is to predict environmental variables for a fossil sample using a modern training set. This involves regression that models the relationship between contemporary diatom assemblages and their associated environmental variables of interest. Calibration then uses this relationship to transform the fossil data into quantitative estimates of past environmental variables (figure 3.1).

Most methods assume a linear or unimodal taxon-environment response model. In nature, most species-environment relationships are unimodal, as most taxa survive best in optimum

environmental conditions (Birks, 1995). However, if the data spans only a narrow range of environmental variation then it may appear linear (Birks, 1995). For reconstruction purposes, it is essential to estimate the gradient length for the environmental variables of interest. CONOCO (version 4.5; ter Braak & Smilauer, 2002) uses Detrended Canonical Correspondence Analysis (DCCA) to estimate the gradient length in standard deviation (SD) units by detrending segments with non-linear rescaling. Gradient length is important as it governs what transfer function models are suitable for the data set.

If the gradient length is short (2 SD units or less), linear regression and calibration methods are appropriate, for example, Partial Least Squares (PLS). If the gradient length is longer (2 SD units or more), several taxa have their optima located within the gradient and unimodal based methods of regression and calibration are best (Birks, 1995). Such models include Weighted Averaging (WA), Weighted Averaging with Tolerance Downweighting (WA-TOL) and Weighted Averaging-Partial Least Squares (WA-PLS), all available within the software package C2 (Juggins, 2003).

Statistical parameters produced during regression and calibration includes the coefficient of determination (r^2) that measures the strength of a relationship between observed and inferred values (Birks, 1995). The Root Mean Square Error of Prediction (RMSEP) measures the predictive abilities of the training set and is calculated by a method called bootstrapping (ter Braak & Juggins, 1993).

When calculating a relative sea-level change between two fossil samples, the change in elevation is simply the difference between the two reconstructed values and calculation of the associated error term uses the formula (Preuss, 1979):

$$\sqrt{(\text{error term } 1^2 + \text{error term } 2^2)}$$

3.3.2 Modern analogue technique

The modern analogue technique (MAT) quantifies the similarity between fossil assemblages and the modern training set (Birks *et al*., 1990) and is particularly useful in identifying whether fossil samples possess good modern analogues (e.g. Birks, 1995; Edwards & Horton, 2000; Zong *et al*., 2003). The computer program C2 (Juggins, 2003) models the full contemporary diatom data set against each fossil data set and determines the minimum dissimilarity coefficient for each fossil sample.

4. Results: Contemporary Samples and Transfer Function

The combination of contemporary diatom data taken from Girdwood, Ocean View and Kenai form the basis of our contemporary training set (figures 4.1, 4.2 and 4.3). Each of the 154 samples has an associated elevation (m) relative to Mean Higher High Water (MHHW) and a calculated Standardised Water Level Index (SWLI). This section aims to describe the contemporary diatom assemblages from tidal flat through to freshwater environments and to produce a quantitative function whose application to the fossil data from the three sites will allow quantitative estimates of relative sea-level change through time.

4.1 Tide Levels

Transfer functions applied in previous studies at Girdwood and Kenai (Hamilton, 2003; Zong *et al*., 2003) use only contemporary samples from Kenai with the resulting fossil reconstructions of elevation for Girdwood re-scaled for difference in tidal range. Tidal range, measured as the difference between MHHW and MLLW, at Anchorage is 8.84 m compared to 6.62 m at Nikiski (Centre for Operational Oceanographic products and Services web page, http://co-ops.nos.noaa.gov). While the contemporary samples from Kenai provide good modern analogues in the majority of fossil reconstructions the tidal range differences

between Kenai and Girdwood introduces a potential error that is difficult to quantify (Hamilton, 2003). In addition, Kenai River shows a significant attenuation of tidal range between the open sea, the City Pier and the Kenai Flats contemporary transect. The greatest effect is river discharge keeping low water levels much higher than those at the estuary mouth. Hamilton (2003) quantified these differences using a series of observations of high and low water compared to tidal predictions at Kenai City Pier. We adopt a similar approach at all three sites (Girdwood, Ocean View, Kenai) but measure high tide at each site in comparison with tide gauge observations, rather than predictions, at Anchorage for Girdwood and Ocean View, and Nikiski for Kenai (Centre for Operational Oceanographic products and Services web page, http://co-ops.nos.noaa.gov).

Figure 4.4 shows the relationship between our observations of high tide and those at the nearest tide gauge. From the best-fit solutions we calculate the elevation for each contemporary sample, levelled relative to a temporary benchmark set up on each transect, relative to mean higher high water (MHHW) at Anchorage or Nikiski. To accommodate tidal range differences between sites we standardise elevations relative to MHHW and the difference in elevation between MHHW and mean sea level (MSL):

$$SWLI_n = \frac{100(h_n - h_{MSL})}{h_{MHHW} - h_{MSL}} + 100$$

Where:
$SWLI_n$ = standardised water level index for sample n
h_n = elevation of sample n, m
h_{MSL} = Mean Sea Level elevation at tide gauge, m
h_{MHHW} = Mean Higher High Water at tide gauge, m

Quantitative diatom transfer functions use the SWLI as the environmental variable for each contemporary sample and produce a reconstructed SWLI for each fossil sample that are recalculated back to give a reconstructed elevation relative to m MHHW. SWLI = 100 represents MSL and SWLI = 200 is MHHW at each site. Use of tidal observations, rather than predictions and reference to the tide gauges at Nikiski and Anchorage mean that the elevations relative to m MHHW in this report differ to those reported by Hamilton (2003) and Zong *et al*. (2003).

4.2 Diatom assemblages of contemporary training set

Unconstrained cluster analysis using Chord distance (square root transformation of the data) aids in the description of contemporary diatom assemblages. The dendrogram produced identifies six major classes within the contemporary diatom data from Girdwood, Ocean View and Kenai (classes produced are in a random order and class numbers do not relate to any environmental variable). Figures 4.5a and b illustrate these classes with only the major taxa present (species above 10% of the total diatoms counted), figure 4.6 shows their elevation range by SWLI and table 4.1 describes their main characteristics.

Using Chord distance, samples from Girdwood, Ocean View and Kenai are comparable to one another as samples from each site are located within the same class. Class 1 from Ocean View and Kenai occupy the largest elevation range. When combined, class 1 occupies a range of 39.48 to 202.04 SWLI (figure 4.6d). Major sub-divisions do not appear in samples found on the tidal flat indicating that diatom assemblages are similar over a large elevation range. Possible explanations may include the effect of river discharge at Kenai, intense mixing of tidal flat sediment during the winter months by ice or it being a residual assemblage where dead diatoms are washed away by tidal currents as described by Sawai (2001). This may potentially affect the accuracy of the transfer function. At higher elevations the classes are more constrained by elevation. These results also illustrate the

need for quantitative reconstructions as diatom salinity classifications are based primarily on assemblages found in north-west Europe and this is not a sound basis to reconstruct elevation since different processes may control diatom distributions in Alaska. A primary example is *Navicula cari* var. *cincta* that occurs on the tidal flat and low marsh and yet in the halobian classification for north-west Europe, it is classified as freshwater within the oligohalobous-halophile group.

Table 4.1 Characteristics of contemporary diatom classes

Class	Dominant diatom species	SWLI range
1	Polyhalobous species dominate class 1, for example, *Cocconeis peltoides*, *Delphineis surirella*, *Paralia sulcata* and *Thalassiosira eccentrica*. It also contains *Navicula cari* var. *cincta* and *Cymbella ventricosa*	39.48-202.04
2	*Navicula cari* var. *cincta* dominates class 2 together with lower counts of other polyhalobous and mesohalobous species	170.12-221.57
3	Class 3 contains a broad range of diatoms including *Navicula cari* var. *cincta*, *Achnanthes minutissima* and *Nitzschia pusilla*	193.10-242.89
4	*Navicula salinarum*, *Navicula cari* var. *cincta*, *Navicula protracta* and *Nitzschia fruticosa* dominate class 4 together with smaller amounts of other polyhalobous, mesohalobous and oligohalobous species	213.05-234.94
5	Oligohalobous-indifferent species dominate class 5, for example, *Navicula brockmanii*, *Nitzschia fruticosa*, *Nitzschia pusilla* and *Pinnularia lagerstedtii*	224.89-240.45
6	A mixture of oligohalobous-indifferent and halophobous species dominate class 6, for example, *Achnanthes minutissima*, *Diploneis ovalis*, *Eunotia exigua* and *Tabellaria fenestrata*. Class 6 also contains KE 01/S38, dominated by the planktonic taxa *Aulacoseira granulata*	232.74-247.44

4.3 Quantitative techniques

Detrended Canonical Correspondence Analysis (DCCA) determines whether linear or unimodal methods are appropriate for the contemporary training set. Regression of the contemporary data can then produce a relationship between the contemporary diatom data and associated environmental variable (SWLI). Statistical parameters, for example, the coefficient of determination (r^2), which is a measure of the strength of the relationship between observed and inferred values and the Root Mean Square Error of Prediction (RMSEP), which is a measure of the predictive abilities of the training set help determine the best models. The modern analogue technique (MAT) provides a measure of the similarity between each fossil sample and those in the contemporary data set.

Previous investigations (Hamilton, 2003) suggest that the full contemporary data set may introduce error when using regression of SWLI against diatom data and so it is divided into smaller training sets summarised in table 4.2 and described later.

Table 4.2 Summary of contemporary training sets

Model	Name	Description
2	Full data set	154 contemporary samples from Girdwood, Ocean View and Kenai
3	Full excluding lowest samples from Kenai	Full data set excluding the 7 lowest samples from Kenai
4	Ocean View only	Ocean view samples only
5	Kenai only	Kenai samples only
6	Girdwood only	Girdwood samples only
8	SWLI>225	Combined data set including only samples above SWLI>225
9	SWLI>180	Combined data set including only samples above SWLI>180
12	Full excluding outliers >1σ	Full data set excluding outliers >1σ

4.3.1 Detrended Canonical Correspondence Analysis

Detrended Canonical Correspondence Analysis (DCCA) estimates the gradient length for the environmental variable of interest, SWLI and hence elevation (m) relative to MHHW. It is a pre-requisite to determine the appropriate numerical model. Table 4.3 summarises DCCA values for the different training sets and as results are greater than two standard deviation (SD) units, unimodal methods of regression and calibration are appropriate for each model.

Table 4.3 DCCA results for the contemporary data sets

Model	Name	DCCA axis 1 length for SWLI (SD units)
2	Full data set	3.277
3	Full excluding lowest samples from Kenai	3.707
4	Ocean View only	3.473
5	Kenai only	3.366
6	Girdwood only	2.026
8	SWLI>225	3.528
9	SWLI>180	3.144
12	Full excluding outliers >1σ	3.558

4.3.2 Optimum conditions for diatom species

The unimodal method of Weighted Averaging (C2, Juggins, 2003) calculates the optimum (the maximum of the response curve) and tolerance (breadth of the response curve) with reference to height (m MHHW) for each individual diatom species ($u \pm t$). Figure 4.7 shows the most abundant taxa (those that reach more than 10% in at least one sample). The inset illustrates the entire data set. Species with optima below SWLI 220 have very large tolerances and those with optima above SWLI 220 generally occur within a smaller elevation range.

The optima and tolerances of contemporary tidal flat diatoms again suggest that there may be potential problems with developing an accurate transfer function for the mudflat samples

as species occur over a large elevation range. It indicates that a transfer function should perform well once on the salt marsh surface, supporting the results from cluster analysis (section 4.2).

4.3.3 Transfer function – Regression of the contemporary data sets

Previous investigations (Hamilton, 2003) suggest that Weighted Averaging-Partial Least Squares (WA-PLS) is the most accurate unimodal model (e.g. ter Braak *et al*., 1993), producing the best relationship between observed and predicted values.

Table 4.4 summarises the r^2 and RMSEP using WA-PLS for each of the training sets described in table 4.2. Figures 4.8a to c illustrate the relationship between observed and predicted SWLI for each of the best models. Best models were chosen based upon a high r^2 and low RMSEP and inspection of the scatter plots.

Table 4.4 Summary statistics for the contemporary training sets using WA-PLS components 1 to 4 from C2. Highlighted values show the best models illustrated in figures 4.9a to c

		r^2				RMSEP			
	Model	**1**	**2**	**3**	**4**	**1**	**2**	**3**	**4**
02	Full data set	0.65	**0.75**	0.79	0.82	24.04	**21.95**	21.97	22.90
03	Full excl lowest samples from Kenai	0.77	0.86	**0.90**	0.92	13.81	11.87	**11.44**	11.56
04	Ocean View only	0.92	**0.95**	0.96	0.97	8.86	**8.25**	8.43	8.85
05	Kenai only	0.67	**0.75**	0.81	0.85	30.58	**29.52**	30.28	32.33
06	Girdwood only	0.77	0.89	**0.95**	0.98	20.44	18.16	**17.03**	16.74
08	SWLI>225	0.75	0.89	**0.93**	0.95	3.19	2.99	**2.90**	2.93
09	SWLI>180	0.71	0.83	**0.89**	0.91	9.61	8.35	**7.79**	7.85
12	Full excl outliers >1σ	0.79	0.88	**0.91**	0.93	13.80	11.58	**11.17**	11.41

Full data set – Model 2

The regression models for the full training set result in a high RMSEP of approximately 22 and a low r^2 suggesting that the predictive abilities of these models and the relationship between observed and inferred values are poor. Therefore, any reconstruction based on these models will have a high associated error. The best model, chosen by the highest r^2 and lowest RMSEP is WA-PLS component 2. Figure 4.8 illustrates observed against predicted SWLI and shows that a linear relationship only exists above approximately SWLI 175. For this reason, the contemporary data set is divided into subsets (table 4.2) to try and increase the transfer functions predictive ability and accuracy.

Site specific training sets – Models 4, 5 and 6

Models 4, 5 and 6 show the observed against predicted SWLI for individual sites. The regression models for Girdwood and Ocean View (r^2 = 0.95) perform a lot better than that for Kenai (r^2 = 0.75). At Kenai, a non-linear relationship exists for samples found below SWLI 175. The non-linearity of the results (figure 4.8), cluster analysis suggesting that there are no distinct classes below MHHW (figure 4.6) and the large tolerances of tidal flat diatoms (figure 4.7) indicate samples below MHHW create difficulties for the transfer function, addressed below.

Combined smaller training sets – Models 3, 8, 9 and 12
In order to try and decrease the non-linearity present in the tidal flat samples, two methods are used. The first excludes the lowest tidal flat samples from Kenai (model 3) and the second (model 12) applies a statistical cut-off value and excludes all samples with absolute residuals greater than the SWLI standard deviation (Jones & Juggins, 1995). Model 12 performs slightly better than model 3 as illustrated by the higher r^2 and lower RMSEP (table 4.4). To increase the predictive powers of the regression models further more samples are excluded. Model 8 only includes samples that have a SWLI>225 and model 9 only includes samples that have a SWLI>180. Model 8 has the lowest RMSEP of 2.90. The following section explains the selection of these cut off SWLI values.

4.3.4 Selection of regression models for the calibration of fossil data
Calibration of the fossil data from sites around the Cook Inlet requires the selection of the best regression model or models to estimate relative sea-level changes through time. Different regression models should perform better in certain parts of the environmental range and litho-stratigraphy provides an independent assessment over which model or models are applicable. On this basis, following sections define the models most suitable for the calibration of fossil data.

Calibration of marsh and raised bog sediments
In the modern day environment diverse raised bog and other peat forming environments occur above an SWLI>230. Therefore, where peat occurs in the stratigraphy, model 8 using samples SWLI>225 is acceptable as peat only forms above this elevation, allowing for some variation at the lower end. WA-PLS component 3 is the best model. It accurately predicts SWLI for the fossil samples that can then be converted to elevation (m) relative to MHHW for the salt marsh and raised bog samples. This model gives a high r^2 (0.93) and lowest RMSEP (2.90) and so reconstructions are more precise.

Calibration of tidal flat to salt marsh sediments
Transfer function model 8, using samples above SWLI>225, is unsuitable for interpreting changes throughout silt units because of the imposed cut-off value compared to the full elevation range of tidal flat sediments. Three suitable models exist, models 3, 9 and 12 and litho-stratigraphy helps indicate which model is most suitable. If the silt contains *in situ* rootlets, the model including only samples SWLI>180 (model 9) is appropriate and more precise, as vegetation does not live below this elevation, again, allowing for some variance at the lower limit. WA-PLS component 3 is best.

If the silt does not contain any rootlets then the models excluding the lowest ones found at Kenai (model 3) or excluding those with absolute residuals greater than the SWLI standard deviation (model 12) are acceptable, as it is possible that silt deposition occurred below SWLI 180. It allows the prediction of lower elevations (m) relative to MHHW, but due to the non-linear relationship between predicted and observed values and the scatter contained within the data set it has a high associated error (RMSEP) and a low r^2. Model 12 appears to perform slightly better than model 3 with WA-PLS component 3 best for both models.

4.3.5 The modern analogue technique
The modern analogue technique (MAT) allows identification of fossil samples that have 'poor' modern analogues when compared to the contemporary training set (e.g. Birks, 1995). This is important, as the calibration results using the transfer function may be less accurate where 'poor' modern analogues exist.

There is no set method to determine if the lowest dissimilarity found between a fossil sample and a modern sample represents a convincing match and analogue (Birks, 1995). To assess whether the lowest dissimilarity coefficient found between a fossil sample and a modern sample represents a convincing match, the extreme 2.5% and 5% of the

dissimilarities calculated between all modern samples represent suitable thresholds. Table 4.5 summarises the values and descriptions used and these descriptions appear in following result sections.

Table 4.5 Thresholds and descriptions of modern analogues

Extreme percentage of data set	Description	Dissimilarity coefficient values
2.5% and less	'poor' analogue	>92.15
2.6 to 5%	'close' analogue	74.01-92.15
5.1% and above	'good' analogue	<74.01

4.4 Winter samples 2002

The March 27, 1964 earthquake occurred when the marshes and tidal flats were frozen. Field observations during March 2002 aimed to investigate the potentially significant influence of sea ice in the transport of sediment and microfossils. Large ice flows covered the tidal flats at Girdwood and Ocean View (figures 4.9 a and b) and snow covered much of the vegetated marshes. A 3 m high ice dam 1500 m out on the tidal flat at Ocean View restricted tidal inundation to the adjacent area. We observed numerous potentially significant processes.

4.4.1 Sediment mixing on tidal flats

The build up of ice on the tidal flat could potentially disturb all tidal flat sediments (figure 4.9). If the ice is transported significant distances this could diminish any spatial or elevation zoning of microfossils. Alternatively, if the features we observed result from *in situ* freezing of the tidal flat, with localised movement (vertically and spatially) the effect on microfossil zoning may be less and tidal-controlled zoning may be more important. Nevertheless, it could lead to vertical mixing of microfossil assemblages and this may blur the signal of small RSL changes in tidal flat sequences.

In contrast to the ridges and blocks of ice at Girdwood and Ocean View (figure 4.9), retrieval of the transplant experiment sample at Kenai River (section 8) suggested less distortion of sediments. Approximately 30 cm of ice, with bands of sediment, covered the stakes used to mark the position of each transplant. In digging through the ice we uncovered the stake to find it still vertical and undisturbed. On a subsequent visit in the summer, all the other remaining stakes were vertical.

4.4.2 Transport of ice blocks and sediment onto tidal marshes

The highest tides carry ice blocks onto the tidal marsh where they become stranded. Once melted, they leave accumulations of melt out sediment on the marsh surface (figure 4.9). In 2002 they were restricted to the marsh front and alongside creeks. We also noted a thick cover of silt on marsh plant leaves, significantly thicker than seen during our summer fieldwork. We sampled both the melt out sediment from ice blocks and the silt covering the vegetation. We also observed slabs of sediment, up to ~1.5 x 0.8 x 0.3 m, transported onto the marsh. The silt cover on leaves (that washed off with the first rainfall) and the melt out accumulations seem to be part of the annual transport of sediment and microfossils alongside regular tidal inundation. However, large slabs of sediment deposited by ice melt were preserved as a whole and started to become colonised by marsh plants in the following summer.

4.4.3 Diatom analysis of ice and associated sediment

We took samples to investigate first whether diatoms were preserved in the ice and associated sediments and secondly whether they represent unique assemblages. This was

a preliminary study to assess the potential significance of ice processes. Figure 4.10 shows diatoms that account for at least 2% total diatom valves counted in the ice and sediment samples. Samples taken from the frozen salt marsh surface contain a broad range of diatoms from polyhalobous through to oligohalobous-indifferent species, for example, *Paralia sulcata*, *Navicula cari* var. *cincta* and *Nitzschia fruticosa*. Samples taken from the frozen mudflat, melt out sediment and ice flows are dominated by polyhalobous species, particularly, *Cocconeis peltoides*, *Delphineis surirella*, *Paralia Sulcata* and *Thalassiosira eccentrica*.

Application of MAT and the contemporary transfer function to this data (table 4.6) suggests that each of the winter samples has a 'good' modern analogue when compared to the contemporary training sets from Girdwood, Ocean View and Kenai. Table 4.6 shows that for all of the melt out samples and sediment contained within ice flows, the closest modern analogue comes from the contemporary mudflat, suggesting that the ice is capable of transporting sediment and diatoms from the tidal flat up onto the vegetated marsh. The transfer function estimates their original elevation to be between -0.89 and -1.25 m MHHW. Samples taken from the frozen *Carex* marsh have close modern analogues from the contemporary *Carex* marsh.

Table 4.6 Ice and associated sediment samples, best-fit modern analogue ("Good Fit"=MinDC<74.01) and apparent elevation derived from the transfer function (TF) described in section 4.3. Sample codes prefixed G are from Girdwood, OV from Ocean View and KE from Kenai

Code	Sample description	Approximate elevation of sampling location	Closest match in contemporary data set	MAT Min DC value	Reconstructed elevation using the TF (m MHHW)
OV/02/s101	Sediment in ice flow on tidal flat	0.7	OV/s21, tidal mudflat	32.44	-1.24
OV/02/s102	Sediment in ice flow on tidal flat	0.6	OV/s21, tidal mudflat	35.08	-1.11
G02/s1	Melt out sediment at *Carex* marsh front	1.0	OV/s21, tidal mudflat	34.30	-1.12
G02/s5	Melt out sediment at *Carex* marsh front	1.0	G/s38, tidal mudflat	46.05	-1.25
G02/s6	Melt out sediment on *Carex* marsh	1.2	OV/s21, tidal mudflat	37.01	-1.05
G02/s8	Melt out sediment on *Carex* marsh	1.2	KE/s1, tidal mudflat	36.45	-0.89
G02/s9	Melt out sediment on *Carex* marsh	1.2	OV/s21, tidal mudflat	33.67	-1.24
G02/s7	Frozen tidal flat at base of marsh cliff	-0.2	OV/s21, tidal mudflat	31.01	-1.24
G02/s2	Sediment film on *Carex* marsh	1.2	G/s30, *Carex* marsh	61.81	1.02
G02/s3	Sediment film on *Carex* marsh	1.2	G/s30, *Carex* marsh	44.28	0.92
G02/s4	*Carex* marsh with standing frozen water	1.2	G/s30, *Carex* marsh	48.36	0.83
G02/s10	*Carex* marsh, frozen sediment	1.2	G/s30, *Carex* marsh	46.05	0.26

5. Results: Girdwood

5.1 The earthquake deformation cycle at Girdwood

Plafker *et al*. (1969) suggest 1.5 m regional subsidence and up to 0.9 m local subsidence of unconsolidated sediment accompanied the 1964 earthquake at Girdwood. The bank section at Girdwood contains two extensive peat layers, the upper buried in 1964 and the lower buried approximately 850 cal yr BP (figure 5.1 & table 5.1).

The upper peat layer (figure 5.2) is visible along the entire marsh front with its upper boundary varying in depth from approximately 30 to 100 cm below present day marsh surface which consists of low growing *Carex lyngbyei* and *Triglochin maritima*. Ghost forests visible on the surface today are rooted in this peat. All depths relate to the top of the bank section, which is approximately 34 cm below the general level of the vegetated marsh. At the sampling site, GW-1, the upper peat layer is brown herbaceous peat and occurs at a depth of 69 to 112 cm. From 82 to 91 cm, it contains a small amount of silt. Approximately 100 cm below the top of this peat at GW-1 is the lower peat layer. The intervening silt ranges in thickness from ~70 cm to over 100 cm. This silt is laterally extensive but the lower peat is only visible at certain times due to the ever-changing thickness of tidal silt at the marsh front. The lower peat layer at GW-1 is a predominantly herbaceous peat and occurs at a depth of 179 to 188 cm. Coarse sand layers do not overlie any of the buried peat surfaces suggesting there is no tsunami evidence.

The buried peat layers are laterally extensive and have sharp upper boundaries separating them from overlying silt, following the criteria described by Nelson *et al*. (1996). This section aims to investigate how the stratigraphy of Girdwood records relative sea- and land-level movements associated with the earthquake deformation cycle (EDC).

5.2 Chrono-stratigraphy of Girdwood

Figure 5.1 and table 5.1 show radiocarbon dates from peat layers at Girdwood and figure 5.3 shows ^{137}Cs and ^{210}Pb concentrations around the upper peat-silt boundary. AMS dating of *in situ* macrofossils found at the base of the upper peat and top and base of the second buried peat layer reveal similar ages for GW-1 and GW-2 (figure 5.1). The lower peat formed ~850 to 1100 cal yr BP and the upper peat between ~450 cal yr BP and 1964 AD. In addition, a tephra found beneath the base of the uppermost peat layer correlates with the Augustine tephra, deposited approximately 500 cal yr BP (Combellick, unpublished data), in good agreement with the radiocarbon results. Despite showing significant scatter in the silt and the upper 18 cm of the uppermost peat, the ^{210}Pb data indicate a 20th century age for this section of the upper peat.

Table 5.1 Radiocarbon results from Girdwood

Site	Lab Code	Stratigraphic context	^{14}C age ± 1σ	Calibrated age BP Median, minimum and maximum ages		
GW-1	CAMS-93957	Base of Girdwood peat H	395±80	455	318	515
GW-1	CAMS-93958	Top of Girdwood peat G	955±80	856	764	948
GW-1	CAMS-93959	Base of Girdwood peat G	945±80	853	744	932
GW-2	Beta-184321	Top of Girdwood peat G	890±80	817	714	919
GW-2	Beta-184322	Base of Girdwood peat G	1170±80	1087	971	1175

Radionuclide data, taken from a monolith adjacent to GW-1, shows that maximum ^{137}Cs concentrations occur at the upper peat-silt boundary, supporting co-seismic submergence,

followed by burial by intertidal silts and clays during the 1964 earthquake. The 1954 horizon occurs approximately 5 cm below.

5.3 Bio-stratigraphy of GW-1

Sampling intervals for diatom analysis varied depending on stratigraphy, ranging from 8 cm to 1 cm intervals where greater resolution was required. Detailed microfossil analysis of the 1964 event undertaken by Shennan *et al*. (1999) and Zong *et al*. (2003) concentrates only on the few centimetres surrounding the upper peat-silt boundary.

Figure 5.4 shows the lithology of the section, AMS dates and summarises the bio-stratigraphy of Girdwood GW-1, from the surface down to a depth of 195 cm. It shows diatoms that account for at least 2% total diatom valves at each level along with summary salinity classes. Zones produced during stratigraphically constrained cluster analysis aid the description of diatom changes through the core. Following paragraphs introduce and summarise the main changes in diatom assemblages and present an initial interpretation of sea-level tendencies that will be fully analysed and quantified in later sections.

Zone A: 194.5 to 185.5 cm

Oligohalobous-indifferent diatoms dominate zone A, particularly *Pinnularia lagerstedtii*. The decline in polyhalobous diatoms towards the top of this zone, together with a gradual change in lithology from silt to peat indicates a gradual negative sea-level tendency and suggests a relative sea-level fall.

Zone B: 185.5 to 178.5 cm

Halophobous diatoms, for example, *Eunotia exigua* and *Pinnularia subcapitata* increase to a peak at 181 to 182 cm suggesting a continued negative sea-level tendency (relative sea-level fall). However, above 180.5 cm they start to decline together with an increase in oligohalobous-indifferent species, in particular, *Navicula variostriata* and *Nitzschia pusilla*. At the very top of zone B, polyhalobous species increase (e.g. *Delphineis surirella*). These changes above 180.5 cm suggest a positive sea-level tendency (relative sea-level rise) within the top few centimetres of the lower peat layer. The boundary between zone B and zone C is a sharp contact between this peat layer and overlying silt with herbaceous rootlets.

Zone C: 178.5 to 164 cm

Diatom assemblages are significantly different compared to zone B. Polyhalobous diatoms dominate especially, *Actinoptychus senarius*, *Delphineis surirella*, *Odontella aurita* and *Paralia sulcata*. The change in diatom assemblages, alongside the rapid change in lithology from freshwater peat to silt with herbaceous rootlets represents a sudden positive sea-level tendency (relative sea-level rise). Towards the top of this zone, polyhalobous diatoms decrease slightly with an associated increase in mesohalobous and oligohalobous species suggesting the start of a negative sea-level tendency (relative sea-level fall).

Zone D: 164 to 124 cm

The lithology of zone D is silt with herbaceous rootlets. Polyhalobous diatoms, for example, *Delphineis surirella* and *Paralia sulcata* dominate. However, they continue to decline throughout this zone together with an increase in mesohalobous and oligohalobous species, particularly *Nitzschia fruticosa*. This suggests the negative sea-level tendency (relative sea-level fall) started in zone C continues throughout zone D.

Zone E: 124 to 111 cm

Polyhalobous diatoms (e.g. *Delphineis surirella* and *Paralia sulcata*) continue to decline and mesohalobous and oligohalobous species dominate, for example, *Navicula cari* var. *cincta*, *Navicula protracta* and *Nitzschia fruticosa*. The negative sea-level tendency (relative sea-level fall) continues through zone E.

Zone F: 111 to 102 cm
Zone F contains two smaller clusters illustrated on figure 5.4 as dashed lines. The lower cluster from 111 to 107 cm shows an increase in oligohalobous-indifferent and halophobous diatoms, for example, *Nitzschia palustris*, *Stauroneis anceps* and *Pinnularia subsolaris* together with a general decline in polyhalobous, mesohalobous and oligohalobous-halophile species. The second cluster from 107 to 102 cm indicates a continued decline of the more salt tolerant species and the introduction of *Eunotia exigua*. The general trend of decreasing salt tolerant diatoms and the introduction of halophobous species, together with the change in lithology from silt with herbaceous rootlets to freshwater peat suggests a continued negative sea-level tendency (relative sea-level fall).

Zone G: 102 to 68.5 cm
In the absence of any lithological evidence of local channel migration the bio-stratigraphy of zone G suggests a complex pattern of relative sea-level movements within the upper peat layer. It contains three smaller clusters illustrated by dashed lines on figure 5.4.

Oligohalobous-indifferent and halophobous diatoms dominate the lowest cluster from 102 to 94 cm, for example, *Achnanthes minutissima*, *Eunotia lunaris* and *Eunotia exigua*. Halophobes peak at 100 cm, suggesting a continued negative sea-level tendency (relative sea-level fall) followed by a slight positive sea-level tendency (relative sea-level rise). Within the second cluster from 94 to 82 cm, halophobes continue to decline to a low at 84 cm. There is an associated increase in more salt tolerant species, for example, *Delphineis surirella*, *Nitzschia obtusa*, *Luticola mutica*, *Navicula brockmanii* and *Pinnularia lagerstedtii*. This suggests a positive sea-level tendency (relative sea-level rise) and accompanies an increase in silt content. The third cluster ranges from 82 to 68.5 cm. At the base of this cluster, halophobes increase to a peak at 76 cm, for example, *Eunotia exigua* and *Pinnularia subcapitata*. This suggests a negative sea-level tendency (relative sea-level fall). However, above 76 cm halophobes decline and more salt tolerant diatoms increase, for example, *Nitzschia obtusa*, *Navicula begeri* and *Pinnularia lagerstedtii*. This suggests a positive sea-level tendency (relative sea-level rise) within the upper few centimetres of the peat. The boundary between this zone and zone H is a sharp contact between the peat layer and silt.

Zone H: 68.5 to 12 cm
At the base of this zone, there is a sudden change in diatom assemblage compared to zone G. Polyhalobous diatoms, for example, *Actinoptychus senarius*, *Cocconeis peltoides*, *Delphineis surirella*, *Odontella aurita* and *Paralia sulcata* dominate. This change, together with the sharp contact between the peat and silt with herbaceous rootlets indicates a rapid positive sea-level tendency (relative sea-level rise).

Between 67 and 44 cm oligohalobous diatoms increase, for example, *Nitzschia fruticosa*. The one sample at 40 cm suggests a slight reversal in this trend with polyhalobous species dominating once again. Above 40 cm, polyhalobous diatoms decline and there is a general increase in mesohalobous and oligohalobous species, for example, *Navicula cari* var. *cincta*, *Navicula protracta*, *Nitzschia fruticosa* and *Nitzschia pusilla*. Salinity groupings suggest a general negative sea-level tendency (relative sea-level fall) within the upper silt layer and later sections quantify these changes.

Zone I: 12 cm to ground surface
Throughout this zone, there is decrease in polyhalobous species and an increase in oligohalobous-indifferent species, in particular, *Achnanthes minutissima* and *Nitzschia pusilla*. This suggests a continued negative sea-level tendency (relative sea-level fall) to the present day.

5.4 Numerical analysis – calibration of GW-1

This section aims to analyse and quantify relative sea-level changes recorded by the bio-stratigraphy of Girdwood GW-1 using the contemporary training set from Kenai, Ocean View and Girdwood, described in section 4.

Reconstruction of relative sea level only requires one model, chosen using the established litho-stratigraphic constraints (see section 4.3.4). Table 5.2 describes the calibration model chosen for different parts of GW-1.

Table 5.2 Calibration models used to reconstruct RSL change in different parts of GW-1

Depth ranges (cm)	Model used	Reason
178 to 116 68 to 0	SWLI> 180	Lithology indicates silt with rootlets. The SWLI>180 model is appropriate
188 to 179 112 to 69	SWLI> 225	Lithology indicates peat and so the SWLI>225 model is best

Figure 5.5 shows the results from the modern analogue technique (MAT). In summary, MAT indicates one fossil sample (2%) has a 'poor' modern analogue, 11 (23%) have 'close' modern analogues and 35 (74%) have 'good' modern analogues. Only the sample from 110 cm depth has a 'poor' modern analogue compared to the contemporary training set.

Figure 5.6 is a composite diagram illustrating the main changes in predicted elevation (m) relative to MHHW for Girdwood GW-1, drawn using the transfer function models specified in table 5.2. Sample 110 cm (highlighted in red) has a 'poor' modern analogue, identified using figure 5.5. Sea level tendency (SLT) phases aid in the description of relative sea-level changes through the section.

5.5 Relative sea- and land-level changes through GW-1

Following sections interpret the relative sea-level changes shown in figure 5.6 in chronological order, testing periods of the EDC model and where appropriate suggesting alternative mechanisms. In this location, the EDC model could contain up to four main periods:

1. Rapid co-seismic submergence (sudden relative sea-level rise) during a large magnitude earthquake
2. Rapid post-seismic uplift (relative sea-level fall) immediately following the event on the timescale of decades
3. Slower inter-seismic uplift (relative sea-level fall) on the timescale of centuries
4. Pre-seismic relative sea-level rise immediately before the next co-seismic event

Identification of these four periods, together with the criteria reviewed by Nelson *et al*. (1996) are important when determining if a buried peat layer results from co-seismic submergence or non-seismic changes in relative sea level.

Development of the lower peat - SLT phase A

This phase could represent the inter-seismic period of the EDC model where strain accumulation at the plate boundary gradually causes land to rise and relative sea level to fall allowing the development of peat at approximately +1.44 ± 0.12 m MHHW. Alternatively, it could represent a change in non-seismic processes, for example, isostatic adjustments or

local processes such as a change in sedimentary conditions. Peat development started approximately 850-1100 cal yr BP, earlier at GW-2 than GW-1.

RSL changes associated with the penultimate event – SLT phases B to D
RSL changes surrounding the burial of the lower peat layer, approximately 850 cal yr BP conform to periods of the EDC model.

Pre-seismic RSL rise associated with the penultimate event - SLT phase B
This phase occurs within the upper three centimetres of the lower peat layer with diatom assemblages suggesting a positive sea-level tendency. Quantitative reconstructions suggest a relative sea-level rise of +0.13 ± 0.14 m from a ground level of +1.47 ± 0.12 m MHHW to +1.34 ± 0.11 m MHHW. Evidence to suggest these assemblages are not a result of mixing includes an increase in *Navicula variostriata* and *Nitzschia pusilla* within this phase. These species only occur in small numbers in the above silt.

Co-seismic submergence associated with the penultimate event - SLT phase C
Evidence suggesting co-seismic submergence ~850 cal yr BP (table 5.1) includes a laterally extensive buried peat layer with a sharp upper boundary together with polyhalobous diatoms dominating the overlying silt. This indicates a sudden change from a freshwater peat environment to one regularly inundated by the tide and fulfils three of the five criteria suggested by Nelson *et al*. (1996). There is no evidence of any tsunami deposit and later sections investigate synchroneity of submergence when bringing all three sites together. Quantitative reconstructions indicate a rapid relative sea-level rise of +1.63 ± 0.39 m to a new ground height of -0.29 ± 0.37 m MHHW, assuming the first couple of elevation reconstructions within the silt unit are due to mixing following burial. Both Shennan *et al*. (1996) and Zong *et al*. (2003) suggest calculation of the amount of subsidence equals the maximum difference estimated from the marsh top and the minimum value indicated in the overlying minerogenic sequence. This may over estimate the value if it refers to a single sample that is an outlier in the model.

Post-seismic recovery of the land - SLT phase D
Rapid relative sea-level fall follows co-seismic submergence in SLT phase C allowing development of the upper peat approximately 450 cal yr BP. Quantitative reconstructions indicate a relative sea-level fall of -1.85 ± 0.39 m to a new ground height of +1.56 ± 0.10 m MHHW, representing post-seismic and inter-seismic recovery of the land combined with sediment accumulation.

RSL oscillation within the upper peat unit - SLT phase E
There is an oscillation in relative sea level below the pre-seismic signal of the 1964 earthquake occurring between 1954 AD and 450 cal yr BP. Quantitative reconstructions suggest a relative sea-level rise of +0.18 ± 0.14 m to a new ground height of +1.38 ± 0.11 m MHHW. Following this RSL rise, relative sea-level falls by -0.13 ± 0.14 m and the ground surface returns more or less to its previous elevation. Following sections test possible hypotheses for this RSL oscillation.

Possible hypotheses include:

1. RSL oscillation associated with co-seismic submergence of a small magnitude earthquake
2. RSL oscillation associated with non-seismic processes, for example, the combination of eustatic and glacio-isostatic changes
3. RSL oscillation associated with co-seismic submergence superimposed upon a background non-seismic RSL change

Hypothesis 1 - The RSL oscillation within SLT phase E results from co-seismic submergence

Lateral extent, amount and suddenness of submergence (Nelson *et al*., 1996) together with the identification of pre-seismic, co-seismic and post-seismic relative sea-level movements are important when deciding if SLT phase E records an episode of co-seismic submergence. Immediately before the event, there is no evidence of a pre-seismic relative sea-level rise. After possible co-seismic submergence of +0.18 ± 0.14 m, the land returns to its previous elevation, suggesting recovery of the same magnitude. This oscillation corresponds to a slight increase in silt content between 91 and 82 cm. The hypothesis that the relative sea-level oscillation observed in SLT phase E results from co-seismic submergence remains valid, although to fulfil the criteria of Nelson *et al*. (1996) further investigation of other cores is required to see if it becomes a sharp peat-silt boundary.

Hypothesis 2 - The RSL oscillation within SLT phase E results from non-seismic processes, including eustatic and glacio-isostatic changes

A combination of eustatic, isostatic and local processes could account for the relative sea-level oscillation observed in SLT phase E. Isostatic adjustments could have taken place during the Little Ice Age, 650 to 100 cal yr BP. Advance of the surrounding glaciers in Portage Valley and adjacent mountains reached their maximum extent before 140 cal yr BP (Crossen, 1992) causing depression of the earths crust. Following melting, isostatic uplift returns the land to its previous position and these responses would be rapid due to its proximity to the subduction zone. James *et al*. (2000) and Clague and James (2002) investigate postglacial rebound at the northern Cascadia subduction zone and indicate that postglacial rebound was rapid following disappearance of the Cordilleran ice sheet at the end of the Pleistocene, suggesting it was complete by the middle Holocene. Other non-seismic factors include local changes, for example, a change in sedimentary processes, but as this relative sea-level rise corresponds to the relative sea-level rise at Kenai (see later sections), it is likely to be a response to a regional or global factor. This hypothesis also remains valid.

Hypothesis 3 - The RSL oscillation within SLT phase E results from co-seismic submergence superimposed upon a non-seismic RSL change

As both hypotheses 1 and 2 are possible explanations of the relative sea-level oscillation observed in SLT phase E, some combination of both is also possible. It may represent small co-seismic submergence superimposed upon some background non-seismic RSL change, whether eustatic, isostatic or local, for example, migration of the tidal channel or a change in marsh sedimentary processes.

In summary, the relative sea-level oscillation observed in SLT phase E could result from co-seismic submergence, non-seismic changes or a combination of both but as the relative sea-level changes are so small, it is difficult to distinguish between them. Given that the event occurs at both Kenai and Girdwood, it is unlikely that local scale processes are the cause. Without further evidence we cannot attribute it to co-seismic submergence.

Quantitative changes associated with the 1964 event – SLT phases F to H

Identification of pre-, co- and post-seismic periods of the EDC model occurs at or around the upper peat-silt boundary. ^{137}Cs relates this peat-silt boundary to the 1964 earthquake and following sections examine these relative sea-level changes in detail.

Pre-seismic relative sea-level rise - SLT phase F

Quantitative reconstructions indicate an increase in tidal inundation immediately before the 1964 earthquake with a relative sea-level rise of +0.16 ± 0.14 m to a new ground height of +1.35 ± 0.11 m MHHW. It is unlikely that these diatom assemblages are a result of mixing at the peat-silt boundary because species such as *Nitzschia obtusa*, *Navicula begeri*, *Navicula brockmanii* and *Pinnularia lagerstedtii* increase and do not occur in the overlying silt.

Three other exposures of the 1964 peat at Girdwood record the same trend (Shennan *et al*., 1999; Zong *et al*., 2003). Zong *et al*. (2003) suggest this change started around the beginning of the 1950's (using ^{137}Cs) and calculated a relative sea-level rise of +0.16 ± 0.13 m using diatom transfer functions and +0.15 ± 0.11 m using pollen transfer functions. Zong *et al*. (2003) used an incorrect calculation for the error term leading to an underestimate.

In addition, there is also observational data indicating a relative sea-level rise before the event. Karlstrom (1964) reports that storm tides that did not flood the marsh surface before 1953 began depositing a thin surface silt layer that became progressively thicker.

Co-seismic submergence associated with the 1964 event - SLT phase G
Evidence suggesting co-seismic submergence includes a laterally extensive sharp boundary between the peat and overlying silt with herbaceous rootlets together with diatom assemblages showing a rapid change to dominance by polyhalobous species. ^{137}Cs dates this contact to 1964 and quantitative reconstructions indicate a positive sea-level tendency of +1.69 ± 0.35 m to a new ground level of -0.28 ± 0.33 m MHHW. This is of the same magnitude as the sum of regional subsidence, ~1.5 m, and local subsidence of unconsolidated sediment, up to ~0.9 m (Plafker *et al*., 1969).

These figures also compare favourably with the results of Zong *et al*. (2003) who estimate co-seismic submergence between +1.59 ± 0.22 m and +1.98 ± 0.23 m using diatom transfer functions and greater than +1.07 ± 0.42 m using pollen transfer functions (note comment above about error terms).

Post-seismic recovery - SLT phase H
Immediately after the 1964 earthquake, rapid uplift of the land and sedimentation occurs and this is continuing to the present day (e.g. Atwater *et al*., 2001; Bartsch-Winkler, 1988; Bartsch-Winkler & Schmoll, 1992; Brown *et al*., 1977; Combellick, 1997; Cohen, 1996, 1998; Plafker *et al*., 1992). Repeated levelling at Girdwood by Brown *et al.* (1977) suggests a cumulative uplift of approximately 2 cm from 1964 to 1965, 12 cm from 1964 to 1968 and 40 cm from 1964 to 1975. Quantitative reconstructions using the microfossil data suggest 0.84 ± 0.47 m recovery by 2000 suggesting most recovery occurs in the post-seismic period of the EDC model.

5.6 Summary of GW-1
The stratigraphy of GW-1 records up to three episodes of co-seismic submergence. Each has an event name, GW-1a to c, for ease of comparison with other sites in section 9.

The uppermost peat-silt boundary (GW-1c) relates to co-seismic submergence associated with the 1964 event and figures obtained from this study are similar to both observational data (e.g. Plafker *et al*., 1969) and those estimated previously from fossil data by the transfer function method (e.g. Zong *et al*., 2003). Quantitative reconstructions clearly identify different periods of the EDC model: pre-seismic, co-seismic and then post-seismic and inter-seismic together. The peat-silt boundary is laterally extensive and represents large, sudden submergence of the peat into the intertidal zone.

The oscillation in relative sea level below the 1964 event (GW-1b) is directly comparable to that found in Kenai (section 7) suggesting that the oscillation is due to regional or global factors, rather than local processes. It could result from a small co-seismic event, non-seismic relative sea-level change or a combination of them both but as the relative sea-level changes are so small, it is difficult to differentiate between them. Given there is observational data of glacier oscillations during this period, non-seismic explanations seem the simplest.

The laterally extensive lower peat-silt boundary (GW-1a) records the penultimate great earthquake to affect Girdwood and it is directly comparable to the 1964 event in sea-level tendencies and magnitude. Before the event, there is a pre-seismic relative sea-level rise, followed by large, sudden co-seismic submergence. Immediately after, relative sea-level falls, indicating the post-and inter-seismic periods of the EDC model together with sediment accumulation. There is no evidence of any tsunami deposit. The above interpretation of GW-1 fulfils three out of the five criteria described by Nelson *et al*. (1996) and later sections investigate synchroneity of submergence when bringing all three sites together.

6. Results: Ocean View

6.1 The earthquake deformation cycle at Ocean View

From estimates based on mapping in the summers of 1964 and 1965 Plafker (1969) estimates 0.7 to 1.5 m co-seismic subsidence at Anchorage during the 1964 earthquake. No previous publications identify Ocean View as recording evidence of the 1964 or earlier earthquakes. It is a key site being so close to downtown Anchorage.

6.2 Litho-stratigraphy of Ocean View

Coring along three transects at Ocean View (figure 6.1) reveal up to five buried peat layers with sharp upper contacts. A maximum of three buried peat layers are found at Shore Drive and up to five at Coral Lane. Each peat layer is given a name (A at the base to E closest to the surface) to make descriptions of stratigraphy easier. This project concentrates on the upper two peat layers found at Shore Drive (peats D and E) with further analyses currently underway in our 2003-04 NEHRP project.

The upper herbaceous peat layer (peat E) is characteristically 27 to 156 cm thick and the upper peat-silt boundary is typically found 20 to 60 cm below present marsh surface (figure 6.2). Towards the landward extremes of all transects this peat merges with the second buried peat layer, peat D. In core locations close to the Cook Inlet peat D is a distinct buried peat layer. This second buried peat layer (peat D) is herbaceous and bryophytic. It is generally thinner than peat E (ranging between 14 and 94 cm) and is typically found 125 to 175 cm below current marsh surface. Both occur at similar depths along the three transects.

6.3 Chrono-stratigraphy of Ocean View

Radiocarbon, ^{137}Cs and ^{210}Pb data (figures 6.1 & 6.3; table 6.1) determine the chrono-stratigraphy at Ocean View. Radiocarbon results show that peat D started to accumulate at OV-6 ~1175 cal yr BP and was subsequently buried ~850 to 950 cal yr BP. At this stage it is not possible to say whether burial was synchronous across transects. Detectable levels of ^{210}Pb throughout the whole of the monolith recovered at OV-15 indicate a 20th century age for at least 8 cm below the upper peat silt transition. ^{137}Cs peaks at 25 cm (in the transition zone) indicating that burial of the upper peat layer coincided with the 1964 earthquake.

Table 6.1 Radiocarbon results from Ocean View

Site	Lab Code	Stratigraphic context	^{14}C age ± 1σ	Calibrated age BP Median, minimum and maximum ages		
OV-2	Beta-184317	Top of Ocean View peat D	940±100	849	739	946
OV-6	Beta-184315	Top of Ocean View peat D	1070±80	979	929	1056
OV-6	Beta-184316	Base of Ocean View peat D	1250±120	1176	1013	1289
OV-15	Beta-184320	Base of Ocean View peat E	920±80	843	741	926

6.4 Bio-stratigraphy of peats D and E

Waterlogged ground conditions made sampling of undisturbed cores very difficult during the 2002 summer field season. The upper part of peat E was successfully sampled from the face of a shallow pit at location OV-15 and a Russian corer was used to sample peat D at site OV-6. Both sites currently lie within the *Carex* marsh zone, and site OV-15 is close to an area of dead spruce trees, rooted in peat E. To obtain better samples from other parts of the sequence we used a 50 mm diameter piston corer during the 2003 field program of our 2003-04 NEHRP project.

Tables 6.2 and 6.3 describe diatom assemblages through peats D (figure 6.4) and E (figure 6.5).

Table 6.2 Diatom assemblages of Peat D, OV-6

Zone	Depth (cm)	Diatom description	Lithology	Sea-level tendency
A	161-142.5	Throughout zone A there is a gradual decrease in polyhalobous species and increase in halophobous species. At the base dominant species include *Paralia sulcata*, *Navicula peregrina* and *Navicula cari* var. *cincta*. These taxa are then replaced by *Rhopalodia operculata*, *Diploneis ovalis*, *Epithemia turgida* and *Rhopalodia gibba*. Towards the top of this zone, *Staurosirella pinnata* and *Nitzschia sinuata* increase	Silt to peat	Negative (RSL fall)
B	142.5-140.5	Oligohalobous-indifferent diatoms dominate zone B, particularly, *Diploneis ovalis*, *Epithemia turgida, Pinnularia intermedia* and *Rhopalodia gibba.* Polyhalobous and mesohalobous taxa increase and halophobous species decline	Peat	Positive (RSL rise)
C	140.5-138	Polyhalobous and mesohalobous diatoms dominate this zone, e.g., *Delphineis surirella, Achnanthes delicatula, Cyclotella striata* and *Rhopalodia operculata*	Silt	Positive (RSL rise)

Table 6.3 Diatom assemblages of Peat E, OV-15

Zone	Depth (cm)	Diatom description	Lithology	Sea-level tendency
A	42-28.5	A broad range of diatoms dominate zone A, from polyhalobous through to oligohalobous-indifferent species. Dominant taxa include *Nitzschia sigma* and *Navicula cari* var. *cincta.* At 30 cm the assemblage changes to dominance by *Nitzschia fruticosa*, *Pinnularia lagerstedtii* and *Eunotia exigua*	Peat	Stable
B	28.5-24.5	Polyhalobous species dominate zone B, in particular, *Cocconeis peltoides*, *Delphineis surirella*, *Paralia sulcata* together with smaller amounts of *Nitzschia sigma* and *Navicula cari* var. *cincta*	Silty peat	Positive (RSL rise)

C	24.5-surface	A broad range of diatoms dominate zone C, from polyhalobous through to oligohalobous-indifferent species. Dominant taxa include *Gyrosigma wansbeckii*, *Paralia sulcata, Nitzschia sigma*, *Rhopalodia operculata* and *Navicula cari* var. *cincta*	Silt	Negative (RSL fall) then stable

6.5 Numerical analysis – calibration of peats D and E

This section aims to analyse and quantify relative sea-level changes recorded by the bio-stratigraphy of Ocean View using the contemporary data set described in section 4. It follows the same procedures explained in detail under section 5 for Girdwood.

Table 6.4 describes the calibration model chosen for different parts of OV-6 and OV-15 depending on litho-stratigraphy (section 4.3.4) and figure 6.6 plots the minimum dissimilarity coefficient for samples against depth (cm). It shows that for peat D (OV-6), 19 of the fossil samples (79%) have 'poor' modern analogues, four (17%) have 'close' modern analogues and one (4%) has a 'good' modern analogue. So many of the fossil samples have 'poor' modern analogues because assemblages dominated by *Epithemia turgida*, *Rhopalodia gibba* and *Staurosirella pinnata* do not exist in our contemporary training set. For peat E (OV-15) none of the fossil samples have 'poor' modern analogues, four (16%) have 'close' modern analogues and 21 (84%) have 'good' modern analogues.

Table 6.4 Calibration models used to reconstruct RSL change in different parts of OV-6 (161 to 138 cm) and OV-15 (42 cm to surface)

Depth ranges (cm)	Model used	Reason
161-160 140-138 29-0	SWLI>180	These samples are found within silt containing rootlets
159-141 42-30	SWLI>225	These samples are within peat

Figure 6.7 plots relative sea-level reconstructions through OV-6 and OV-15 using the transfer function models specified in table 6.4 together with calibrated AMS dates and litho-stratigraphy. Sea-level tendency phases help interpret changes through the sequence, described in the following section.

6.6 Relative sea-level changes through peats D and E

Our current quantitative transfer function is problematic when estimating relative sea-level changes through peat D due to the poor modern analogue situation when compared to the contemporary training set. As very few modern analogues exist, the quantitative reconstructions need to be treated with extreme caution and are compared in following sections with our qualitative interpretation.

Development of peat D – SLT phase A

Calibration of the fossil data suggests that relative sea level falls by -0.34 ± 0.32 m from the underlying silt into the base of peat D. Within this peat unit, quantitative reconstructions suggest that relative sea level oscillates. This is in contrast to the diatom data that suggests a gradual relative sea-level fall throughout this unit with a decline in polyhalobous species and associated increase in oligohalobous-indifferent and halophobous taxa (figure 6.4). As

mentioned earlier, this is likely to result from poor modern analogue situations for the assemblages dominated by *Epithemia turgida*, *Rhopalodia gibba* and *Staurosirella pinnata*.

Pre-seismic relative sea-level rise – SLT phase B
During SLT phase B, in the upper three centimetres of the peat unit, the transfer function indicates a relative sea level rise of +0.52 ± 0.33 m to a new ground height of +0.82 ± 0.20 m MHHW. We doubt the validity of these reconstructions, not only because of the poor modern analogue situation, but also because the predicted ground elevation is well below present day peat forming communities at Ocean View (>1 m MHHW). Nevertheless, diatom assemblages do suggest a slight relative sea-level rise in SLT phase B (figure 6.4, diatom zone B). Within this phase polyhalobous species increase and halophobous species decrease. In addition, a number of species found in the overlying silt do not occur in this phase, suggesting that sediment mixing is not the main process to explain the change in diatoms. This could possibly represent a pre-seismic relative sea-level rise immediately before the peat-silt boundary.

Co-seismic submergence – SLT phase C
It is difficult to quantify the change across the sharp upper peat-silt boundary formed by co-seismic submergence. The transfer function reconstruction estimates RSL fall but with no modern analogue. Qualitatively, the diatom assemblages, with a large increase in the frequencies of polyhalobous and mesohalobous species, do suggest a rapid relative sea-level rise across the litho-stratigraphic boundary but we are unable to quantify this change with our current contemporary training set.

Development of peat E – SLT phase D
Throughout the upper part of peat E, at OV-15, ground elevation lies between +1.07 ± 0.11 m MHHW and +1.19 ± 0.11 m MHHW apart from at the very top where relative sea-level falls and ground height changes to +1.36 ± 0.11 m MHHW.

Transitional peat-silt boundary – SLT phase E
Relative sea-level movements surrounding the upper, 1964, peat-silt boundary are also problematic, in this case due to the diffuse lithologic boundary (figure 6.2) in contrast to the abrupt change in diatom stratigraphy. Between the top of SLT phase D and the top of SLT phase E relative sea-level rises by +1.06 ± 0.32 m, and then falls across the transition to phase F. This pattern of RSL change, associated with the 1964 earthquake, does not follow the usual trends across a peat-silt boundary and is discussed further below.

Upper silt unit – SLT phase F
Within the upper silt unit relative sea-level reconstructions oscillate, but all lie between a minimum of +0.30 ± 0.30 m MHHW, at the top of SLT phase E and +1.11 ± 0.29 m MHHW. The estimate for the present surface, +0.94 ± 0.29 m MHHW, is in good agreement with the levelled height of OV-15, 0.96 m MHHW.

6.7 Summary of Ocean View

Multiple peat-silt couplets, with sharp upper contacts on each peat, suggest recurring great earthquakes associated with marsh subsidence similar to that identified at Girdwood. Analyses of the two most recent events, OV-6a and OV-15b, ~850-950 cal yr BP and 1964 AD respectively, is slightly complicated. The lack of modern analogues throughout peat D and the adjoining silt layers hinders a quantitative reconstruction of RSL changes. Nevertheless diatom assemblages confirm colonisation of tidal mudflat by salt marsh, dated in OV-6 ~1175 cal yr BP, and a continued negative sea-level tendency as an increasingly freshwater peat environment develops. The top 3 cm of the peat records a change in freshwater diatom assemblages, with a decrease in salt-intolerant species and renewed occasional tidal inundation indicated by low but increasing frequencies of tidal flat

polyhalobous and mesohalobous species. The overlying silt is dominated by polyhalobous and mesohalobous species.

This sequence is consistent with pre-seismic RSL rise followed by co-seismic marsh submergence ~850-950 cal yr BP but the two radiocarbon ages only just overlap at the 95% confidence level. Although not quantifiable by the transfer function reconstruction, the pre-seismic signal comprises changes in freshwater species as well as low frequencies of some species common in the overlying silt. Significantly, a number of species present in the silt do not occur in the top 3 cm of the peat, showing that the pre-seismic signal is not the result of sediment mixing. To confirm the co-seismic explanation we require analysis from another core at the site.

Peat E stated to form ~850 cal yr BP and ^{137}Cs data confirm its burial in 1964 (at OV-15). Transfer function reconstructions through peat E at OV-15 all have good modern analogues. They record development of peat more than 1 m above contemporaneous MHHW, followed by rapid RSL rise and tidal flat sedimentation before recovery to the present *Carex* marsh environment. Dead spruce trees rooted in peat E also demonstrate the rapid change in environment. However, complications exist when attributing the sequence to co-seismic subsidence during the 1964 earthquake, primarily in correlating the litho-stratigraphy, bio-stratigraphy and RSL reconstructions.

The main problem arises from the peat-silt contact not being sharp, but transitional over 5 cm. This 5 cm zone does not have the characteristics of an extended pre-seismic phase since it contains the most marine diatom assemblages of the whole sequence. Observations of winter conditions in March/April 2002 and 2003 lead us to suggest that the sequence at OV-15 results from co-seismic subsidence of a peat environment with standing water that was frozen in March 1964 (figure 6.8). We hypothesise that clastic tidal sedimentation in the weeks after the earthquake became mixed with the top of the peat layer during the spring thaw. This would mask any pre-seismic signal contained in the top of the peat. Subsequently marsh vegetation recolonised the site, aided by post-seismic recovery producing RSL fall. Transfer function reconstructions indicate 1.06 ± 0.32 m co-seismic subsidence, in good agreement with Plafker's (1969) estimate of 0.7 to 1.5 m. Following submergence 0.64 ± 0.30 m post-seismic recovery occurs combined with sediment accumulation. This agrees with observations of rapid post-seismic uplift experienced since the 1964 earthquake (e.g. Brown *et al*., 1977; Cohen, 1996, 1998; Cohen & Freymueller, 1997, 2001; Cohen *et al*., 1995; Freymueller *et al*., 2000; Plafker *et al*., 1992; Savage & Plafker, 1991; Savage *et al*., 1998; Zweck *et al*., 2002).

7. Results: Kenai

7.1 The earthquake deformation cycle at Kenai

Plafker (1969) suggests approximately 0.5 m co-seismic subsidence accompanied the 1964 earthquake at Kenai but this interpolation was from three observations, at Anchorage, Homer and Nikiski (figure 1.1). The value for Nikiski, 15 km away, was 0.27 m submergence.

7.2 Litho-stratigraphy of Kenai

A series of cores taken along the contemporary surface transect at Kenai reveals two to three buried peat layers. Figure 7.1 summarises the litho-stratigraphy across the marsh. The upper boundary of the lowest peat and overlying silt varies in depth between 100 to 250 cm below present marsh surface, and it is sharp, apart from in KE-7 where it is transitional over 5 cm. Its thickness ranges from 10 to 128 cm and it is typically humified herbaceous peat with some *Sphagnum* species and bryophytes. It contains up to three distinct tephras,

one likely to be the Hayes tephra (Combellick & Pinney, 1995), dated to 3591-4411 cal yr BP (Riehle, 1985). This peat layer is absent in KE-9, probably due to its proximity to the small tidal channel.

The uppermost-buried peat layer is present in KE-2 to KE-10 with traces of silt found within the peat in KE-11 and KE-12 (figures 7.1 and 7.2). The peat ranges in depth from 5 to 19 cm below current marsh surface. It generally thickens towards the landward end of the transect, ranging from 8 cm by the riverbank to 27 cm at KE-10. It is typically brown herbaceous peat with some *Sphagnum* species and bryophytes. This peat contains up to two distinct tephras. Present day peat accumulation starts along the coring transect at KE-7 where there is 1 cm of silty peat at the surface. At KE-16, a floating mat of vegetation occurs from the surface down to a depth of 83 cm.

Further investigations concentrate on KE-7, as this is the only location where the upper boundary of the second buried peat layer is transitional over five centimetres. This potentially minimises any effect of sediment erosion, possible sediment mixing and does not bias the sampling design by assuming rapid events. At all other locations along the coring transect this boundary appears sharp.

7.3 Chrono-stratigraphy of KE-7

Radiocarbon, ^{137}Cs and ^{210}Pb data provide the chronology for KE-7 (figures 7.1 and 7.3; table 7.1). Radiocarbon dates show that the lower peat accumulated ~6500-1575 cal yr BP and the upper peat started to form ~400 cal yr BP. ^{210}Pb data indicate 20th century ages for the uppermost 12 cm. Figure 7.3 shows first detectable levels of ^{137}Cs start at a depth of 7.5 cm, corresponding to the 1954 horizon. ^{137}Cs peaks at 4.5 cm, directly above the peat-silt boundary confirming that the change in lithology from peat to silt coincided with the 1964 event. Zong *et al*. (2003) also found peak ^{137}Cs concentrations just above the peat-silt boundary in three other cores at Kenai and the base of detectable concentrations approximately 3 to 4 cm below.

Table 7.1 Radiocarbon results from Kenai

Site	Lab Code	Stratigraphic context	^{14}C age ± 1σ	Calibrated age BP Median, minimum and maximum ages		
KE-5	Beta-184332	Top of Kenai peat A	1670±80	1575	1421	1694
KE-5	Beta-184333	Base of Kenai peat A	5780±80	6581	6453	6718
KE-7	CAMS-93963	Base of Kenai peat B	425±80	485	324	535
KE-7	CAMS-93964	Top of Kenai peat A	1670±90	1576	1421	1695
KE-7	AA-48152	Base of Kenai peat A	5685±110	6470	6313	6635

7.4 Bio-stratigraphy of KE-7

Sampling intervals for diatom analysis varied from 1 to 8 cm intervals. Figures 7.4 (a) and (b) summarise the lithology, AMS dates and bio-stratigraphy of KE-7, showing diatoms that account for at least 2% all diatom valves counted. Zones produced during stratigraphically constrained cluster analysis aid the description of diatom changes through the core. Table 7.2 summarises the main changes in diatom assemblages and presents an initial interpretation of sea-level tendencies.

Table 7.2 KE-7 diatom assemblages

Zone	Depth (cm)	Diatom description	Lithology	Sea-level tendency
A	205.5-196.5	Polyhalobous diatoms, e.g., *Cocconeis peltoides* and *Paralia sulcata* dominate at the base of this zone. They decline upwards with an increase in oligohalobous and halophobous groups, e.g., *Eunotia lunaris*, *Pinnularia lagerstedtii* and *Pinnularia subcapitata*	Silt to peat	Negative (RSL fall)
B	196.5-180.5	Oligohalobous-indifferent and halophobous diatoms dominate, in particular, *Eunotia* species. *Tabellaria flocculosa* starts to increase towards the top of this zone	Peat	Negative (RSL fall)
C	180.5-165.5	Zone C contains 3 smaller clusters. *Tabellaria flocculosa* dominates cluster 1 (180.5-175.5 cm). Cluster 2 (175.5-170.5 cm) shows an increase in polyhalobous, mesohalobous and oligohalobous species, e.g., *Delphineis surirella* and *Navicula cari* var. *cincta*. *Eunotia* species and *Pinnularia brevicostata* dominate cluster 3 (170.5-165.5 cm)	Peat	Oscillation (RSL fall, rise and fall)
D	165.5-99.5	From 165.5 to 163.5 cm polyhalobous, mesohalobous and other oligohalobous diatoms increase and halophobous species decline. *Navicula brockmanii* dominates. From 163.5 to 160.5 cm all halophobes disappear, *Navicula brockmanii* declines and *Pinnularia lagerstedtii* becomes dominant. From 160.5 to 99.5 cm there is a decrease in oligohalobous-indifferent taxa and an increase in more salt tolerant species, e.g. *Cocconeis peltoides*, *Delphineis surirella*, *Paralia sulcata* and *Navicula cari* var. *cincta*	Peat to silt	Positive (RSL rise)
E	99.5 to 21.5	*Navicula cari* var. *cincta* dominates the lower part of zone E alongside other polyhalobous, mesohalobous and oligohalobous-halophile taxa. Around 55 cm *Navicula cari* var. *cincta* starts to decline and there is an increase in *Delphineis surirella* and *Paralia sulcata*. At 32.5 cm, polyhalobous species start to decrease together with an associated increase in *Nitzschia obtusa*, *Luticola mutica* and *Pinnularia lagerstedtii*, which becomes more dominant towards the upper part of the zone. Introduction of other oligohalobous-indifferent and halophobous species, e.g., *Pinnularia borealis* occurs towards the top	Silt to peat	Positive then negative (RSL rise followed by RSL fall)
F	21.5 to 5.5	From 21.5 to 10.5 cm oligohalobous-indifferent and halophobous species dominate, particularly *Eunotia* species. From 10.5 cm, there is an increase in *Nitzschia fruticosa*, *Pinnularia lagerstedtii* and *Pinnularia microstauron* together with the introduction of different polyhalobous,	Peat	General positive sea-level tendency (RSL rise)

		mesohalobous and oligohalobous-halophile species, e.g., *Delphineis surirella*, *Paralia sulcata*, *Navicula phyllepta* and *Navicula cari* var. *cincta*. At 8.5 cm, *Eunotia* species start to increase indicating a slight reversal in this trend. However, they disappear by 6.5 cm and *Nitzschia fruticosa*, *Nitzschia pusilla* and *Pinnularia lagerstedtii* replace them		
G	5.5 cm to surface	At the base of zone G, *Cocconeis peltoides*, *Nitzschia fruticosa* and *Pinnularia lagerstedtii* dominate suggesting a rapid positive sea-level tendency in relation to zone F. Towards the top, mesohalobous diatoms increase and *Navicula phyllepta*, *Navicula protracta* and *Navicula salinarum* dominate alongside *Navicula cari* var. *cincta* and *Nitzschia fruticosa*	Silt to silty peat	Negative (RSL fall)

7.5 Numerical analysis – calibration of KE-7

This section aims to analyse and quantify relative sea-level changes recorded by the bio-stratigraphy of KE-7 using the contemporary data set described in section 4. Table 7.3 describes the calibration model chosen for different parts of the core using the litho-stratigraphic constraints. Figure 7.5 plots the minimum dissimilarity coefficient for samples in KE-7 against depth (cm). It shows 13 of the fossil samples (12%) have 'poor' modern analogues, nine (9%) have 'close' modern analogues and 83 (79%) have 'good' modern analogues.

Figure 7.6 shows changes in relative sea level through KE-7 using the transfer function models specified in table 7.3, calibrated radiocarbon ages and lithology. Section 7.6 investigates these changes in greater detail.

Table 7.3 Calibration models used to reconstruct RSL change in different parts of KE-7

Depth ranges (cm)	Model used	Reason
205 to 199 163 to 22 5 to 2	SWLI>180	These samples are found within silt containing rootlets
198 to 164 21 to 6 1 to surface	SWLI>225	These samples are within peat units

7.6 Relative sea- and land-level changes through KE-7

This section investigates relative sea-level (RSL) changes shown in figure 7.6 in chronological order. It tests periods of the EDC model and suggests alternative explanations where appropriate.

Development of lowest peat - SLT phases A and B

The relative sea-level fall in SLT phase A of -1.22 ± 0.26 m to a ground height of approximately +1.18 ± 0.08 m MHHW could represent the inter-seismic period of the EDC model, where strain accumulation at the plate boundary causes land to rise and hence relative sea level to fall. Alternatively, peat formation approximately 6500 cal yr BP could

result from non-seismic processes, for example on a global scale, a slowing down in the rate of eustatic sea-level rise approximately 7000 cal yr BP (e.g. Fleming *et al*., 1998; Peltier, 1998) allowing colonisation of freshwater environments over tidal flats.

Oscillation in RSL within lowest peat layer - SLT phase C
SLT phase C records an oscillation in relative sea level but there is no obvious change in litho-stratigraphy and so it is unknown if it is laterally extensive. Relative sea level rises by +0.16 ± 0.13 m and then falls by -0.21 ± 0.11 m. It could result from a number of processes and possible hypotheses include:

1. RSL oscillation associated with co-seismic submergence during a small magnitude earthquake
2. RSL oscillation associated with non-seismic processes, including eustatic and glacio-isostatic changes
3. RSL oscillation associated with co-seismic submergence superimposed upon a background non-seismic RSL change

All three hypotheses are possible explanations of the relative sea-level oscillation observed in this phase. It could result from co-seismic submergence, non-seismic processes or a combination of them both. Wiles and Calkin (1994) suggest three major intervals of Holocene glacier expansions in the Kenai Mountains around 3600 cal yr BP, 1350 cal yr BP and the Little Ice Age (650 to 100 cal yr BP). The expansion 3600 cal yr BP could correlate with the oscillation in SLT phase C. During this period, the mass of ice overlying the Kenai Mountains could isostatically depress the crust resulting in a relative sea-level rise. Following deglaciation, removal of ice could result in isostatic uplift and return the marsh to its previous elevation. Effects of glacio-isostatic deformation should be rapid in this tectonically active area due to the thin lithosphere.

Detailed microfossil evidence from other cores taken from Kenai, together with similar analyses from other sites could help to correlate this possible event and help resolve this question.

Burial of the lower peat layer - SLT phases D to F
Burial of the lower peat layer dates to 1421-1695 cal yr BP. At KE-7 this event occurs at the transitional boundary between the lowest bryophyte herbaceous peat and overlying silt with herbaceous rootlets. In all other locations along the coring transect this boundary appears sharp, similar to that observed for the 1964 event, and has the same age at KE-5 (table 7.1). Figure 7.6 shows that relative sea level movements around this boundary are complicated and until the diatoms in KE-5 are investigated the following interpretation of sea-level change remains provisional. SLT phase D commences in the top of the bryophyte peat characterised by oligohalobous-indifferent and halophobous diatoms (figure 7.4). It records a relative sea-level rise of +0.08 ± 0.11 m, from +1.22 ± 0.08 m MHHW to +1.14 ± 0.08 m MHHW. There is then a rapid relative sea-level rise to +0.86 ± 0.08 m MHHW, representing possible co-seismic submergence of 0.28 ± 0.11 m. SLT phase E shows a temporary stabilisation of relative sea level, before gradual RSL rise in phase F.

Development of the uppermost peat - SLT phase G
This general relative sea-level fall of -1.16 ± 0.26 m to a ground height of +1.17 ± 0.08 m MHHW may represent the inter-seismic period of the EDC model and sediment accumulation resulting in the development of peat, approximately 400 cal yr BP. Alternatively, it could represent a change in non-seismic processes, for example, eustasy, isostasy and local factors. Section 9 compares this phase with simultaneous changes at Girdwood and Ocean View.

Oscillation in RSL within the upper peat - SLT phase H
Within the upper peat layer there is a relative sea-level oscillation between 11.5 and 7.5 cm, similar to that recorded in SLT phase C. Quantitative reconstructions suggest a RSL rise of +0.10 ± 0.11 m followed by a RSL fall of -0.07 ± 0.11 m. The limit of detectable ^{137}Cs occurs at 8 cm depth, indicating these changes occur before 1954. There is no change in litho-stratigraphy and so it is difficult to say whether this oscillation is laterally extensive. Possible explanations include co-seismic origin, non-seismic origin or a combination of both. Isostatic adjustments could have taken place during the Little Ice Age, 650 to 100 cal yr BP (Wiles & Calkin, 1994), where advance of the surrounding glaciers in the Kenai Mountains caused depression of the earths crust. As the relative sea-level changes are so small, it is difficult to say which hypothesis is most likely. Detailed microfossil work on other cores from Kenai together with other sites in the area will test these hypotheses further.

RSL changes associated with the 1964 event – SLT phases I to K
This section investigates relative sea-level changes associated with the 1964 earthquake in detail. ^{137}Cs confirms the burial of the upper peat layer resulted from co-seismic submergence associated with the 1964 event (figure 7.3).

Pre-seismic relative sea-level rise - SLT phase I
A pre-seismic RSL rise of +0.07 ± 0.12 m starts within the peat (7.5 cm), directly below the peat-silt boundary. ^{137}Cs data indicates that this period started approximately 10 years before the 1964 event (figure 7.3). Evidence suggests it is not a result of mixing because it has a distinct diatom assemblage (figure 7.4). *Gomphonema olivaceum* and *Nitzschia fonticola* are not present in the underlying peat or overlying silt. There are also no *Eunotia* species above 7 cm and *Pinnularia lagerstedtii* increases immediately below the peat-silt boundary.

Co-seismic submergence - SLT phase J
Evidence to suggest co-seismic submergence includes a laterally extensive upper boundary between the peat and overlying silt with herbaceous rootlets and a rapid change in diatom assemblages (figure 7.4). ^{137}Cs confirms the rapid relative sea-level rise observed in SLT phase J results from the 1964 event (figure 7.3). Diatom transfer functions suggest the amount of co-seismic submergence to take place at Kenai was between +0.23 ± 0.24 m and +0.58 ± 0.24 m. The value depends on whether you compare the level at the top of the peat with the first assemblage from the silt unit or from a few centimetres above the contact to make allowance for rapid sedimentation and recovery during and immediately after the event.

Both of these values are comparable to the estimates of Plafker (1965, 1969) and Zong *et al*. (2003). Zong *et al*. (2003) estimate the magnitude of co-seismic land subsidence at Kenai to be 0.17 ± 0.12 m based on diatom transfer functions to 0.31 ± 0.21 m based on pollen transfer functions. Plafker (1965, 1969) suggests 0.5 m co-seismic subsidence accompanied the 1964 event at Kenai, interpolated from three observations at Anchorage, Homer and Nikiski. The measured value at Nikiski (15 km away) was 0.27 m submergence (Plafker, 1969), which is extremely close to the lower reconstructed value using the transfer function approach.

Post-seismic recovery of the land - SLT phase K
Post-seismic recovery occurs in SLT phase K and has been rapid on the Holocene timescale, with redevelopment of silty peat at the surface, only 36 years after the event. Quantitative reconstructions record -0.38 ± 0.23 m post-seismic uplift (RSL fall) together with sediment accumulation. From 1964 to 1995, GPS, tide gauge and levelling measurements suggest 0.20 m post-seismic uplift has occurred at Kenai relative to the Seward tide gauge (Cohen & Freymueller, 1997).

Relative sea-level movements surrounding the 1964 event agree with periods of the EDC model. Transfer functions quantify pre-seismic, co-seismic and post-seismic changes around the peat-silt boundary. These movements allow comparisons between this event and older ones affecting the Kenai area.

7.7 Summary of relative sea-level changes at Kenai

The stratigraphy of Kenai records up to four co-seismic events, named KE-7a to d, with the uppermost being a result of co-seismic submergence associated with the 1964 earthquake.

The stratigraphy of KE-7 clearly records the 1964 event by the burial of the uppermost peat layer (KE-7d). Immediately before the event, there is a pre-seismic signal evident from diatom changes in the upper few centimetres of peat and quantitative transfer functions suggesting a relative sea-level rise. ^{137}Cs dates this period to start around 1954. The litho-stratigraphic boundary fulfils four out of the five criteria described by Nelson *et al*. (1996). The peat-silt boundary is laterally extensive, represents a sudden, large submergence event and observations at the time record it as being synchronous over a large area. Estimates of pre-seismic, co-seismic and post-seismic movements obtained in this study compare well to those from earlier studies (e.g. Zong *et al*., 2003).

The RSL oscillations within SLT phases C (KE-7a) and H (KE-7c) are of similar magnitude but because the relative sea-level changes are so small, it is difficult to discriminate between co-seismic submergence associated with a small magnitude earthquake or non-seismic RSL changes. As they coincide with glacier expansions in the surrounding Kenai Mountains, effects of glacio-isostasy seem the simplest explanation.

The lowest transitional peat-silt boundary in SLT phases D to F (KE-7b) record a similar magnitude relative sea-level rise when compared to the 1964 event. Identical ages from the transitional boundary at KE-7 and the sharp contact at KE-5 support burial by co-seismic submergence but final confirmation requires further diatom analysis.

8. Results: Sediment Mixing Experiment

8.1 Introduction

This section reports results from the first marsh transplant experiment recovered from the tidal flat at Kenai City Pier on April 4th 2002 (section 2.3, figure 2.1). The transplanted block lay beneath ~30 cm of ice that covered the tidal flat and 20 mm of silt-dominated sediment that represents the net sediment accumulation in 320 days since burial. Below were the partially decomposed stems and root layer of the salt marsh plants of the pre-transplant environment. The transplants came from vegetated marsh at 0.8 ± 0.1 m MHHW and were moved to tidal flat at -0.35 ± 0.1 m MHHW, simulating instantaneous submergence of 1.15 m.

8.2 Bio-stratigraphy

Figure 8.1 shows diatom assemblages through the transplanted block of salt marsh sediment (24 to 104 mm) and new silt accumulation on top (0 to 20 mm). The transplanted block of salt marsh sediment is broadly comparable with the post 1964 section from KE-7 (section 7.4). Sample 28 mm had very poor diatom preservation, with insufficient numbers to obtain a statistically significant count. Figure 8.2 shows diatom assemblages from the control block, taken from the salt marsh at the same time and adjacent to the blocks used for transplanting.

The control block (figure 8.2) shows a decrease in polyhalobous species from the base upwards, with an increase in *Navicula cari* var. *cincta*, a common tidal flat and marsh taxa. Above 20 mm the control block shows a continued reduction in tidal inundation as species

with optima at higher elevations (figure 4.7) increase in abundance, especially *Navicula salinarum, Nitzschia sigma, Nitzschia debilis* and *Pinnularia microstauron*. This is consistent with the colonisation of post-1964 tidal flat by salt marsh vegetation and indicative of relative sea-level fall (section 7, Kenai).

Much of the test block (figure 8.1) shows the same trend (104 to 36 mm). However, above 36 mm, no assemblage is similar to any from the top 20 mm of the control block (zone B) characterised by *Navicula salinarum, Nitzschia sigma, Nitzschia debilis* and *Pinnularia microstauron*. In contrast, polyhalobous diatoms from the post-transplant silt (e.g. *Odontella aurita* and *Paralia sulcata*) characterise the assemblages at 24 and 32 mm. These species only occur in very low numbers in the control block.

8.3 Possible sediment mixing

The key question is whether the abundance of polyhalobous diatoms in samples 24 to 32 mm in the test block represents post-burial sediment mixing that could be interpreted as pre-seismic RSL rise in a fossil core. Hamilton (2003) describes a range of evidence for pre-seismic RSL rise, ranging from the very conclusive, where the pre-seismic diatom assemblages comprise mainly species absent from or in lower abundances in the overlying silt, to inconclusive, where the pre-seismic signal is only shown by increasing abundance of species that characterise the overlying silt. Quantitative comparison of the test block and the control block is complicated by the lack of a diatom assemblage equivalent to control block zone B in the test block. It appears that erosion of up to 20 mm may have occurred on the test block prior to deposition of the new silt. Grain size analysis reveals a spike of sand at the boundary, falling from 15% at 20 mm to 6.5 ± 1.0% from 18 to 0 mm.

Qualitative interpretation of the data suggests two possible explanations. First, erosion of the top of the test block, with samples 24 and 32 mm indicating reworked sediment comprising of both the new silt and sediment from the test block. Second, the missing assemblage (control, zone B) reflects microscale variation in the marsh surface from where the test blocks were taken. In this instance, a 20 mm elevation change could result in zone B not existing in the transplanted block. This would suggest that erosion has not taken place and that samples 24 and 32 mm represent downwards mixing during burial, whether by biological processes, e.g. faunal activity, or physical processes, e.g. freeze-thaw or desiccation. In either case, if these diatom assemblages occurred in a fossil sequence, mixing within the top 8 mm of the buried horizon could be misinterpreted as pre-seismic RSL rise where the diatom assemblages comprise only those present in the overlying silt.

Quantitative analyses using the transfer function developed in section 4 reinforce the qualitative interpretations for changes through the test block (figure 8.3). Reconstructed elevations for samples 100 to 36 mm show a gradual development of marsh to +0.75 ± 0.23 m MHHW, in good agreement with the elevation of the marsh from where the transplants were taken, +0.8 ± 0.1 m MHHW. Similarly, reconstructions from the post-transplant silt give elevations close to the transplant elevation of -0.35 ± 0.1m MHHW. Reconstructed values are between -0.21 ± 0.23 m MHHW and -0.37 ± 0.24 m MHHW. The intervening samples, at 24 and 32 mm show that the effect of mixing could be misinterpreted as pre-seismic RSL rise. They have MAT minimum dissimilarity coefficients of 43.4 and 38.6, indicating 'good' modern analogues.

8.4 Summary

This analysis shows that mixing can occur at stratigraphic contacts that record rapid submergence. In this example, mixing is limited to within 8 mm of the boundary but this could be misinterpreted as pre-seismic RSL rise in a fossil record. Unless the pre-submergence assemblages are a distinct assemblage and not a mixture of species found in the underlying peat and overlying silt, it is difficult to say whether there is a pre-seismic

relative sea-level rise or mixing at the peat-silt boundary. We need further criteria to distinguish a 'distinct assemblage'.

We cannot currently use the control block to test hypotheses further due to the significant differences in diatoms within the top 20 mm compared to the test block. We need to analyse one or more of the other recovered test blocks and this will be carried out in our NEHRP 2003-2004 project.

9. Synthesis & Discussion

9.1 Diatom Transfer function for the Cook Inlet

Contemporary diatom assemblages from intertidal and supratidal environments at three sites around the Cook Inlet produce a quantitative diatom transfer function applicable to fossil assemblages from late Holocene sediment sequences. Use of a standardised water level index, based upon the difference between mean higher high water and mean sea level provides a method of allowing for differences in tidal range in this macrotidal environment. This is a substantial improvement to initial analyses that used a transfer function from Kenai only and depended upon upscaling of reconstructed elevations due to difference in tidal range (Hamilton, 2003; Zong *et al*., 2003). In this study, sample specific errors for elevation reconstructions from fossil sequences range from a minimum of ~0.08 m in peat layers to a maximum of ~0.35 m in tidal silt sequences.

9.2 Application to other datasets

Figure 9.1 shows reconstructed elevations associated with the 1964 earthquake from fossil sequences reported by Shennan *et al*. (1999) and Zong *et al*. (2003) based upon the new transfer function described in section 4.

Each of the three reconstructions from different locations on the marsh at Girdwood (figures 1.1 and 5.1) record clear co-seismic submergence in the order of 1.5 m, in good agreement with the observations of Plafker (1969) for land subsidence of 1.7 m, but not indicating the extra 0.9 m suggested for localised sediment compaction. Mixing of sediment within the lowest 1 or 2 cm of the silt above the stratigraphic boundary gives intermediate reconstructions. This phenomenon is reported in numerous studies from the Cascadia subduction zone (e.g. Nelson *et al*., 1996). Pre-seismic RSL rise occurs at all three sites. Pollen analyses reported in the original publications, as well as the detail of the diatom assemblages, offer strong evidence for a pre-seismic RSL rise rather than sediment mixing at the top of the peat (Shennan *et al*., 1999; Zong *et al*., 2003). The only sequence to cover diatom changes up to the present marsh surface, Girdwood 1999 in figure 9.1, clearly records post-seismic recovery.

The two sequences from beneath the salt marsh at Kenai, sites 98-3 and 98-8, record ~0.3 m co-seismic submergence (allowing for sediment mixing 1 cm above the boundary in 98-3) followed by post-seismic recovery. Plafker (1969) recorded 0.27 m at Nikiski, 15 km away (figure 1.1). Both of these sites record pre-seismic RSL rise ~0.1 ± 0.1 m. The site from the raised bog, 98-13, records a pre-seismic RSL rise of similar magnitude, but not a quantifiable co-seismic change. This reinforces the conclusion of Hamilton (2003) that in order to identify small changes in elevation it is necessary to select sites close to thresholds along an environmental gradient. This is an example of the concept of dynamic metastable equilibrium (Chorley & Kennedy, 1971; Shennan, 1995), whereby some locations will respond to a disturbance to the system and others are insensitive. Since such thresholds are difficult to identify in the field it is essential to apply quantitative reconstructions for each event on samples from at least two different locations from each site (Hamilton, 2003).

9.3 Radiocarbon dating of events

Combellick (1991, 1994) and Combellick and Reger (1994) reported significant differences in the chronology of possible co-seismic events between sites around the Cook Inlet. Hamilton (2003) demonstrated that part of the explanation is that diatom analyses show that not all peat-silt couplets result from co-seismic submergence. Nevertheless, significant difficulties remained in establishing a reliable chronology (Hamilton, 2003). Combellick (e.g. 1991) used conventional radiocarbon dating, mostly on bulk peat samples typically 3 cm thick, with a few samples from the outer rings of trees rooted in peat layers. Hamilton (2003) used 1 cm thick bulk peat samples for AMS dating, but still recorded numerous age reversals within and between peat layers. Figure 9.2 shows the results of redating the same peat layers using AMS dates on *in situ* plant macrofossils from the top of each peat layer. Virtually all the samples show a significant older age for the bulk peat sample. While the source of this error remains unidentified (reworking and deposition of older organic material by winter ice seems possible given our observations in 2002 and 2003; figure 4.9) it is very clear that no reliable chronology can be based on bulk peat dates (c.f. Combellick, 1994), whether using AMS or conventional radiocarbon methods.

A new chronology, inter-site correlations and calculation of recurrence intervals requires re-sampling of events from previously investigated sites using diatom analysis to exclude non-events (Hamilton, 2003) and AMS dating methods on *in situ* macrofossils or rooted wood.

9.4 Summary of events

Figure 9.3 shows that the penultimate great earthquake to cause extensive marsh submergence around the upper Cook Inlet occurred ~850-950 cal yr BP. Quantitative reconstructions from Girdwood (section 5) indicate co-seismic submergence of +1.63 ± 0.39 m, similar to that experienced in 1964.

Lack of modern analogues from the diatom samples studied from the same event at Ocean View (section 6) prevents any quantitative estimate of co-seismic submergence.

There is no evidence in the litho-stratigraphy from the transect at Kenai for co-seismic submergence during the ~850-950 cal yr BP event. However it is possible that the bio-stratigraphy and transfer function reconstructions between 40 and 25 cm in KE-7, may record the event. At two different sampling sites along the Kenai River, Combellick and Reger (1994) dated the top of a peat layer to 931-1407 cal yr BP and 1099-1387 cal yr BP indicating that this submergence event may have affected the area. These ages are based on bulk peat samples and so would have to be redated as described above.

During our 2003-2004 NEHRP Project we shall analyse the diatoms within the peat layers dated 1350-1500 cal yr BP at Girdwood and Ocean View.

9.5 Summary of EDC

From studying the stratigraphic evidence of the 1964 earthquake at Girdwood, Shennan *et al*. (1999) propose an EDC model with up to four main periods:

1. Rapid co-seismic submergence (sudden relative sea-level rise) during a large magnitude earthquake (magnitude>8)
2. Rapid post-seismic uplift (relative sea-level fall) immediately following the event on the timescale of decades
3. Slower inter-seismic uplift (relative sea-level fall) on the timescale of centuries
4. Pre-seismic relative sea-level rise immediately before the next co-seismic event

Identification of these four periods is important when determining if a buried peat layer results from co-seismic submergence or non-seismic changes in addition to the criteria reviewed in Nelson *et al*. (1996). This section appraises the four-phase EDC model with reference to the summary data in table 9.1.

Table 9.1 Summary of possible events at Girdwood, Ocean View and Kenai (+ve values represent a relative sea-level rise whereas –ve values suggest a relative sea-level fall)

Event name	Description	SLT Phase	EDC related	Date at contact (cal yr BP)	Pre-event (m) RSL change	Event (m) RSL change	Sharpness of boundary (Troels-Smith)	Lateral extent	Post-event recovery (m) and sediment accumulation
GW-1a	Penultimate event	B - D	Yes	~850	+0.13 ± 0.14	+1.63 ± 0.39	4	Yes	-1.85 ± 0.38
GW-1b	Oscillation within upper peat	E	No?	Between 1954 AD & 450	Not identified	+0.18 ± 0.14	Increase in silt content	Not investigated	-0.13 ± 0.14
GW-1c	1964 earthquake	F - H	Yes	1964 AD	+0.16 ± 0.14	+1.69 ± 0.35	4	Yes	-0.84 ± 0.47
OV-6a	Penultimate event	B - C	Yes?	850-950	RSL rise, not quantified	RSL rise, not quantified	4	Yes	Yes, not quantified
OV-15b	1964 earthquake	D - F	Yes	1964 AD	Not clear	+1.06 ± 0.32	0	Yes	-0.64 ± 0.30
KE-7a	Oscillation within lowest peat	C	No?	Between 1575 & 6500	Not identified	+0.16 ± 0.11	No change in lithology	Not investigated	-0.21 ± 0.11
KE-7b	Penultimate event	D to F	Yes?	1575	+0.08 ± 0.11	+0.28 ± 0.11	0, sharper in other cores	>700 m	No rapid RSL fall
KE-7c	Oscillation within upper peat	H	No?	Between 1954 AD & 500	*Eunotia exigua* declines	+0.10 ± 0.11	No change in lithology	Not investigated	-0.07 ± 0.11
KE-7d	1964 earthquake	I to K	Yes	1964 AD	+0.07 ± 0.12	+0.23 ± 0.24 or +0.58 ± 0.24	2	>400 m	-0.38 ± 0.23

For the six co-seismic events, two at each of Ocean View, Girdwood and Kenai, only the 1964 sequence at Ocean View shows no evidence of pre-seismic RSL rise. In all cases, it is difficult to differentiate between post-seismic RSL fall and inter-seismic RSL fall because of the lack of knowledge on sedimentation rates and the chronology through clastic units. However, observations from the 1964 event (e.g. Brown *et al*., 1977) indicate that post- and inter-seismic periods are separate and there is nothing in the fossil record to suggest otherwise. These results suggest that the four-phase EDC model remains valid.

9.5.1 Pre-seismic relative sea-level rise as a precursor to a major earthquake

Hamilton (2003), Shennan *et al*. (1998, 1999) and Zong *et al*. (2003) record a pre-seismic relative sea-level rise before episodes of co-seismic submergence in the Pacific Northwest of the USA and before the 1964 event in Alaska. Tide gauge records before the 1964 earthquake are available from Women's Bay (Kodiak Island) and Seward (Kenai Peninsula). Both locations experienced co-seismic submergence associated with the 1964 earthquake but the tide gauge measurements did not register any quantifiable pre-seismic relative sea-level rise (Savage & Plafker, 1991). One explanation is that there is differential movement between sites, for example, Cohen and Freymueller (2001) use GPS measurements to establish a different direction and rate of present day movement between Seward and Anchorage against sites along the western Kenai Peninsula. However, Karlstrom (1964) observed that at Girdwood, storm tides that did not flood the marsh surface before 1953 began depositing a thin surface layer of silt that became progressively thicker each year. This date corresponds to the start of the pre-seismic signal identified from the microfossil data at Girdwood, dated using ^{137}Cs.

9.5.2 Other possible explanations for observed pre-seismic changes

If the RSL rise does not form part of the EDC model, other possible explanations include a temporary change in sea level due to the El Nino Southern Oscillation (ENSO). ENSO can cause higher water levels along the west coast of the USA and Alaska, for example, the 1997-1998 El Nino caused a short-lived sea-level rise during the winter of approximately 0.20 m at Seldovia and Seward, Alaska (data from http://pmel.noaa.gov). Any effect before the 1964 event would be as short lived and the magnitude would be even smaller as the only El Nino as large as the 1997-1998 occurred in 1940-1942. Observations at Girdwood by Karlstrom (1964) suggest that the relative sea-level rise started in 1953 corresponds to an El Nino peak but it could not account for continued flooding of the marsh surface between 1954 and 1957 when El Nino was weak. The short-term effect could not account for a relative sea-level rise over the period of several years to a decade and it is hard to envisage how such a process could occur before every peat-silt boundary. Other possibilities include sediment mixing around boundaries due to the flow or percolation of water (e.g. Battarbee, 1986), diatoms burrowing through the sediment column (e.g. Hay *et al*., 1993), tidal inundation and effects of ice.

If it does form part of the EDC model and occurs over several years to a decade, possible mechanisms of pre-seismic RSL rise include aseismic slip (e.g. Dragert *et al*., 2001; Miller *et al*., 2002). For example, tide gauge data in Japan (Katsumata *et al*., 2002) record several centimetres of aseismic subsidence during a five year period before the 1994 Hokkaido-Toho-Oki earthquake (magnitude 8.3). Other possible mechanisms include certain seismic quiescence models (e.g. Kato *et al*., 1997; Wyss *et al*., 1981; Dieterich & Okubu, 1996). Both produce a reduction of uplift caused by inter-seismic strain accumulation (e.g. Long & Shennan, 1998). Pre-seismic RSL rise does appear to be a common feature and seismological models developed on observational data need to take account of these late Holocene relative sea-level movements.

Acknowledgements
NERC Research Studentship GT 04/99/ES/57; NERC radiocarbon allocation number 935 0901; Technician support from the Geography Department, University of Durham; Design and Imaging Unit, University of Durham; Sir James Knott Foundation Fellow; Smiley Shields, Anchorage.

References

Atwater, B. F., Yamaguchi, D. K., Bondevik, S., Barnhardt, W. A., Amidon, L. J., Benson, B. E., Skjerdal, G., Shulene, J. A. & Nanayama, F., 2001. Rapid resetting of an estuarine recorder of the 1964 Alaska Earthquake. *Bulletin of the Geological Society of America*, **113**, 1193-1204.

Bartsch-Winkler, S., 1988. Cycle of earthquake induced aggradation and related tidal channel shifting, upper Turnagain Arm, Alaska, USA. *Sedimentology*, **35**, 621-628.

Bartsch-Winkler, S. & Schmoll, H. R., 1992. Utility of radiocarbon dated stratigraphy in determining late Holocene earthquake recurrence intervals, upper Cook Inlet region, Alaska. *Geological Society of America Bulletin*, **104**, 684-694.

Battarbee, R. W., 1986. Diatom analysis. In: *Handbook of Holocene palaeoecology and palaeohydrology* (ed Berglund, B. E.), pp. 527-541, John Wiley & Sons, Chichester.

Birks, H. J. B., 1995. Quantitative palaeoenvironmental reconstructions. In: *Statistical modelling of Quaternary science data.* (eds Maddy, D. & Brew, J. S.) *Technical Guide No.5*, pp. 161-254, Quaternary Research Association, London.

Birks, H. J. B., Line, J. M., Juggins, S., Stevenson, A. C. & ter Braak, C. J. F., 1990. Diatoms and pH reconstruction. *Philosophical Transactions of the Royal Society of London B*, **327**, 263-278.

Brown, L. D., Reilinger, R. E., Holdahl, S. R. & Balazs, E. I., 1977. Postseismic crustal uplift near Anchorage, Alaska. *Journal of Geophysical Research*, **82**, 3369-3378.

Chorley, R. J. & Kennedy, B. A. 1971. *Physical Geography: a systems approach.* London, Prentice-Hall. 370pp.

Clague, J. J. & James, T. S., 2002. History and isostatic effects of the last ice sheet in southern British Columbia. *Quaternary Science Reviews*, **21**, 71-87.

Cohen, S., 1996. Time-dependent uplift of the Kenai Peninsula and adjacent regions of south central Alaska since the 1964 Prince William Sound earthquake. *Journal of Geophysical Research*, **101**, 8595-8604.

Cohen, S., 1998. On the rapid postseismic uplift along Turnagain Arm, Alaska, following the 1964 Prince William Sound earthquake. *Geophysical Research Letters*, **25**, 1213-1215.

Cohen, S., Holdahl, S., Caprette, D., Hilla, S., Safford, R. & Schultz, D., 1995. Uplift of the Kenai Peninsula, Alaska, since the 1964 Prince William Sound earthquake. *Journal of Geophysical Research*, **100**, 2031-2038.

Cohen, S. C. & Freymueller, J. T., 1997. Deformation of the Kenai Peninsula, Alaska. *Journal of Geophysical Research*, **102**, 20,479-420,487.

Cohen, S. C. & Freymueller, J. T., 2001. Crustal uplift in the south central Alaska subduction zone: new analysis and interpretation of tide gauge observations. *Journal of Geophysical Research*, **106**, 11,259-211,270.

Combellick, R. A., 1991. Palaeoseismicity of the Cook Inlet region, Alaska: evidence from peat stratigraphy in Turnagain and Knik Arms. *Alaska Division of Geological and Geophysical Surveys Professional Report*, **112**, 1-52.

Combellick, R. A., 1994. Investigation of peat stratigraphy in tidal marshes along Cook Inlet, Alaska, to determine the frequency of 1964-style great earthquakes in the Anchorage region. *Alaska Division of Geological and Geophysical Surveys Report of Investigations*, **94-7**, 1-24.

Combellick, R. A., 1997. Evidence of prehistoric great earthquakes in the Cook Inlet region, Alaska. In: *IGCP Project 367. Late Quaternary coastal records of rapid change: Application to present and future conditions. Field trip guide to Portage-Girdwood area, Anchorage lowland and Kenai Fjords* (ed Hamilton, T. D.), pp. 23-40, Anchorage, Alaska.

Combellick, R. A. & Pinney, D. S., 1995. Radiocarbon age of probable Hayes tephra, Kenai Peninsula, Alaska. In: *Short notes on Alaskan geology 1995. Alaska Division of Geological and Geophysical Surveys Professional report 117* (eds Combellick, R. A. & Tannian, F.), pp. 1-9, State of Alaska Department of Natural Resources, Fairbanks.

Combellick, R. A. & Reger, R. D., 1994. Sedimentological and radiocarbon age data for tidal marshes along eastern and upper Cook Inlet, Alaska. *Alaska Division of Geological and Geophysical Surveys Report of Investigations*, **94-6**, 1-60.

Crossen, K. J., 1992. Guide to the Little Ice Age landforms and glacial dynamics of Portage Glacier. In: *Guide to the Little Ice Age landforms and glacial dynamics in Portage Valley and Portage Pass* (ed Crossen, K. J.), pp. 3-15, Alaska Geological Society, Anchorage, Alaska.

Denys, L., 1991. A checklist of the diatoms in the Holocene deposits of the western Belgian coastal plain with a survey of their apparent ecological requirements. *Belgian Geological Survey Professional Paper 1991/2*, **246**, 1-41.

Dieterich, J. H. & Okubu, P. G., 1996. An unusual pattern of recurring seismic quiescence at Kalapana, Hawaii. *Geophysical Research Letters*, **23**, 447-450.

Dragert, H., Wang, K. & James, T. S., 2001. A silent slip event on the deeper Cascadia subduction interface. *Science*, **292**, 1525-1528.

Edwards, R. J. & Horton, B. P., 2000. Reconstructing relative sea-level change using UK salt-marsh foraminifera. *Marine Geology*, **169**, 41-56.

Fleming, K., Johnston, P., Zwartz, D., Yokoyama, Y., Lambeck, K. & Chappell, J., 1998. Refining the eustatic sea-level curve since the Last Glacial Maximum using far- and intermediate-field sites. *Earth and Planetary Science Letters*, **163**, 327-342.

Freymueller, J. T., Cohen, S. & Fletcher, H. J., 2000. Spatial variations in present-day deformation, Kenai Peninsula, Alaska, and their implications. *Journal of Geophysical Research*, **105**, 8079-8101.

Gehrels, W. R., Roe, H. M. & Charman, D. J., 2001. Foraminifera, testate amoebae and diatoms as sea-level indicators in UK salt marshes: a quantitative multiproxy approach. *Journal of Quaternary Science*, **16**, 201-220.

Grimm, E., 1993. *TILIA: A pollen program for analysis and display*. Illinois State Museum, Springfield

Hamilton, S. L., 2003. *Late Holocene relative sea-level changes and earthquakes around the upper Cook Inlet, Alaska, USA.* Unpublished PhD Thesis, University of Durham, Durham, UK.

Hartley, B., Barber, H. G. & Carter, J. R., 1996. *An atlas of British diatoms*. Biopress, Bristol, 601pp.

Hay, S. I., Maitland, T. C. & Paterson, D. M., 1993. The speed of diatom migration through natural and artificial substrata. *Diatom Research*, **8**, 371-384.

Hemphill-Haley, E., 1993. Taxonomy of recent and fossil (Holocene) diatoms (Bacillariophyta) from northern Willapa Bay, Washington. *US Geological Survey Open File Report*, **93-289**, 1-151.

Horton, B. P., Edwards, R. J. & Lloyd, J. M., 1999. A foraminiferal-based transfer function: implications for sea-level studies. *Journal of Foraminiferal Research*, **29**, 117-129.

Horton, B. P., Edwards, R. J. & Lloyd, J. M., 2000. Implications of a microfossil based transfer function in Holocene sea-level studies. In: *Holocene land-ocean interaction and environmental change around the North Sea.* (eds Shennan, I. & Andrews, J.), pp. 41-54, Geological Society, London.

Imbrie, J. & Kipp, N. G., 1971. A new micropaleontological method for quantitative paleoclimatology: application to a Late Pleistocene Caribbean core. In: *The Late Cenozoic Glacial Ages* (ed Turekian, K. K.), pp. 71-181, Yale University Press, New Haven.

James, T. S., Clague, J. J., Wang, K. & Hutchinson, I., 2000. Postglacial rebound at the northern Cascadia subduction zone. *Quaternary Science Reviews*, **19**, 1527-1541.

Jones, V. J. & Juggins, S., 1995 The construction of diatom-based chlorophyll transfer function and its application at three lakes on Signy Island (maritime Antarctica) subject to differing degrees of nutrient enrichment. *Freshwater Biology,* **34**, 433-435

Juggins, S., 2003. *C^2 User guide*. *Software for ecological and palaeoecological data analysis and visualisation.* University of Newcastle, Newcastle upon Tyne, UK. 69pp.

Karlstrom, T. N. V., 1964. Quaternary geology of the Kenai lowland and the glacial history of the Cook Inlet region, Alaska. *US Geological Survey Professional Paper*, **443**, 1-69.

Kato, N., Ohtake, M. & Hirasawa, T., 1997. Possible mechanisms of precursory seismic quiescence: Regional stress relaxation due to preseismic sliding. *Pure and Applied Geophysics*, **150**, 249-267.

Katsumata, K., Kasahara, M., Ozawa, S. & Ivashchenko, A., 2002. A five years super-slow aseismic precursor model for the 1994 M8.3 Hokkaido-Toho-Oki lithospheric earthquake based on tide gauge data. *Geophysical Research Letters*, **29**, 32-1 – 32-4.

Long, A. J. & Shennan, I., 1994. Sea-level changes in Washington and Oregon and the "Earthquake deformation cycle". *Journal of Coastal Research*, **10**, 825-838.

Long, A. J. & Shennan, I., 1998. Models of rapid relative sea-level change in Washington and Oregon, USA. *The Holocene*, **8**, 129-142.

Lu, X. X., 1998. Soil erosion and sediment yield in the upper Yangtze, China. *Unpub. PhD Thesis, University of Durham, Durham.*

Miller, M. M., Melbourne, T., Johnson, D. J. & Sumner, W. Q., 2002. Periodic slow earthquakes from the Cascadia subduction zone. *Science*, **295**, 2423.

Nelson, A. R., Shennan, I. & Long, A. J., 1996. Identifying coseismic subsidence in tidal-wetland stratigraphic sequences at the Cascadia subduction zone of western North America. *Journal of Geophysical Research*, **101**, 6115-6135.

Palmer, A. J. & Abbott, W. H., 1986. Diatoms as indicators of sea-level change. In: *Sea Level Research: a manual for the collection and evaluation of data* (ed Van de Plassche, O.), pp. 457-488, Geobooks, Norwich.

Patrick, R. & Reimer, C. W., 1966. *The Diatoms of the United States. Volume 1. Monographs of The Academy of Natural Sciences of Philadelphia No 13*. Academy of Natural Sciences of Philadelphia, Philadelphia, 688pp.

Patrick, R. & Reimer, C. W., 1975. *The Diatoms of the United States. Volume 2, Part 1. Monographs of The Academy of Natural Sciences of Philadelphia No 13*. The Academy of Natural Sciences of Philadelphia, Philadelphia, 213pp.

Peltier, W. R., 1998. Postglacial variations in the level of the sea: implications for climate dynamics and solid-earth geophysics. *Reviews of Geophysics*, **36**, 603-689.

Plafker, G., 1965. Tectonic deformation associated with the 1964 Alaska earthquake. *Science*, **148**, 1675-1687.

Plafker, G., 1969. Tectonics of the March 27, 1964, Alaska earthquake. *US Geological Survey Professional Paper*, **543-1**, 1-74.

Plafker, G., Kachadoorian, R., Eckel, E. B. & Mayo, L. R., 1969. Effects of the earthquake of March 27, 1964 on various communities. *US Geological Survey Professional Paper*, **542-G**, 1-50.

Plafker, G., Lajoie, K. R. & Rubin, M., 1992. Determining intervals of great subduction zone earthquakes in southern Alaska by radiocarbon dating. In: *Radiocarbon after four decades. An interdisciplinary perspective* (eds Taylor, R. E., Long, A. & Kra, R. S.), pp. 436-452, Springer Verlag, New York.

Preuss, H., 1979. Progress in computer evaluation of sea-level data within the IGCP project no. 61. In: *International Symposium on coastal evolution in the Quaternary, September 11-18, 1978* (eds Suguio, K., Fairchild, T. R., Martin, L. & Flexor, J.), pp. 104-134, Sao-Paulo, Brazil.

Pugh, D. T., 1996. *Tides, Surges and Mean Sea-Level*. John Wiley & Sons, Chichester, 472pp.

Riehle, J. R., 1985. A reconnaissance of the major Holocene tephra deposits in the upper Cook Inlet region, Alaska. *Journal of Volcanology and Geothermal Research*, **26**, 37-74.

Savage, J. C. & Plafker, G., 1991. Tide gage measurements of uplift along the south coast of Alaska. *Journal of Geophysical Research*, **96**, 4325-4336.

Savage, J. C., Svarc, J. L., Prescott, W. H. & Gross, W. K., 1998. Deformation across the rupture zone of the 1964 Alaska earthquake, 1993-1997. *Journal of Geophysical Research*, **103**, 21,275-221,283.

Sawai, Y., 2001. Distribution of living and dead diatoms in tidal wetlands of northern Japan: relations to taphonomy. *Palaeogeography, Palaeoclimatology, Palaeoecology*, **173**, 125-141.

Shennan, I., 1995. Sea-level and coastal evolution: Holocene analogues for future changes. *Coastal Zone Topics: Process, Ecology & Management*, **1**, 1-9.

Shennan, I., 1986. Flandrian sea-level changes in the Fenland II. Tendencies of sea-level movement, altitudinal changes and local and regional factors. *Journal of Quaternary Science*, **1**, 155-179.

Shennan, I., Long, A. J., Rutherford, M. M., Green, F. M., Innes, J. B., Lloyd, J. M., Zong, Y. & Walker, K., 1996. Tidal marsh stratigraphy, sea-level change and large earthquakes, I: a 5000 year record in Washington USA. *Quaternary Science Reviews*, **15**, 1023-1059.

Shennan, I., Long, A. J., Rutherford, M. M., Kirkby, J., Green, F. M., Innes, J. B. & Walker, K., 1998. Tidal marsh stratigraphy, sea-level change and large earthquakes, II: events during the last 3500 years at Netarts Bay, Oregon, USA. *Quaternary Science Reviews*, **17**, 365-393.

Shennan, I., Scott, D., Rutherford, M. & Zong, Y., 1999. Microfossil analysis of sediments representing the 1964 earthquake, exposed at Girdwood Flats, Alaska, USA. *Quaternary International*, **60**, 55-73.

Stuiver, M. & Reimer, P. J., 1993. Extended 14C database and revised CALIB 3.0 radiocarbon calibration program. *Radiocarbon*, **35**, 215-230.

Stuiver, M., Reimer, P. J., Bard, E., Beck, J. W., Burr, G. S., Hughen, K. A., Kromer, B., McCormac, F. G., v.d.Plicht, J. & Spurk, M., 1998. INTCAL98 Radiocarbon age calibration 24,000 - 0 cal BP. *Radiocarbon*, **40**, 1041-1083.

ter Braak, C. J. F. & Juggins, S., 1993. Weighted averaging partial least squares regression (WA-PLS): an improved method for reconstructing environmental variables from species assemblages. *Hydrobiologia*, **269/270**, 485-502.

ter Braak, C. J. F., Juggins, S., Birks, H. J. B. & van der Voet, H., 1993. Weighted averaging partial least squares regression (WA-PLS): definition and comparison with other methods for species-environment calibration. In: *Multivariate Environmental Statistics* (eds Patil, G. P. & Rao, C. R.), pp. 525-560, Elsevier Science Publishers, Amsterdam.

ter Braak, C. J. F. & Smilauer, P., 2002. *CANOCO Reference manual and CanoDraw for Windows User's guide: Software for Canonical Community Ordination (version 4.5).* Microcomputer Power, Ithaca, NY, USA, 500pp.

Troels-Smith, J., 1955. Characterisation on unconsolidated sediments. *Danmarks Geologiske Undersogelse*, **IV**, series 3, 1-73.

Van der Werff, A. & Huls, H., 1958-1974. *Diatomeeenflora van Nederland. 8 parts.* Published privately, De Hoef, The Netherlands.,

Wiles, G. C. & Calkin, P. E., 1994. Late Holocene, high resolution glacial chronologies and climate, Kenai mountains, Alaska. *Geological Society of America Bulletin*, **106**, 281-303.

Wyss, M., Klein, F. W. & Johnston, A. C., 1981. Precursors to the Kalapana M=7.2 earthquake. *Journal of Geophysical Research*, **86**, 3881-3900.

Wyss, M. & Wiemer, S., 1999. How can one test the seismic gap hypothesis? The case of repeated ruptures in the Aleutians. *Pure and Applied Geophysics*, **155**, 259-278.

Zong, Y., Shennan, I., Combellick, R. A., Hamilton, S.L. & Rutherford, M.M., 2003. Microfossil evidence for land movements associated with the AD 1964 Alaska earthquake. *The Holocene*, **13**, 7-20.

Zweck, C., Freymueller, J. T. & Cohen, S. C., 2002. The 1964 great Alaska earthquake: present day and cumulative postseismic deformation in the western Kenai Peninsula. *Physics of the Earth and Planetary Interiors*, **132**, 5-20.

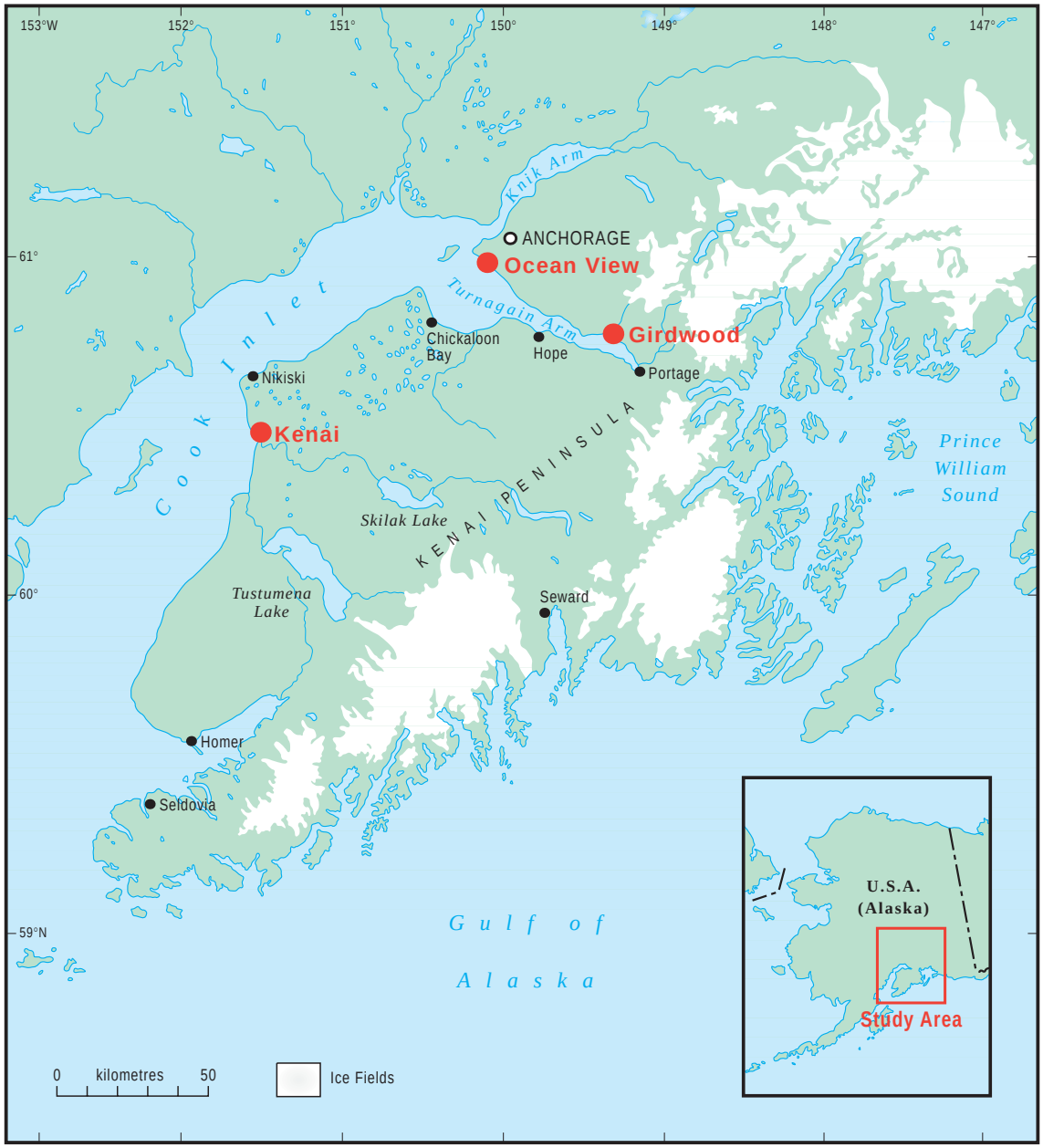

Figure 1.1
Location of field sites around the Cook Inlet

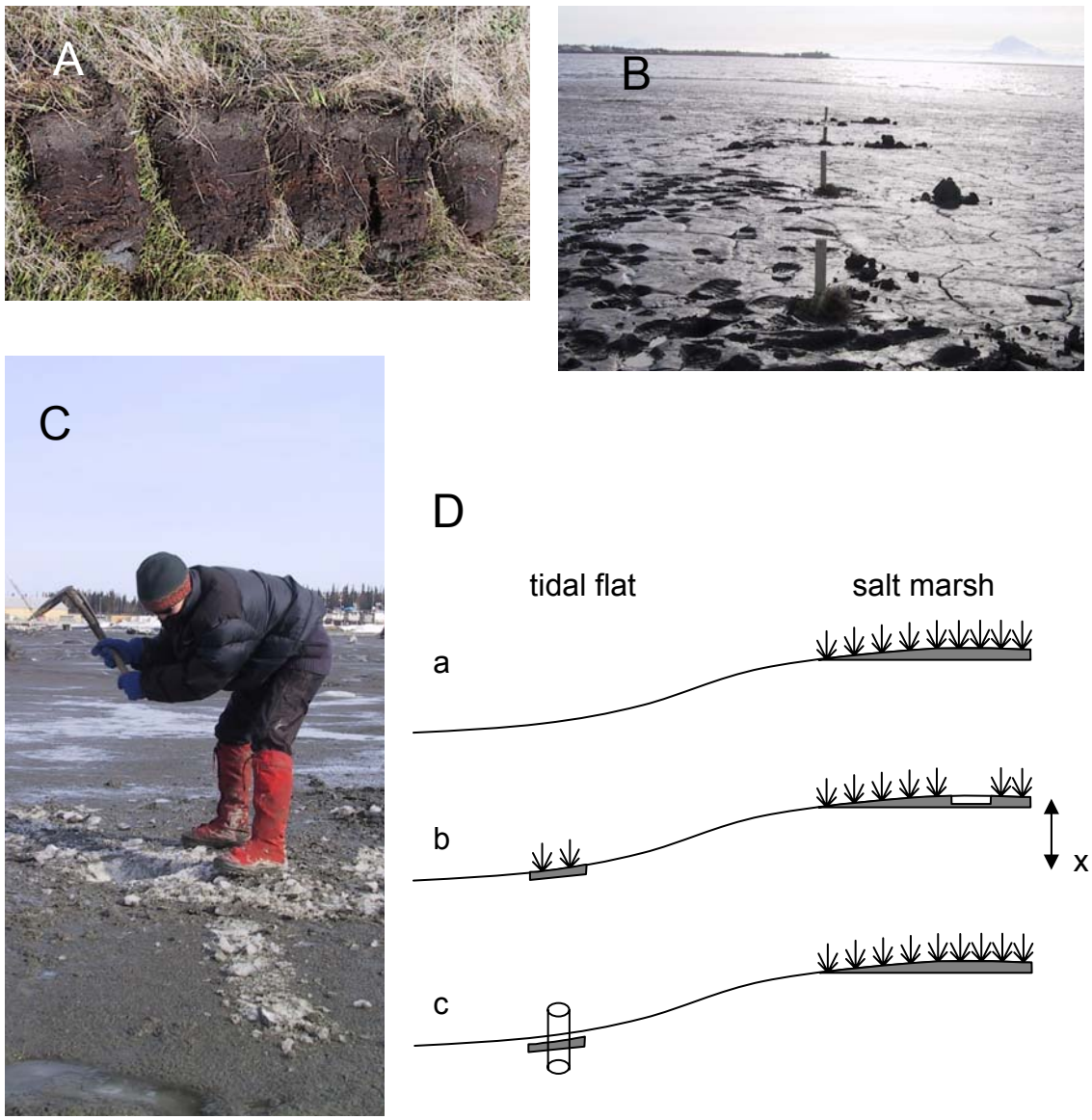

Figure 2.1
Transplant experiments to test diatom mixing at peat-silt boundaries
A Collection of control and test blocks from the vegetated marsh
B Burial of test blocks into the contemporary tidal flat
C Recovery of test blocks after several months of sediment accumulation
D Schematic diagram of an experiment to simulate instantaneous land submergence of ~1.15 m and to measure the associated microfossil changes in surface (filled symbols) and below-surface sediments (core tube symbol)

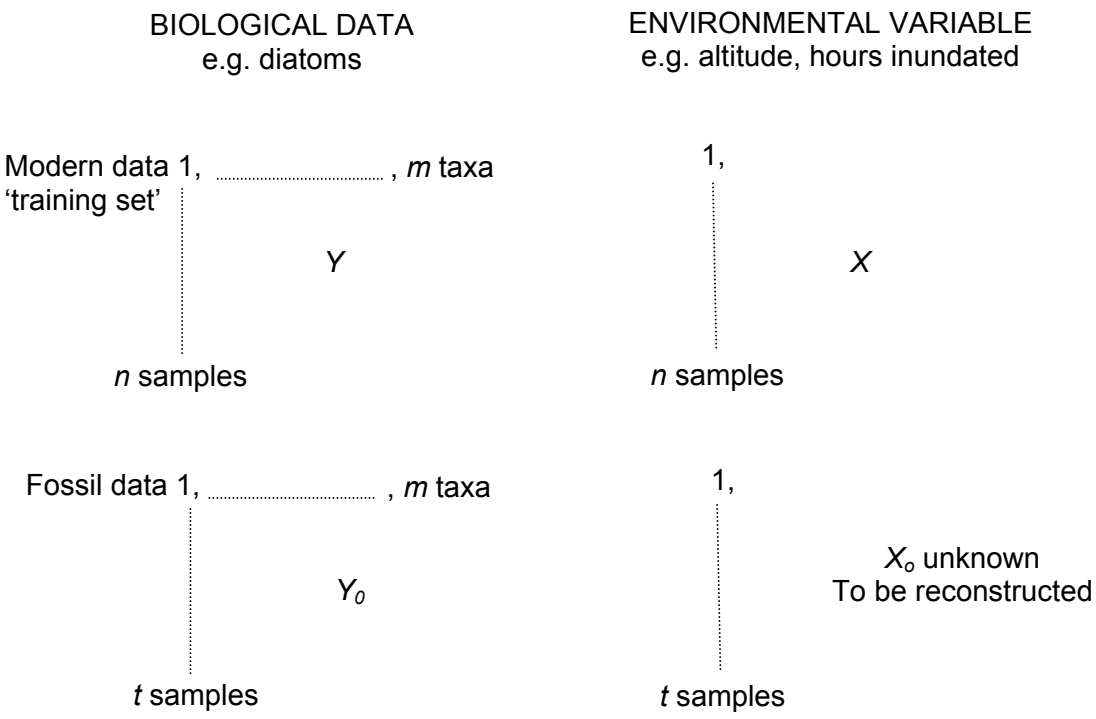

Figure 3.1
The primary aim of a transfer function is to predict the value of one or more environmental variables (*Xo*) from fossil biological data (*Yo*) consisting of *m* species in *t* samples. To estimate values of *Xo* the contemporary response of the same *m* species to the environmental variable(s) of interest is modelled. This involves a contemporary 'training set' of *m* species at *n* sites (*Y*) studied as surface assemblages with an associated set of contemporary environmental variables (*X*) for the same *n* sites. The modern relationships between Y and X are modelled and the resulting function is then used as a transfer function to transform the fossil data (*Yo*) into quantitative estimates of the past environmental variable(s) *Xo* (diagram and text from Birks, 1995)

Figure 4.1
Contemporary environments at Girdwood. A: overview of the marsh (Photograph by Rod Combellick), B: marsh vegetation towards the landward limits of the marsh, C: transitional zone between the vegetated marsh and mudflat and D: unvegetated mudflat

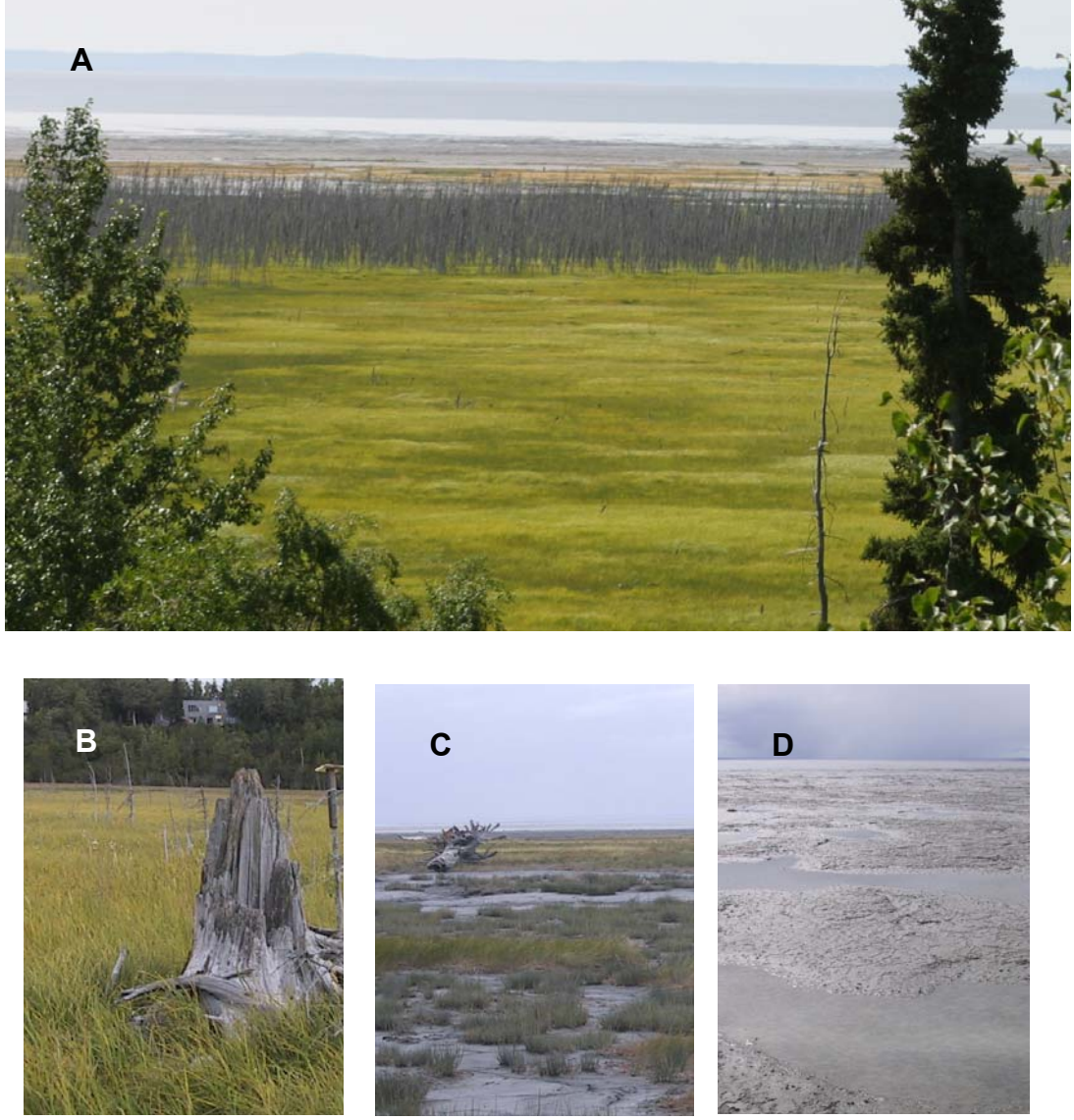

Figure 4.2
Contemporary environments at Ocean View. A: overview of the marsh, B: marsh vegetation towards the landward limits of the marsh, C: transitional zone between the vegetated marsh and mudflat and D: unvegetated mudflat

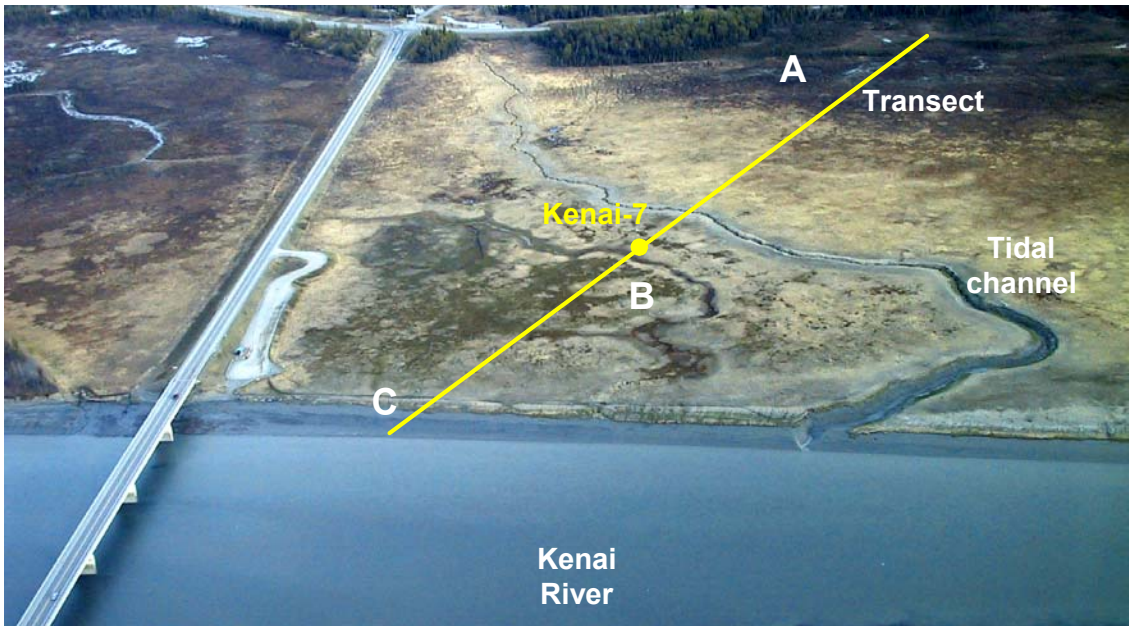

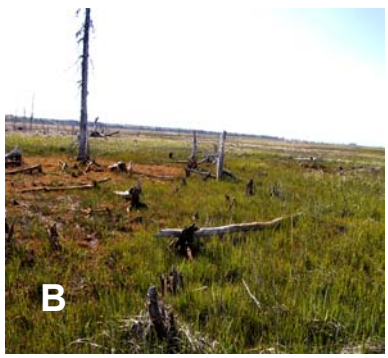

Figure 4.3
Contemporary transect at Kenai showing location of coring site Kenai-7 and different vegetation zones. Zone A is located towards the back of the marsh and consists of freshwater and raised bog environments, zone B is located along the vegetated salt marsh surface and zone C is located at the bank between the vegetated marsh and the mudflat

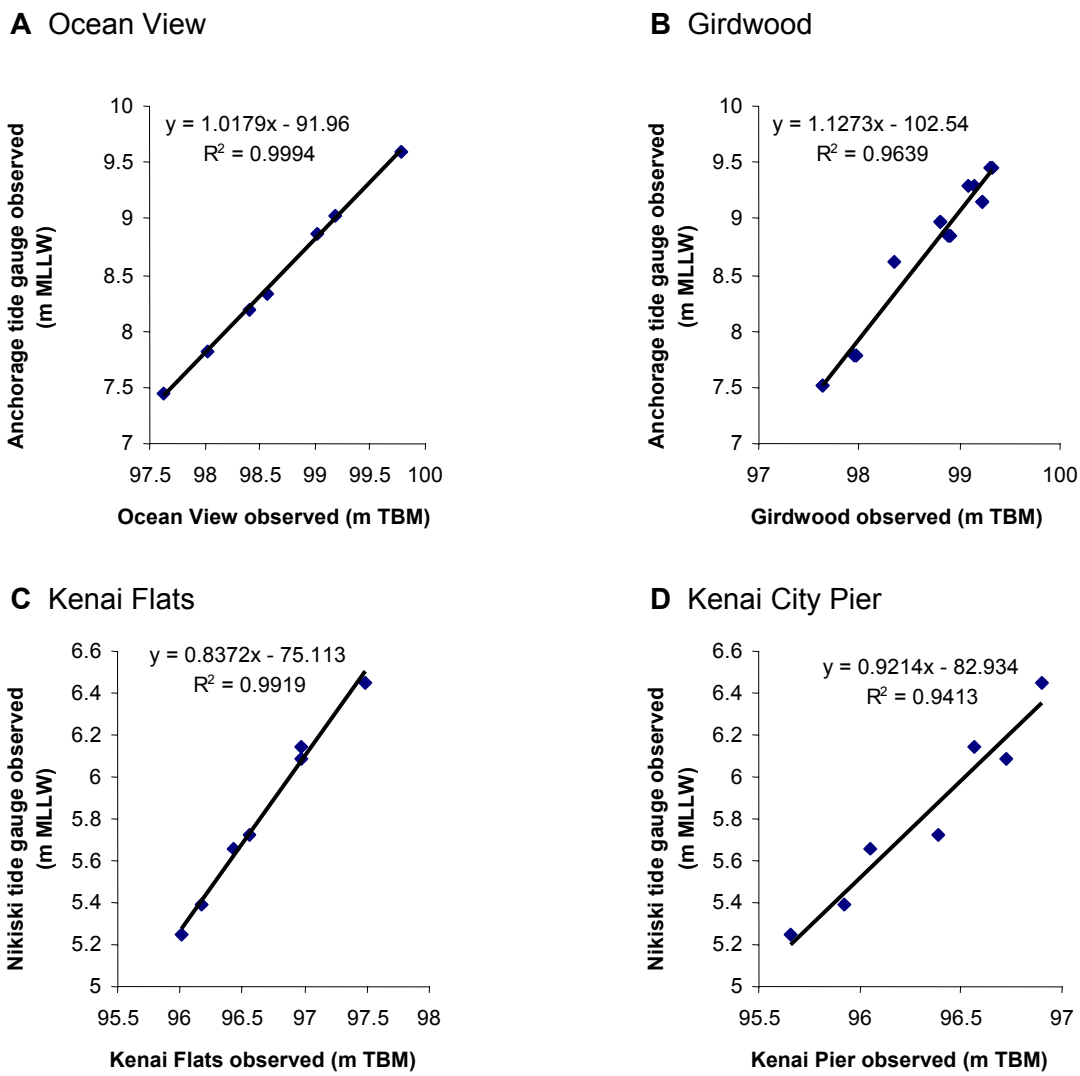

Figure 4.4
High tide level observations at field sites and closest tide gauge station

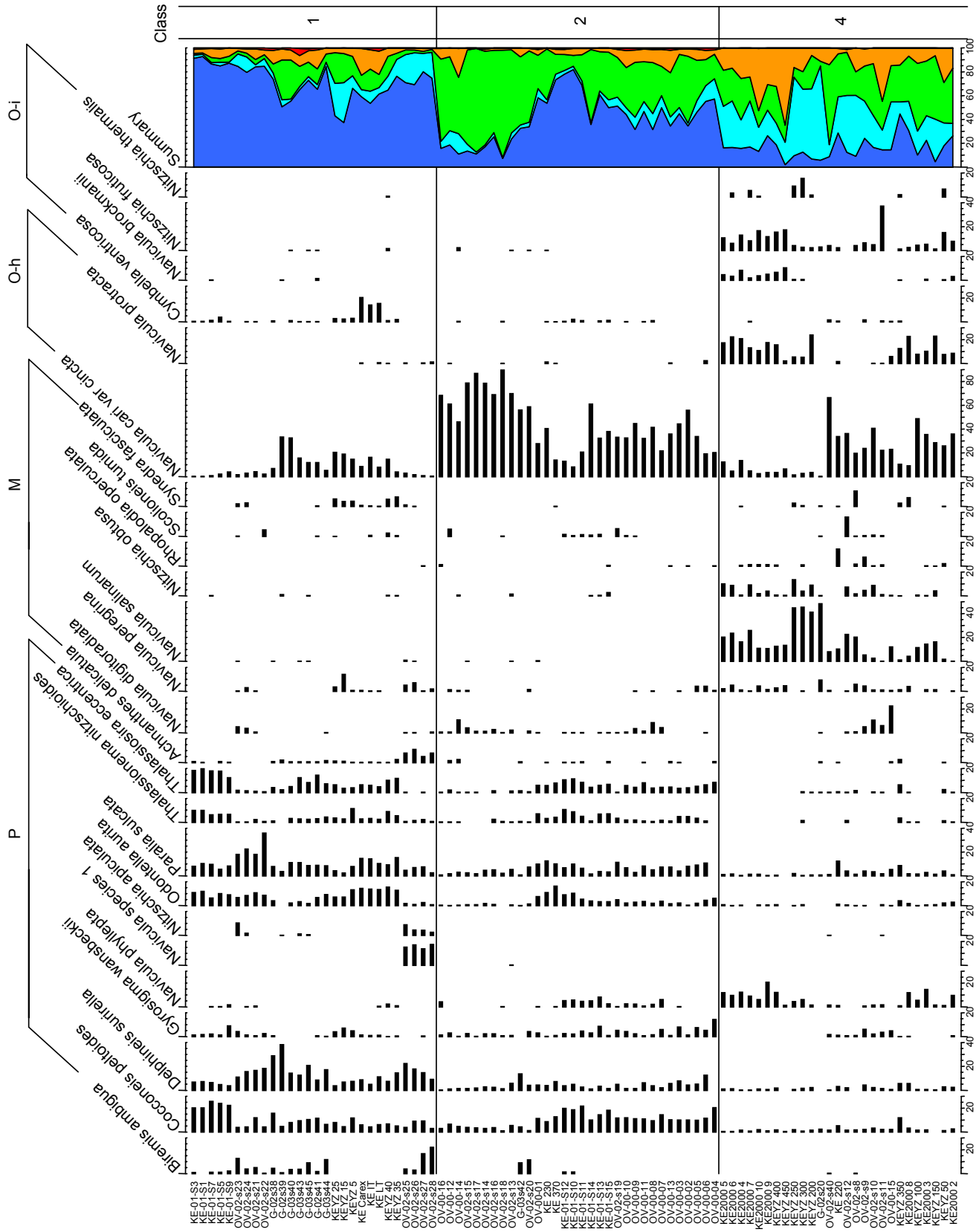

Figure 4.5a
Contemporary diatom data (>10% total diatom valves) and cluster analysis using Chord distance. Summary salinity classes: polyhalobous (P), mesohalobous (M), oligohalobous-halophile (O-h), oligohalobous-indifferent (O-i), halophobous (H), classes 1, 2 and 4

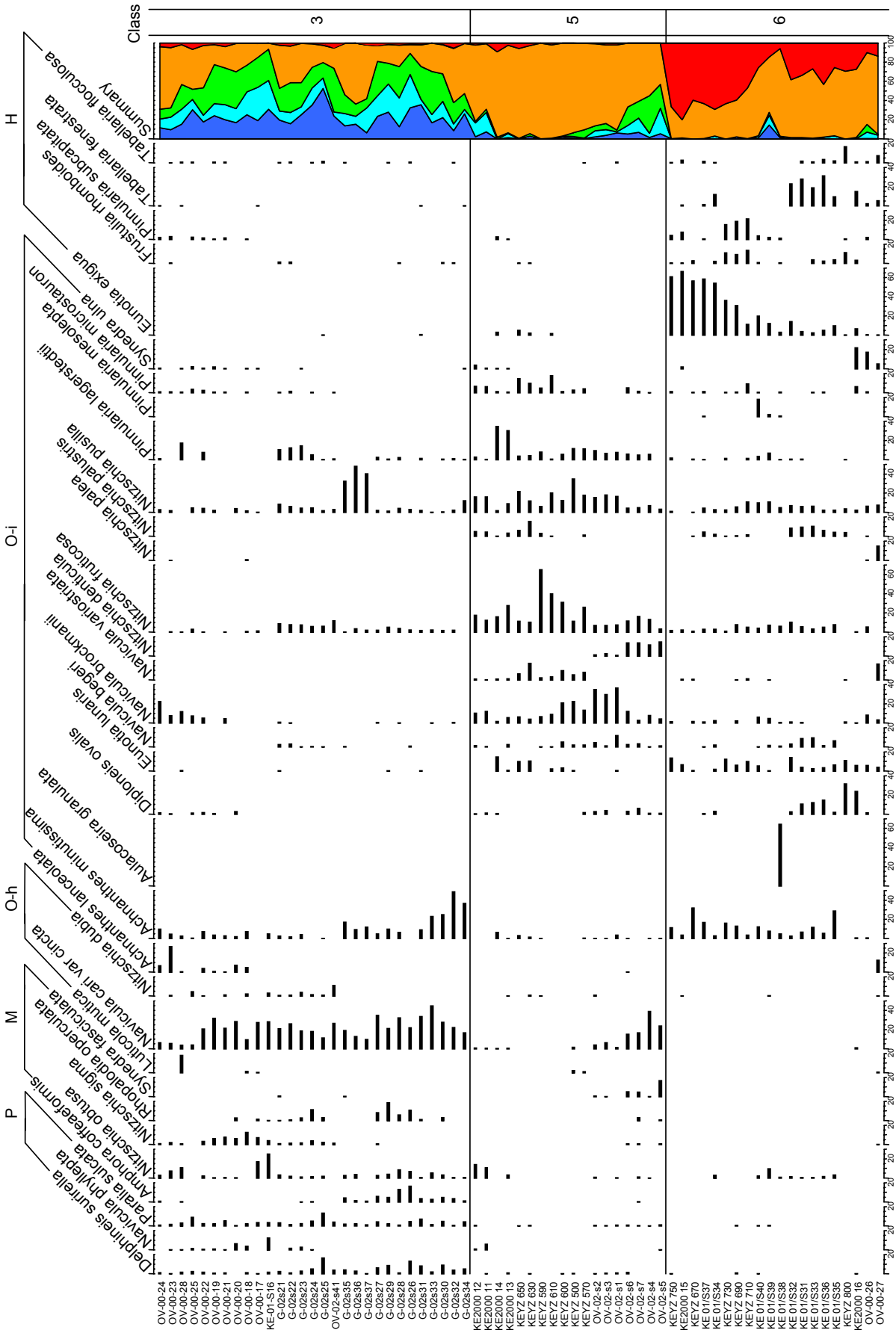

Figure 4.5b

Contemporary diatom data (>10% total diatom valves) and cluster analysis using Chord distance. Summary salinity classes: polyhalobous (P), mesohalobous (M), oligohalobous-halophile (O-h), oligohalobous-indifferent (O-i), halophobous (H), classes 3, 5 and 6

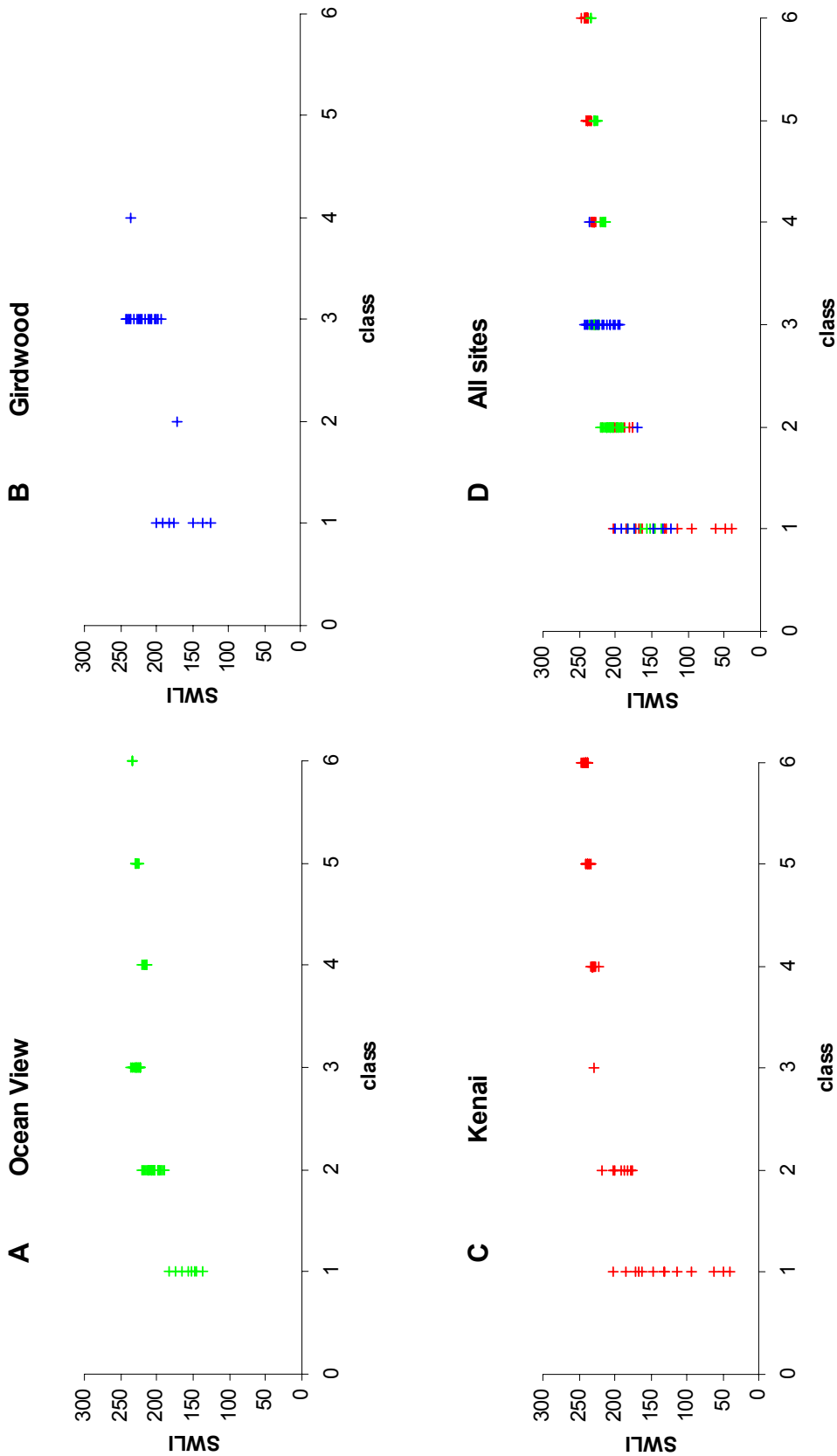

Figure 4.6
Elevation (SWLI) distributions for contemporary samples in classes defined by unconstrained cluster anlaysis

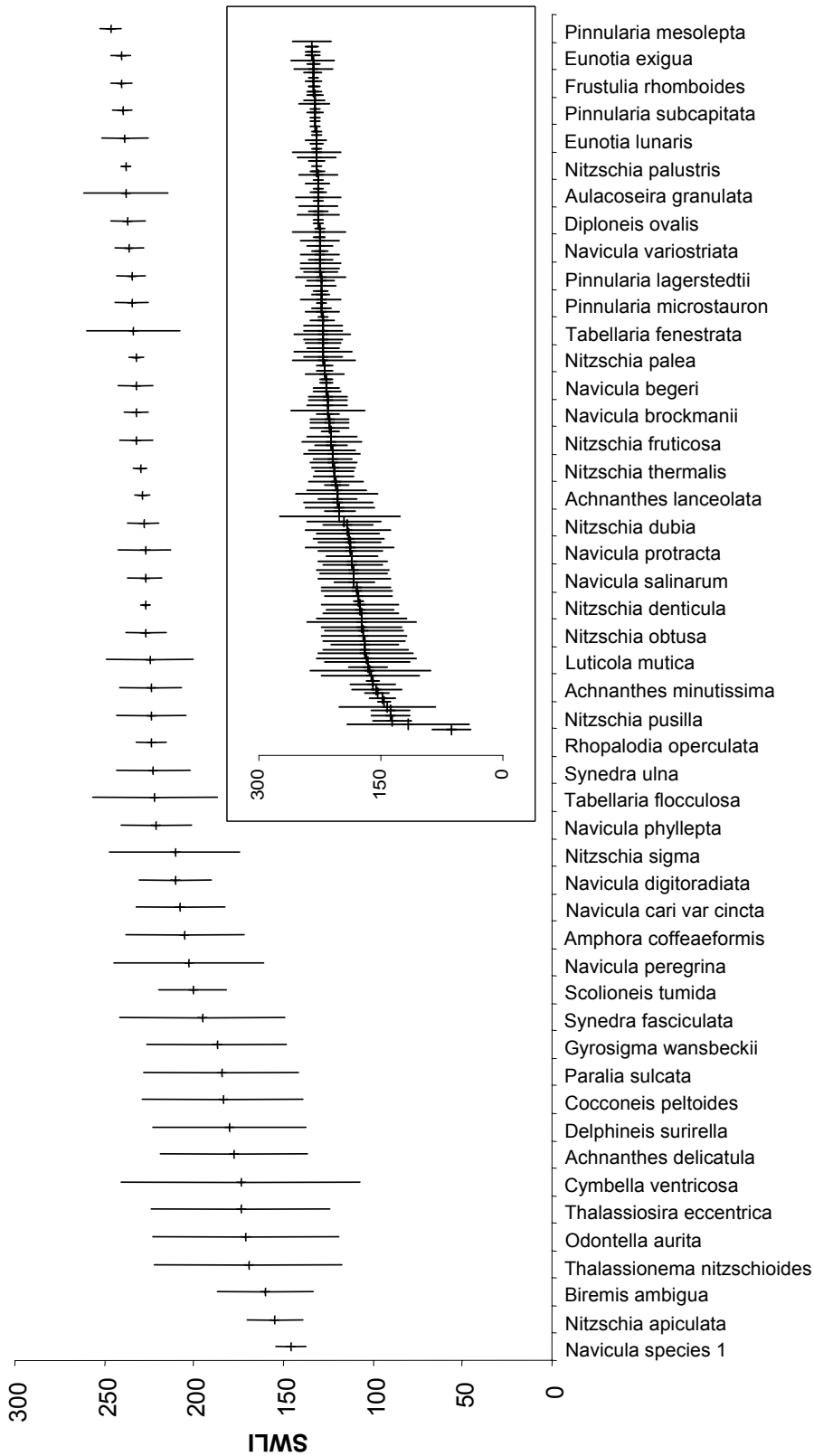

Figure 4.7
Diatom optima and tolerance based upon WA model. Main diagram shows species >10% total diatom valves in at least one sample, inset shows full data set

Model 2: full data set

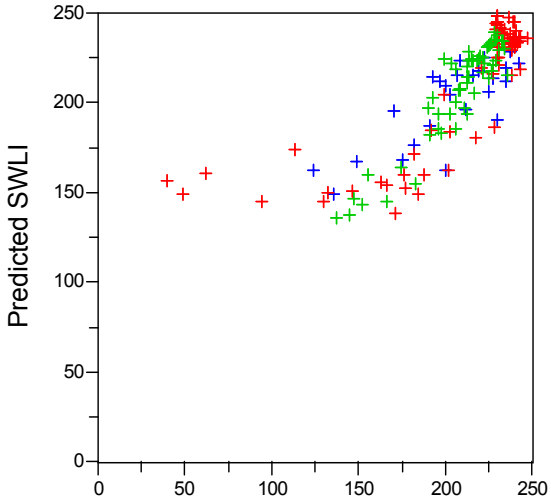

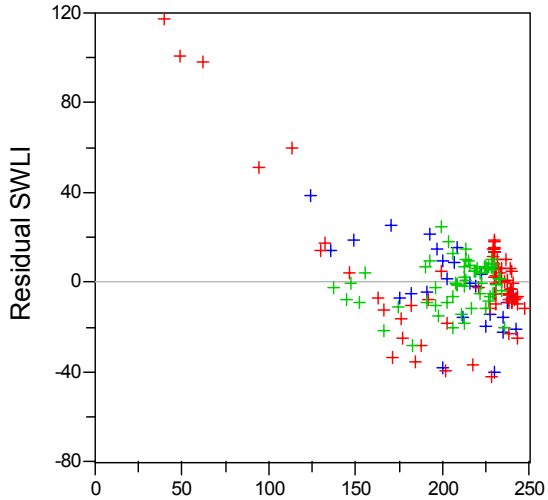

Model 3: excluding lowest samples from Kenai

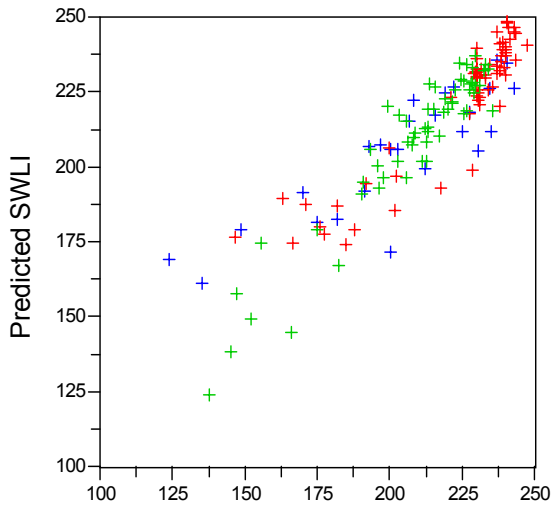

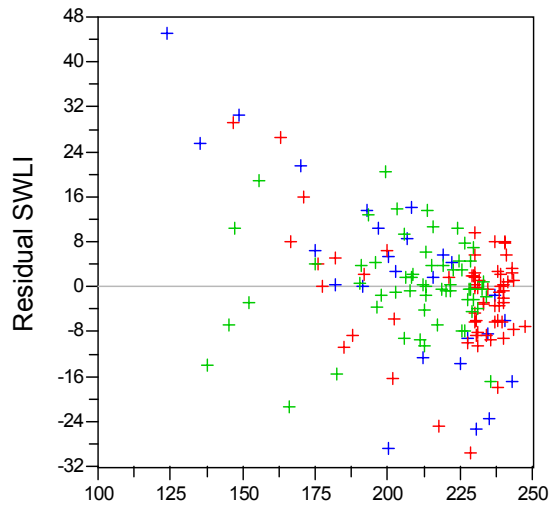

Model 12: excluding outliers >1σ

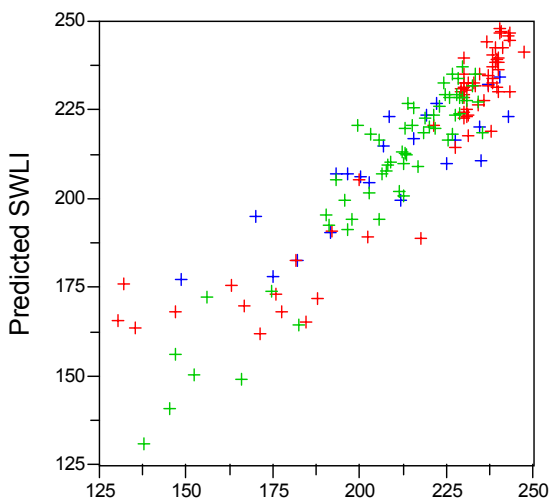

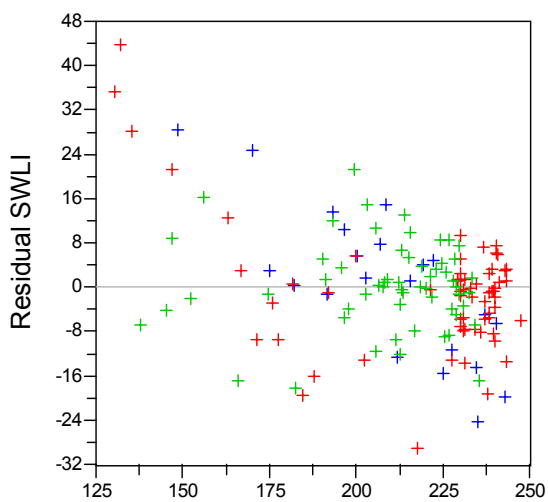

Figure 4.8a

Observed against predicted SWLI and residuals for models described in table 4.4. Colour codes for samples – green: Ocean View; blue: Girdwood; red: Kenai

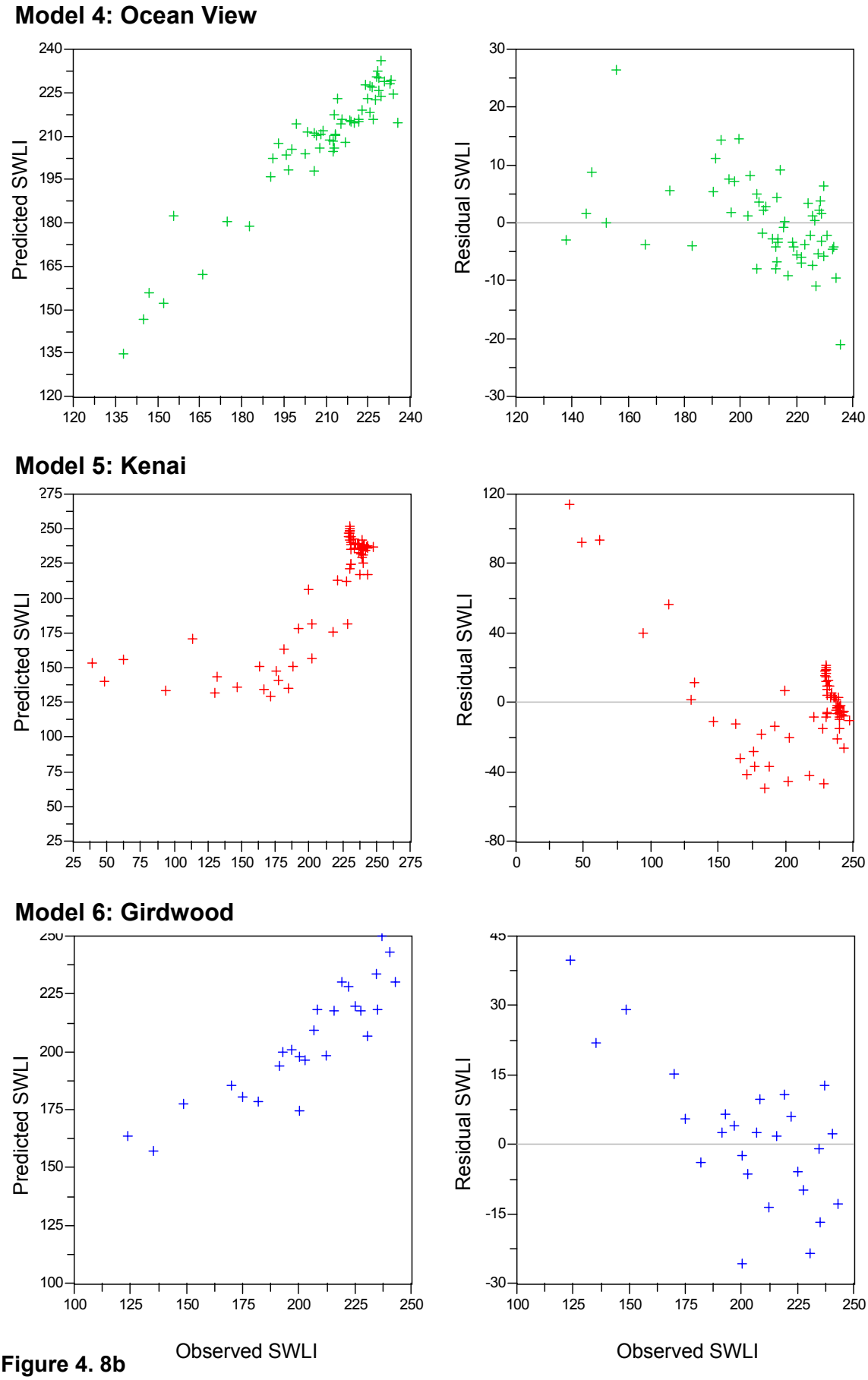

Figure 4. 8b

Observed against predicted SWLI and residuals for models described in table 4.4. Colour codes for samples – green: Ocean View; blue: Girdwood; red: Kenai

Model 8: samples with SWLI >225

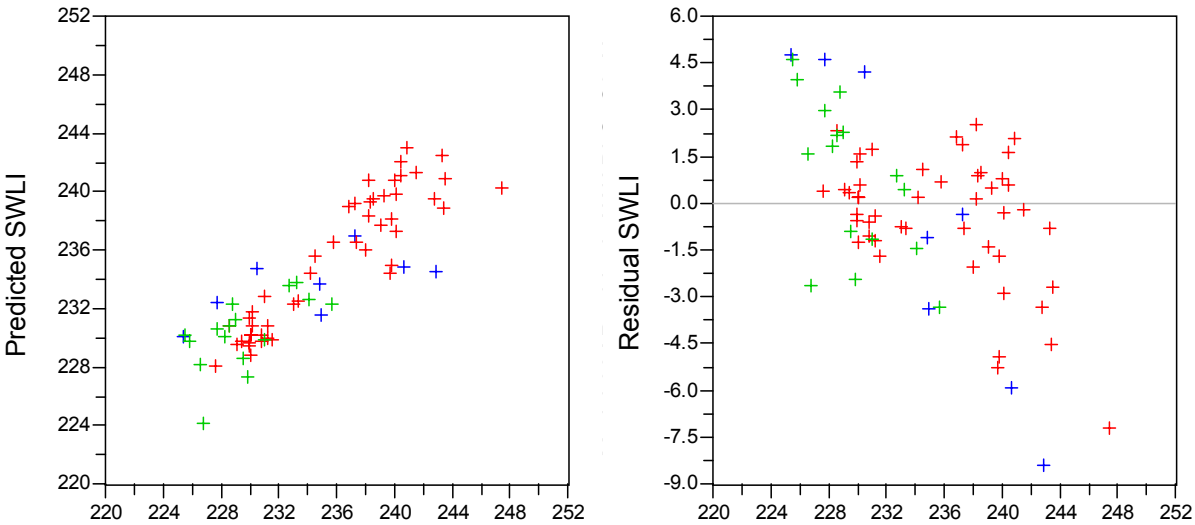

Model 9: samples with SWLI >180

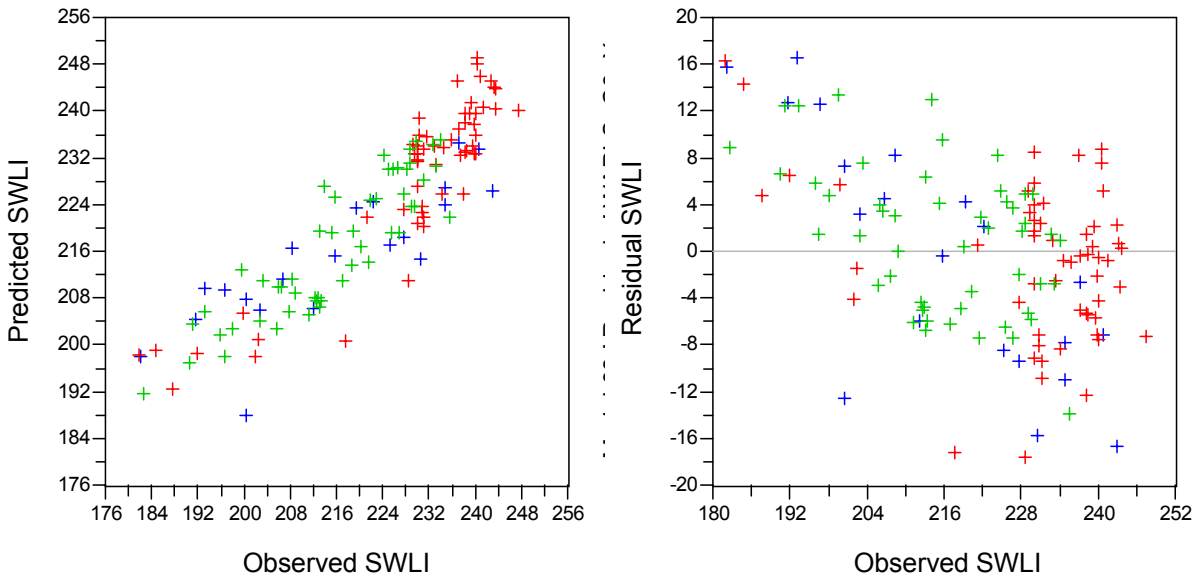

Figure 4.8c
Observed against predicted SWLI and residuals for models described in table 4.4. Colour codes for samples – green: Ocean View; blue: Girdwood; red: Kenai

Ocean View, March 5, 2002: OV02/s101 sediment in ice flow on tidal flat near to transect 1

Ocean View, March 5, 2002: OV02/s102 sediment in ice flow 150 m further seaward

Ocean View, March 5, 2002: 1500 m out on tidal flat, 3 m high ice dam, disseminated sediment throughout the ice

Girdwood, March 15, 2002: Marsh front

Girdwood, March 10, 2002: Frozen mudflat filled with sediment rich ice

Girdwood, March 14, 2002: High tide and stranded ice block at marsh front

Figure 4.9a
Winter conditions at field sites around the Cook Inlet

Girdwood, March 15, 2002: G02/s1, melt out sediment, marsh front

Girdwood, March 15, 2002: G02/s5, melt out sediment, marsh front

Girdwood, March 15, 2002: G02/s6 silt covered Carex from ice melt out

Girdwood, March 16, 2002: Melt out with gravel and cobbles on Carex marsh

Girdwood, March 20, 2002: Carex washed clean of silt following 2 days of rain

Girdwood, Sept 18, 2002: 1.5 m block of ice-rafted sediment deposited on vegetated marsh, still intact

Figure 4.9b
Winter conditions at field sites around the Cook Inlet

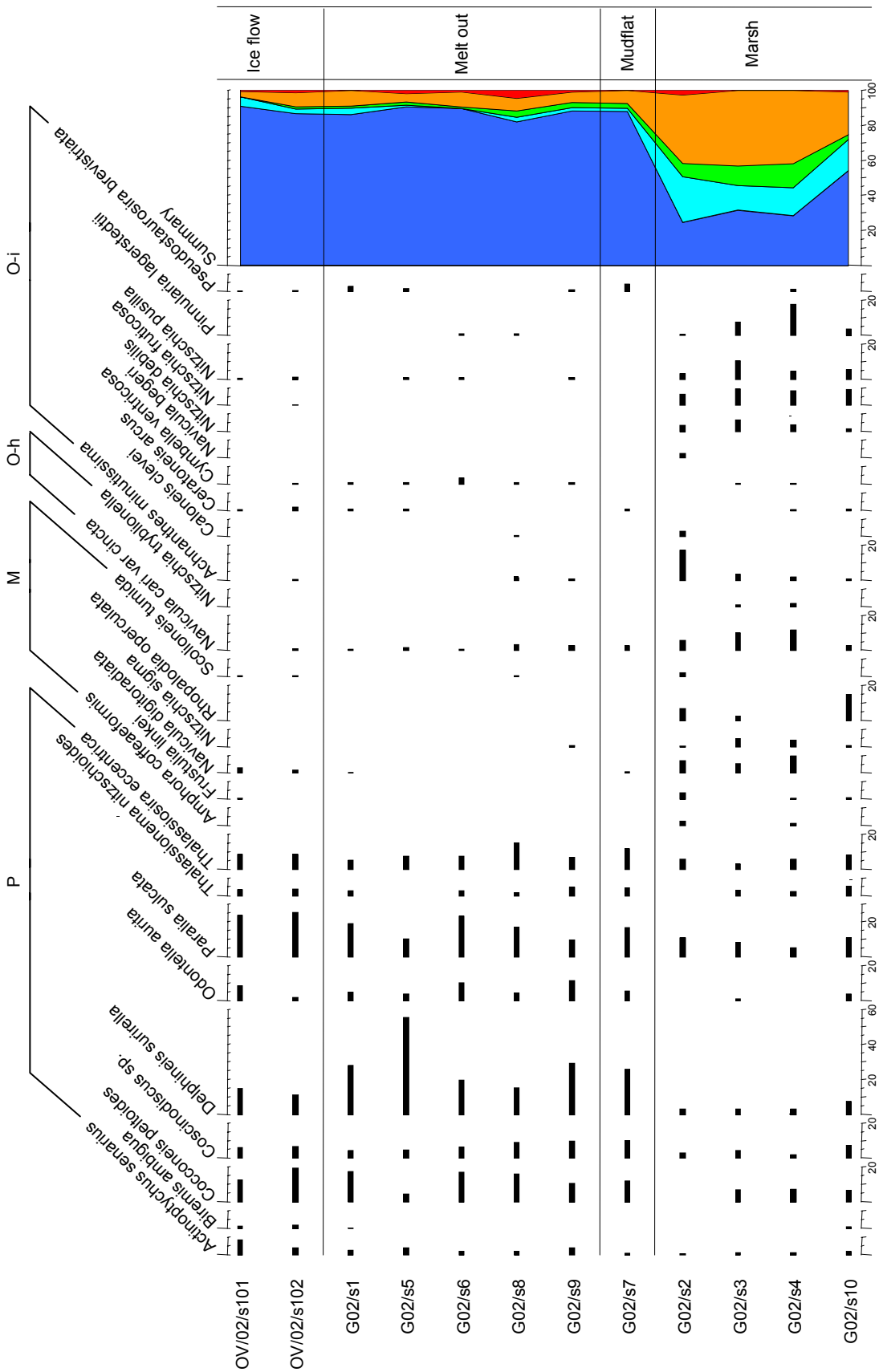

Figure 4.10
Diatom assemblages of winter ice and sediment samples from Girdwood and Ocean View 2002 showing diatoms that account for >2% total counted. P: polyhalobous, M: mesohalobous, O-h: oligohalobous-halophile, O-i: oligohalobous-indifferent, H: halophobous diatom salinity groups ordered left to right in summary graph

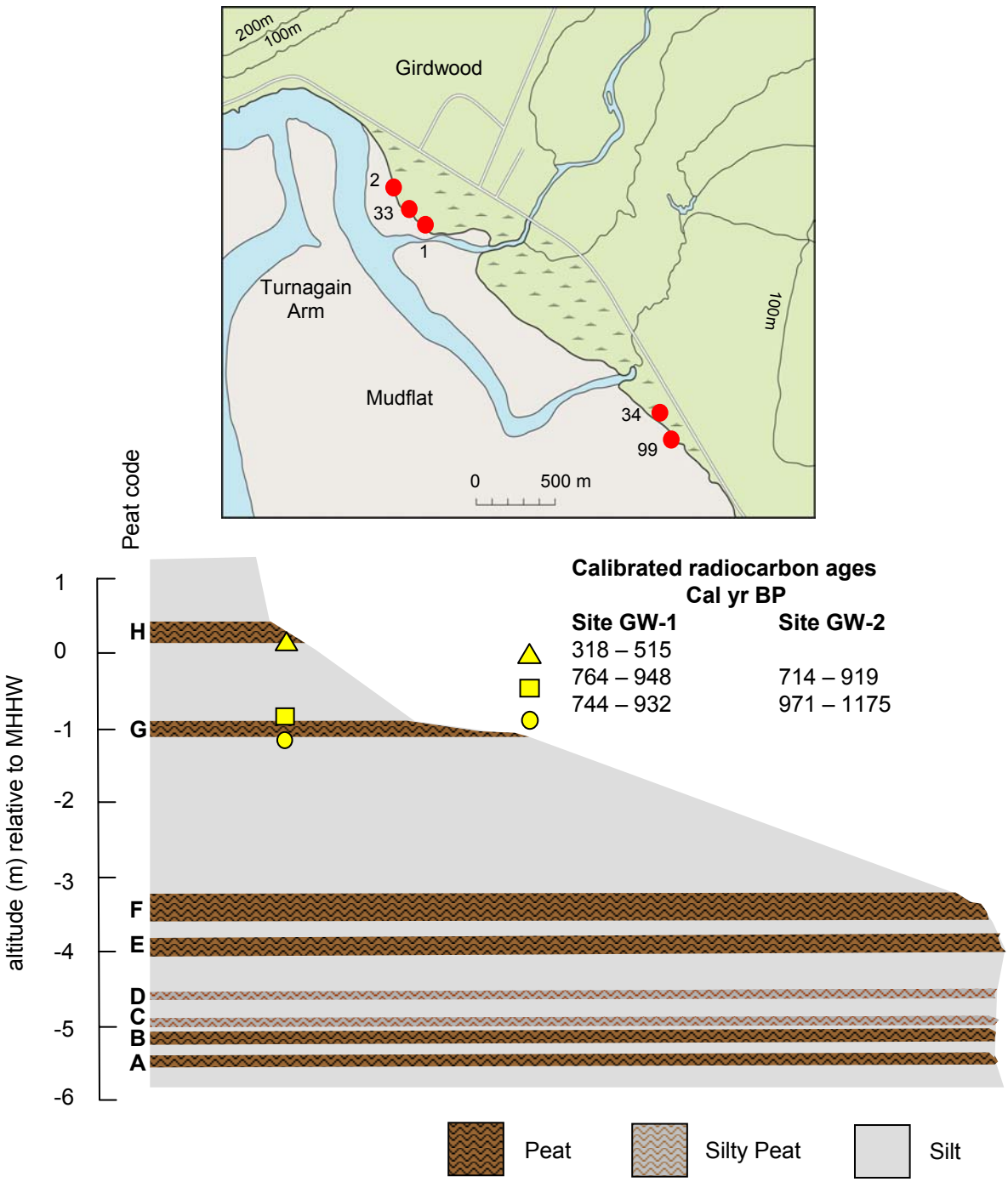

Figure 5.1
Location of sampling sites and schematic section showing the buried peat layers beneath the marsh surface at Girdwood site GW-2, where the outcrop and cores revealed lateral continuity. A smaller outcrop and other cores at GW-1 shows a comparable sequence but with slightly different thicknesses of layers

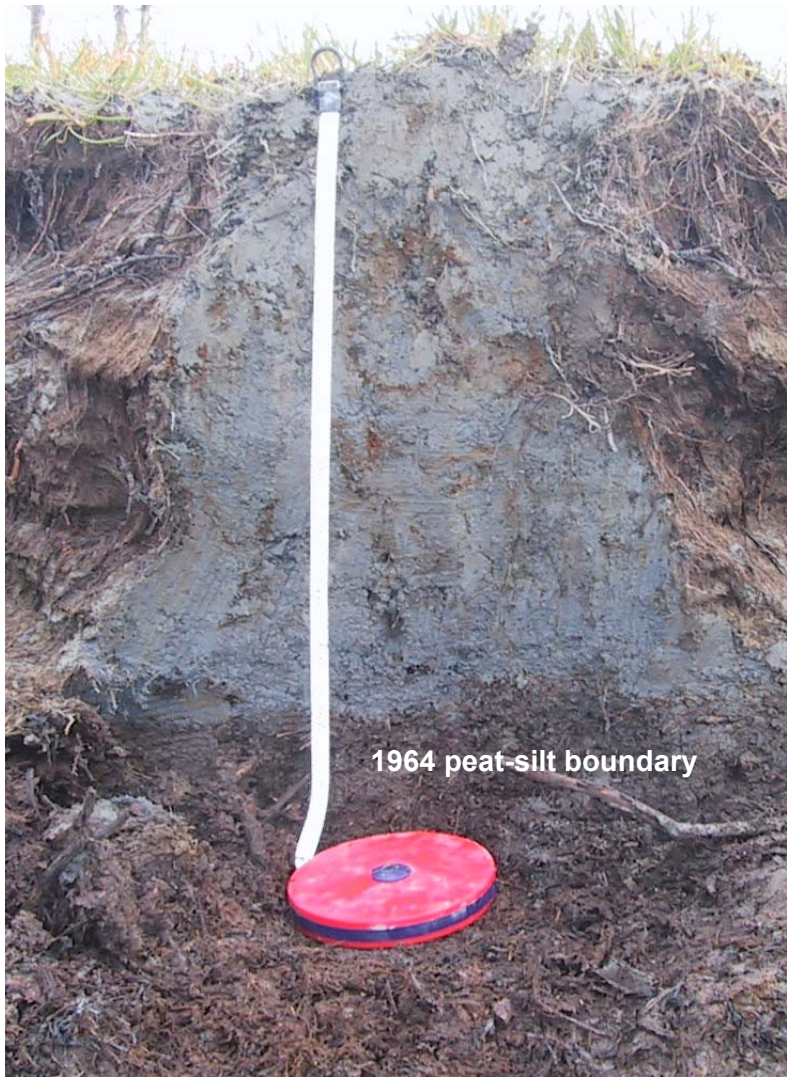

Figure 5.2
Bank section at Girdwood showing peat-silt contact associated with submergence in 1964

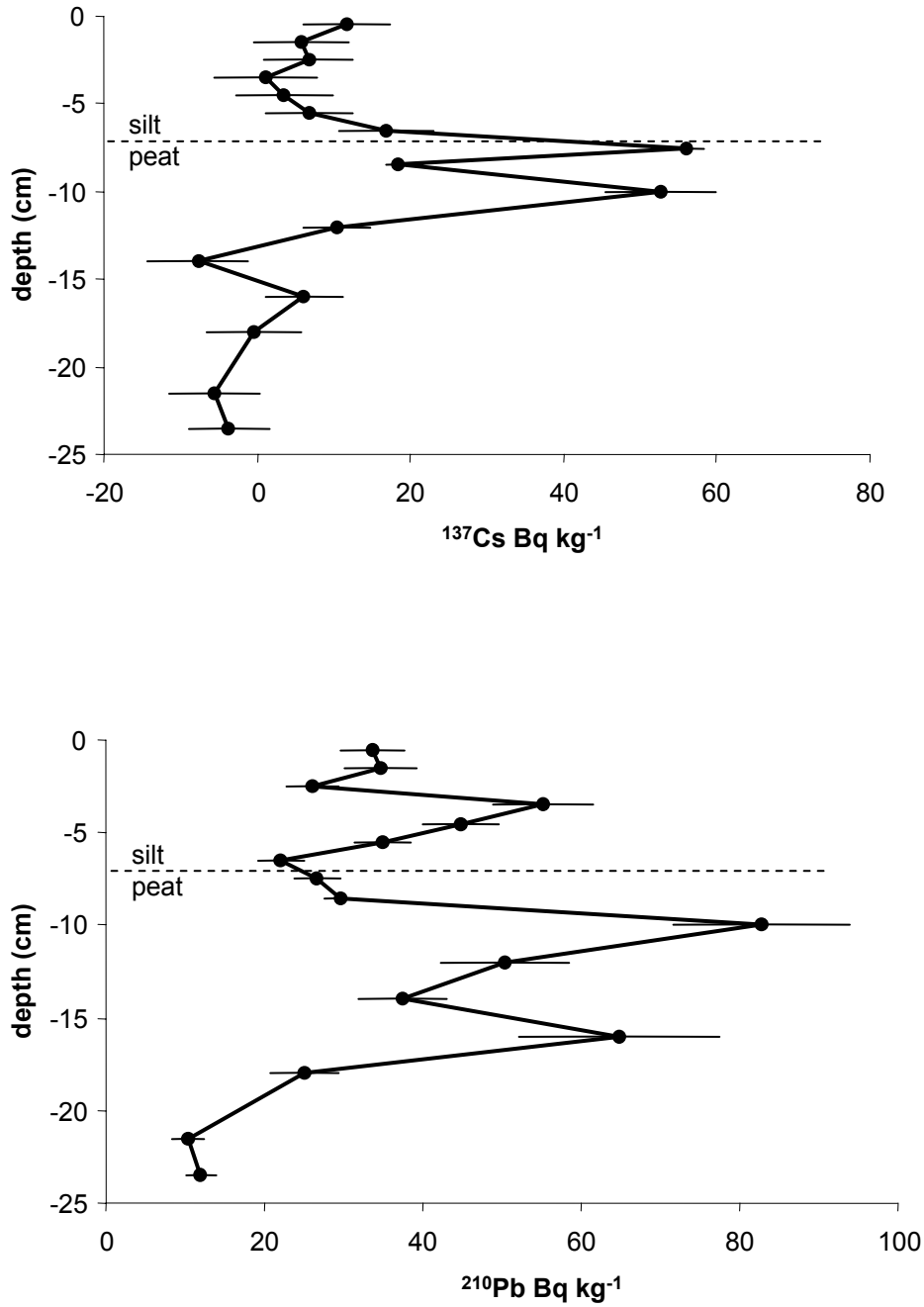

Figure 5.3
Radionuclide data for Girdwood, taken from a monolith sample adjacent to GW-1 (peat silt boundary marked for comparison with GW-1). Minimum detectable limits are 5 Bq kg^{-1} ^{137}Cs and 20 Bq kg^{-1} ^{210}Pb

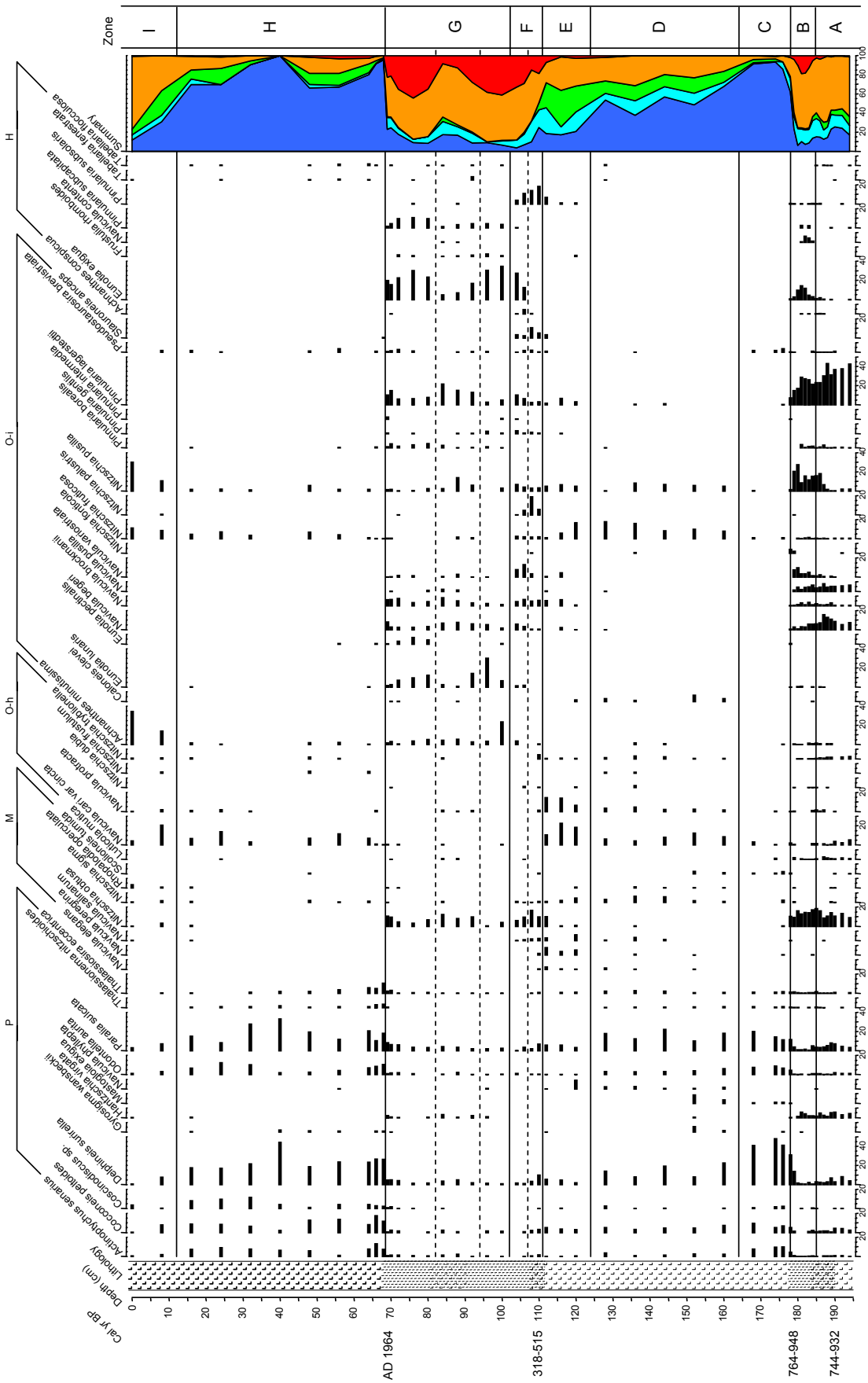

Figure 5.4

Bio-stratigraphy of GW-1 showing diatoms that account for >2% total counted. P: polyhalobous, M: mesohalobous, O-h: oligohalobous-halophile, O-i: oligohalobous-indifferent, H: halophobous diatom salinity groups ordered left to right in summary graph

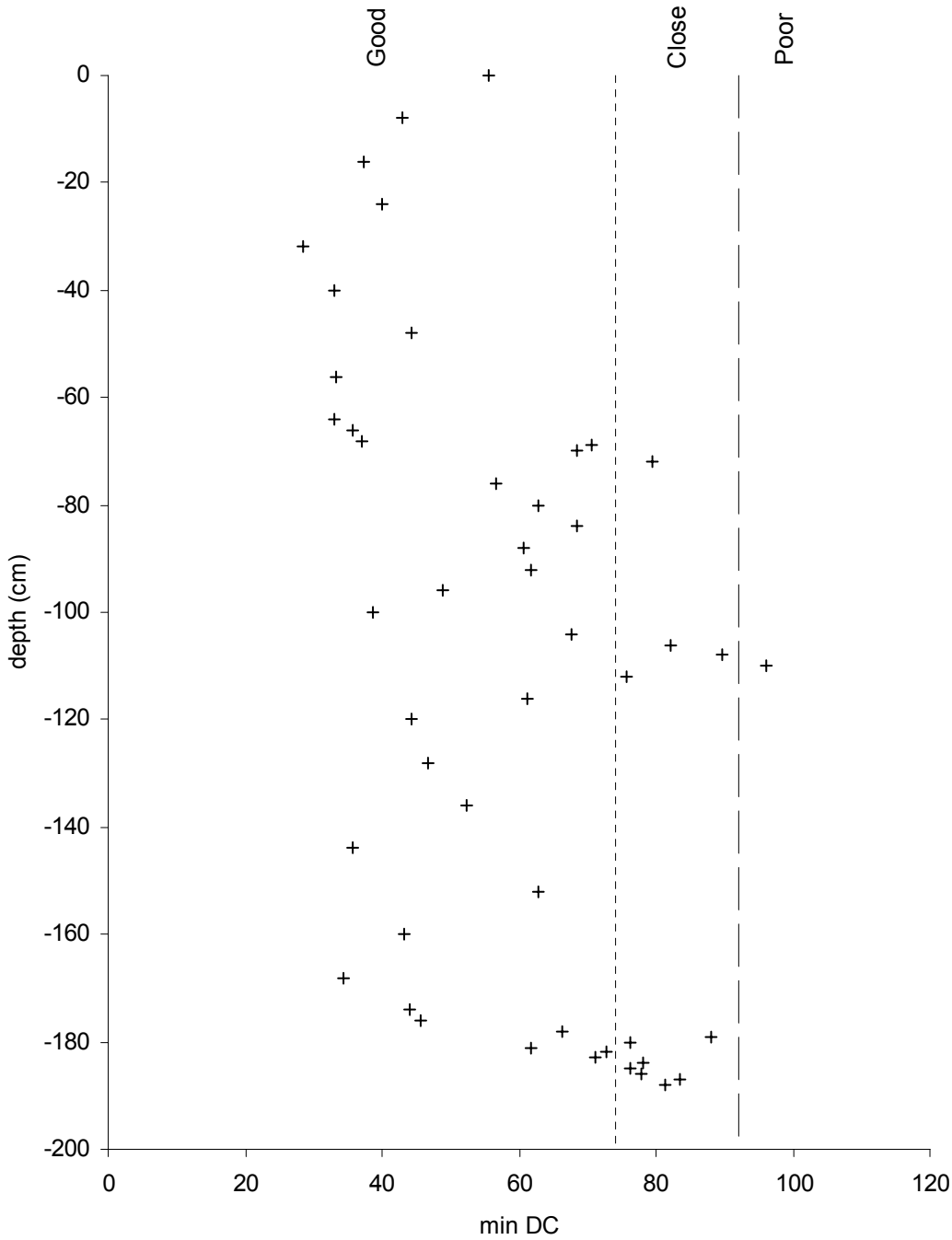

Figure 5.5
Minimum dissimilarity coefficient values from MAT for GW-1

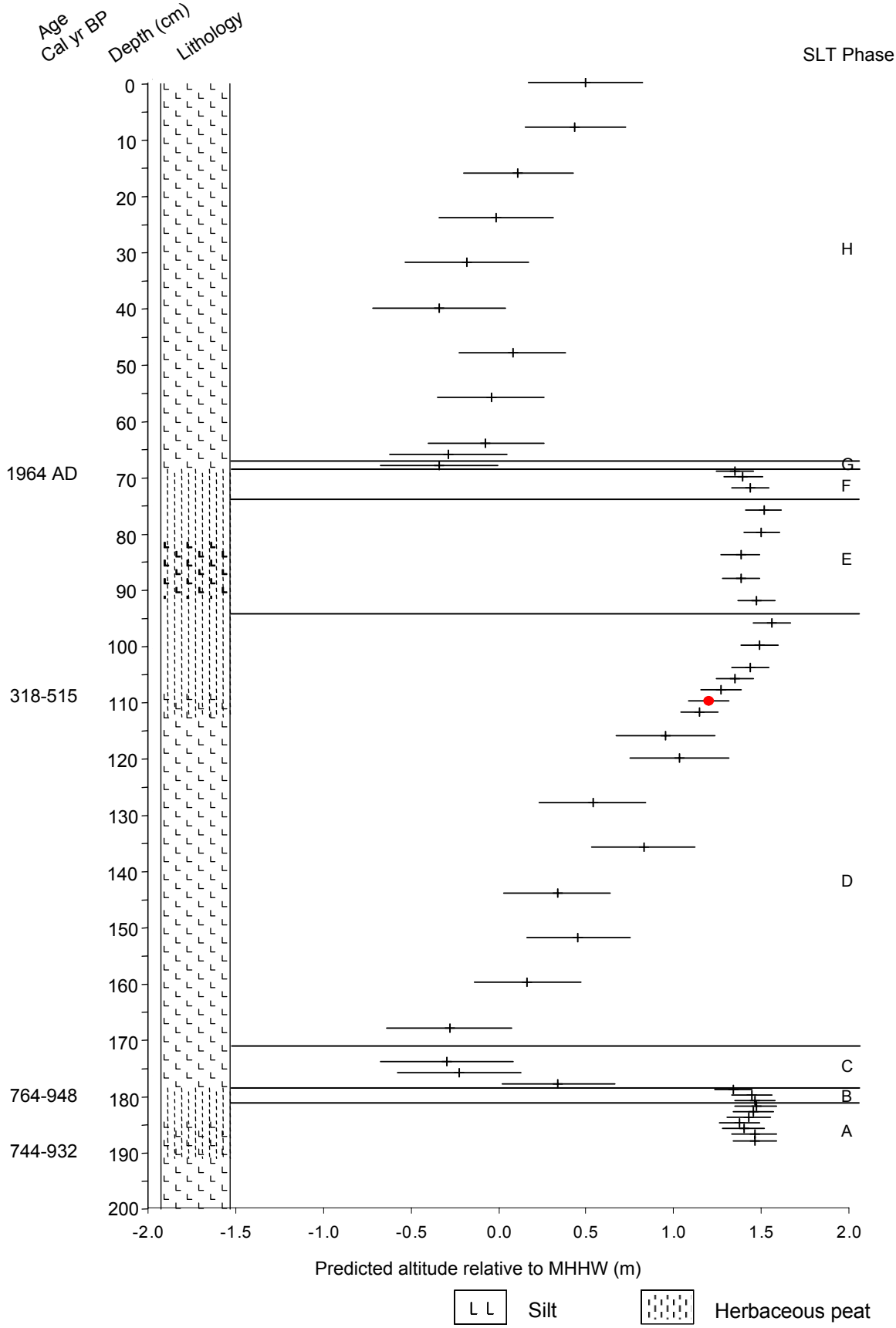

Figure 5.6
Reconstruction of relative sea-level change for Girdwood GW-1 using the best combination of models (table 5.2). The sample in red has a 'poor' modern analogue

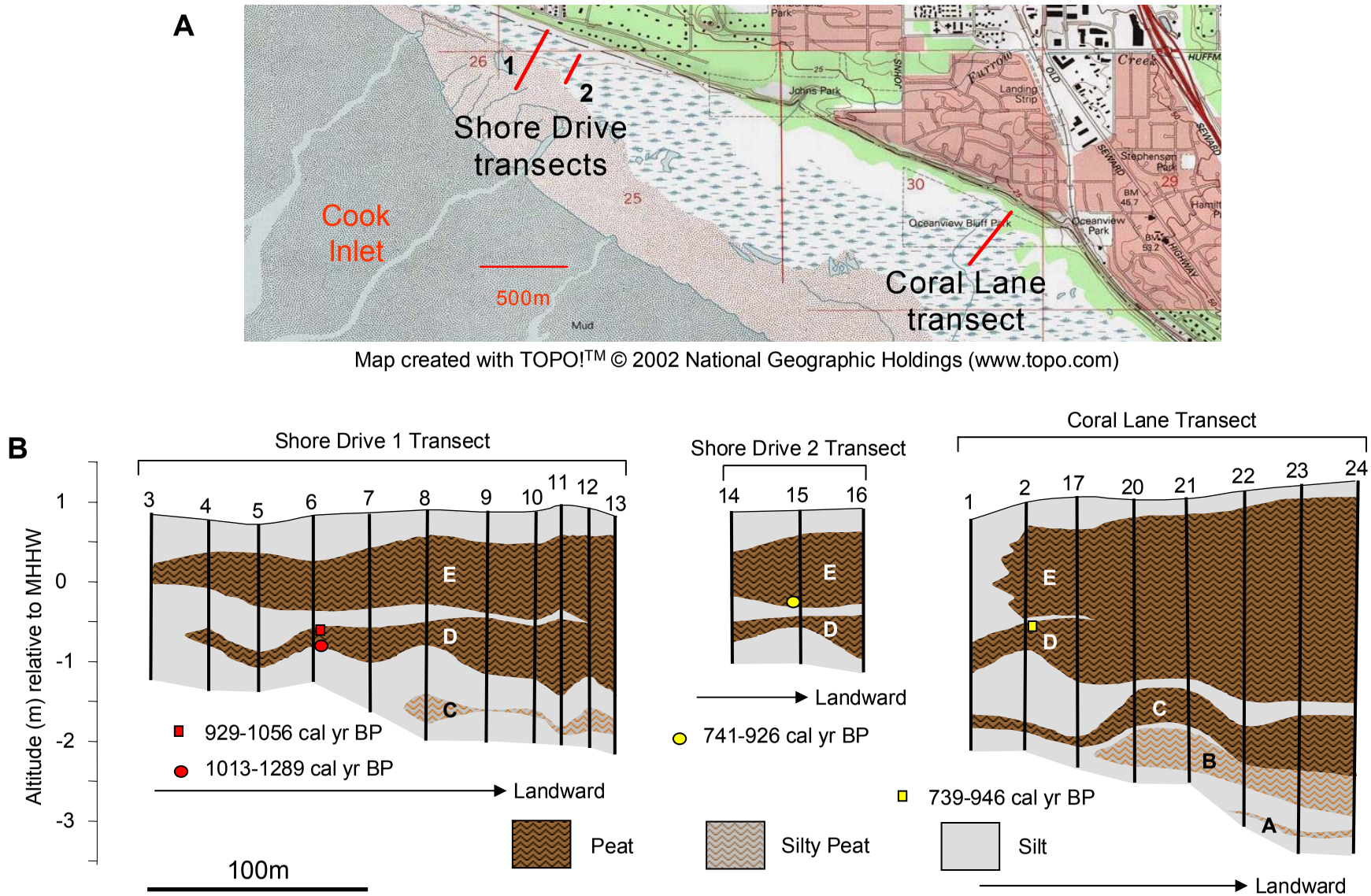

Figure 6.1
Ocean View, Anchorage with (A) showing the location of the coring transects and (B) the litho-stratigraphy of the marsh

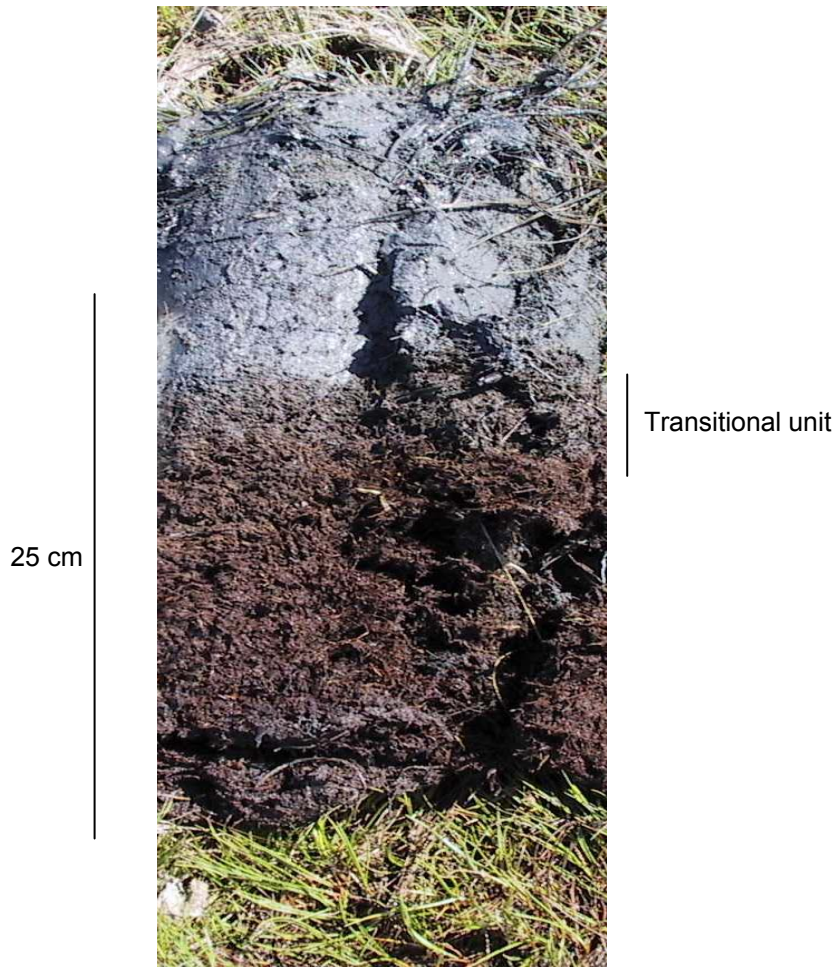

Figure 6.2
Ocean View, peat E OV-15. Peat-silt boundary represents co-seismic submergence during the 1964 earthquake

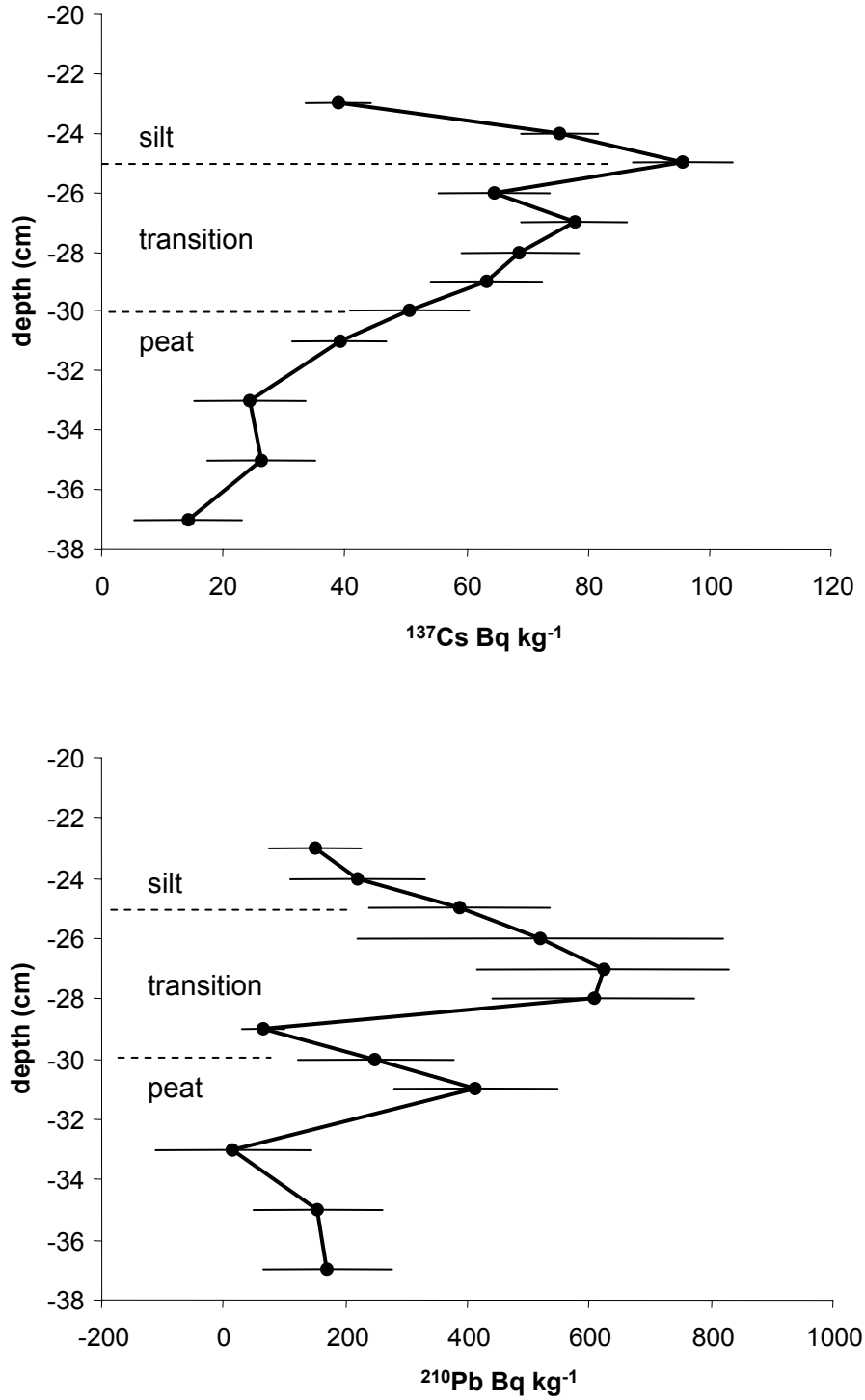

Figure 6.3
Radionuclide data for Ocean View, OV-15. Minimum detectable limits are 5 Bq kg^{-1} ^{137}Cs and 20 Bq kg^{-1} ^{210}Pb

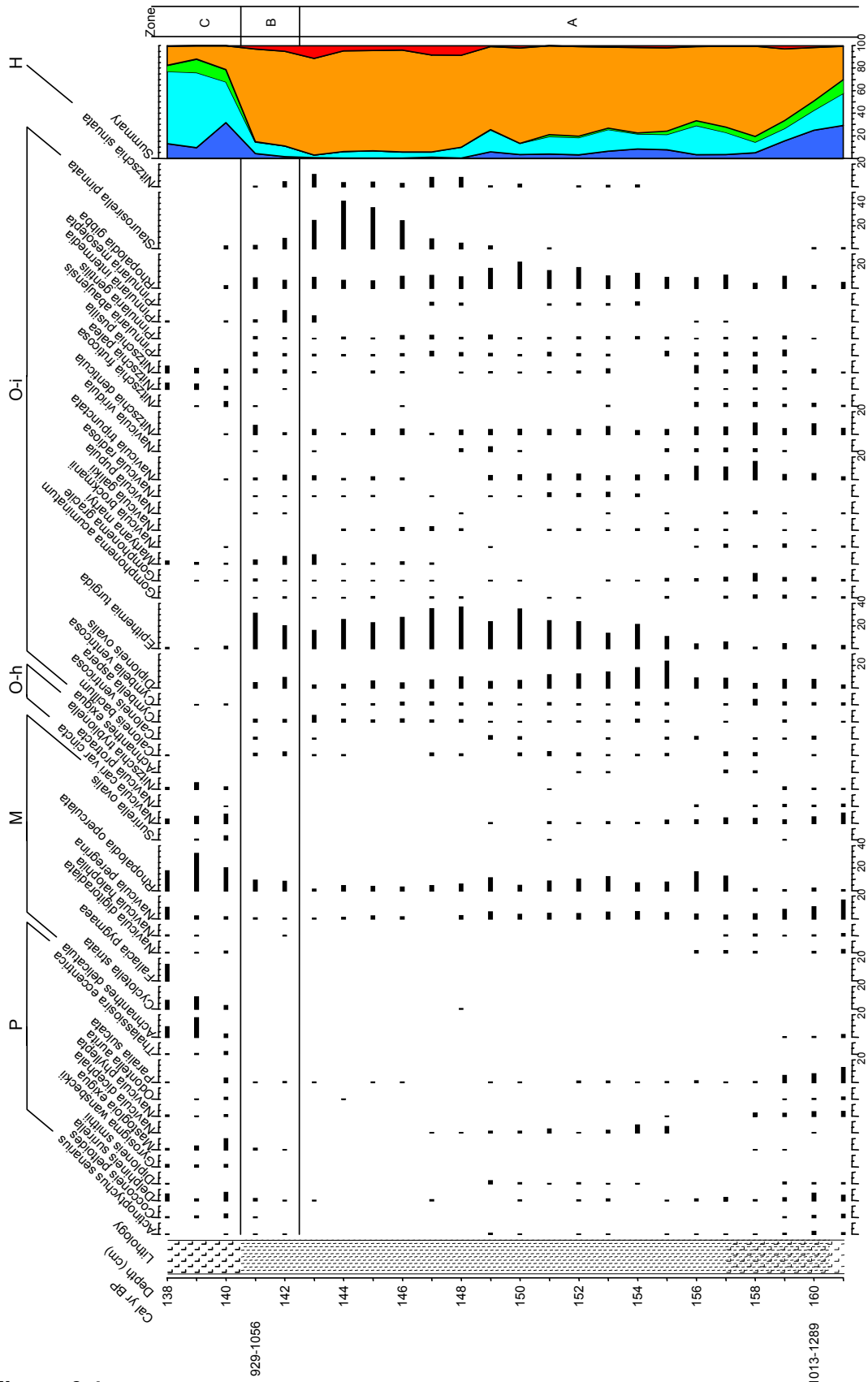

Figure 6.4
Diatom assemblages (>2%) through Peat D, OV-6. P: polyhalobous, M: mesohalobous, O-h: oligohalobous-halophile, O-i: oligohalobous-indifferent, H: halophobous diatom salinity groups ordered left to right in summary graph

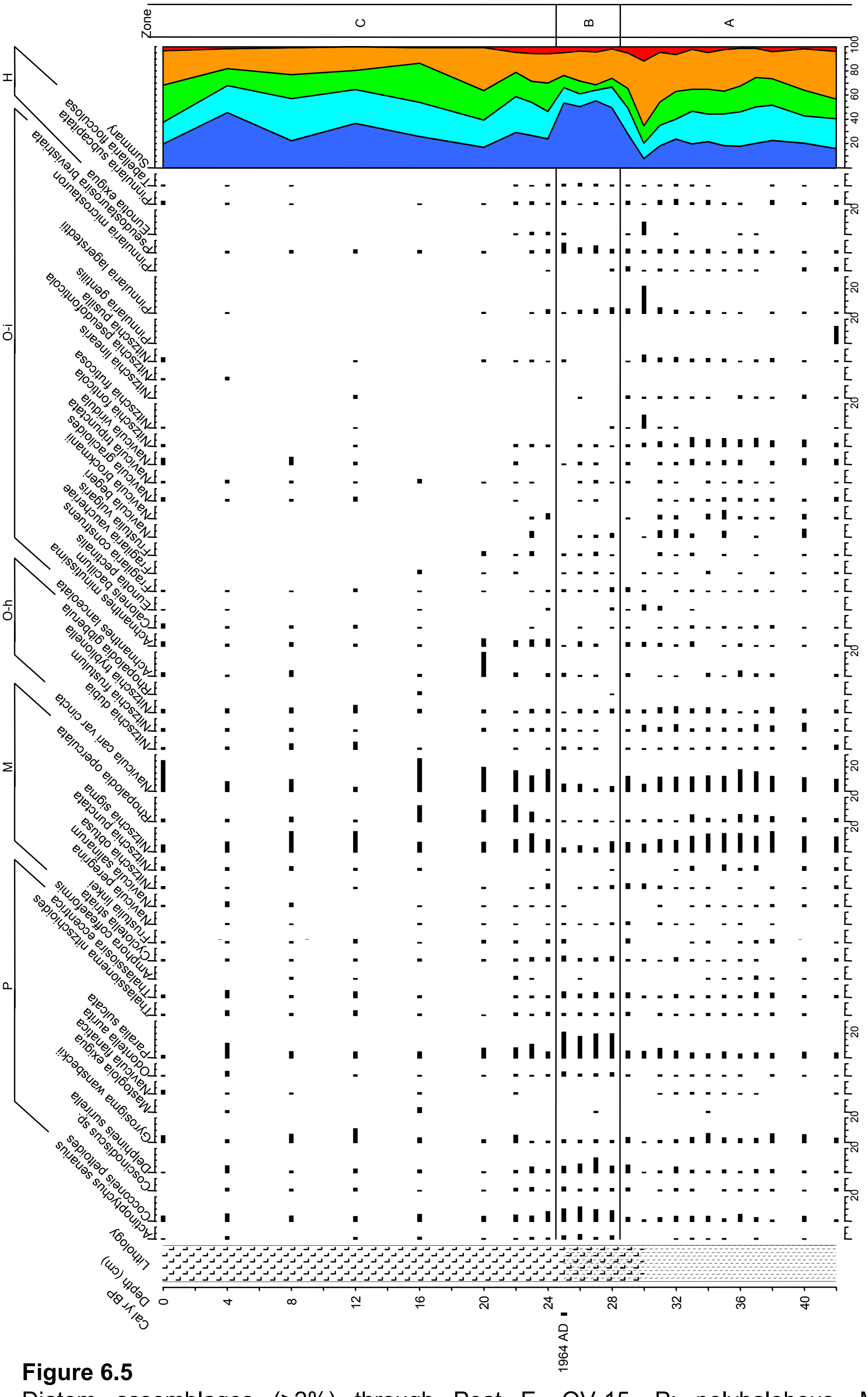

Figure 6.5

Diatom assemblages (>2%) through Peat E, OV-15. P: polyhalobous, M: mesohalobous, O-h: oligohalobous-halophile, O-i: oligohalobous-indifferent, H: halophobous diatom salinity groups ordered left to right in summary graph

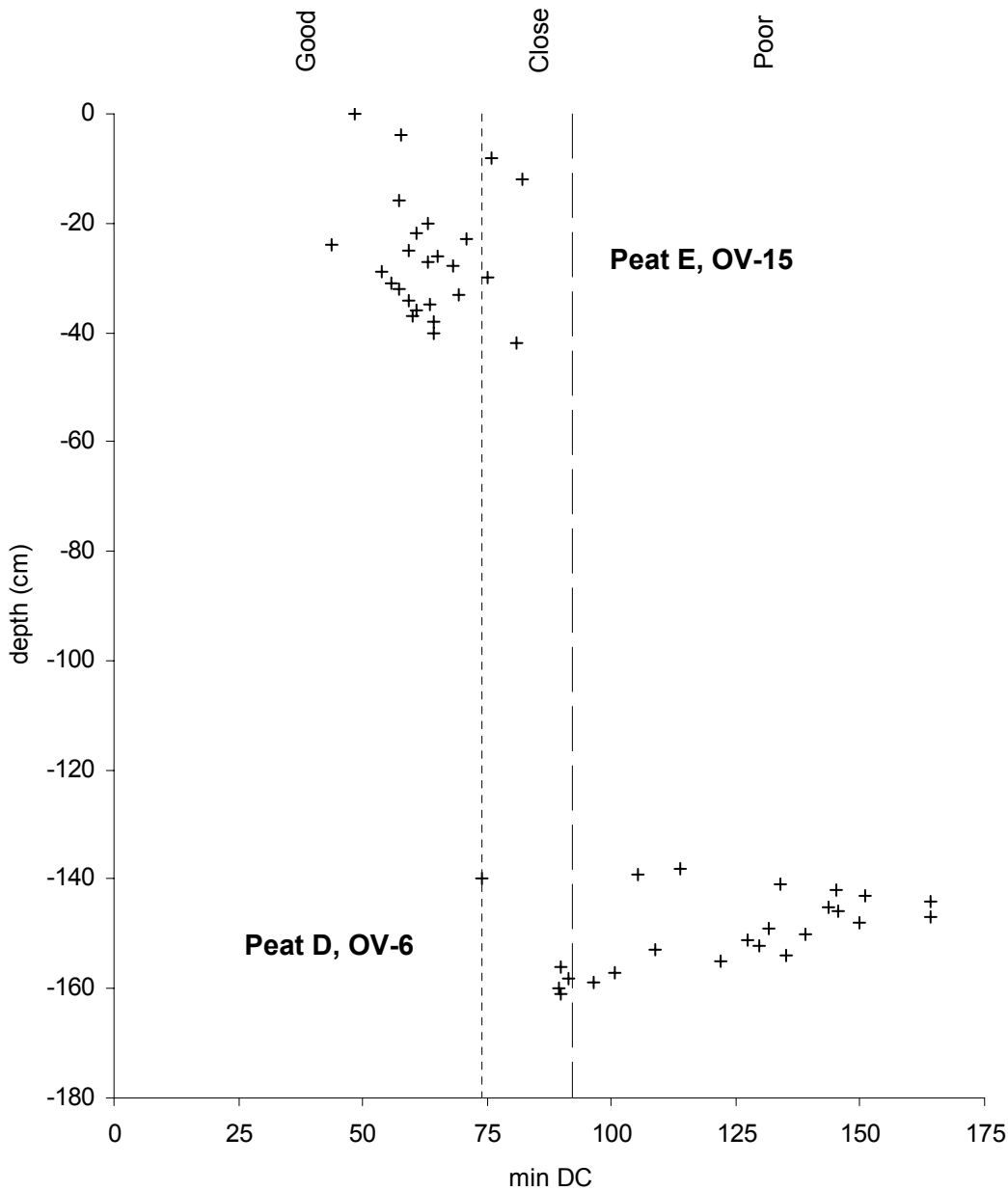

Figure 6.6
Minimum dissimilarity coefficient values from MAT for Ocean View

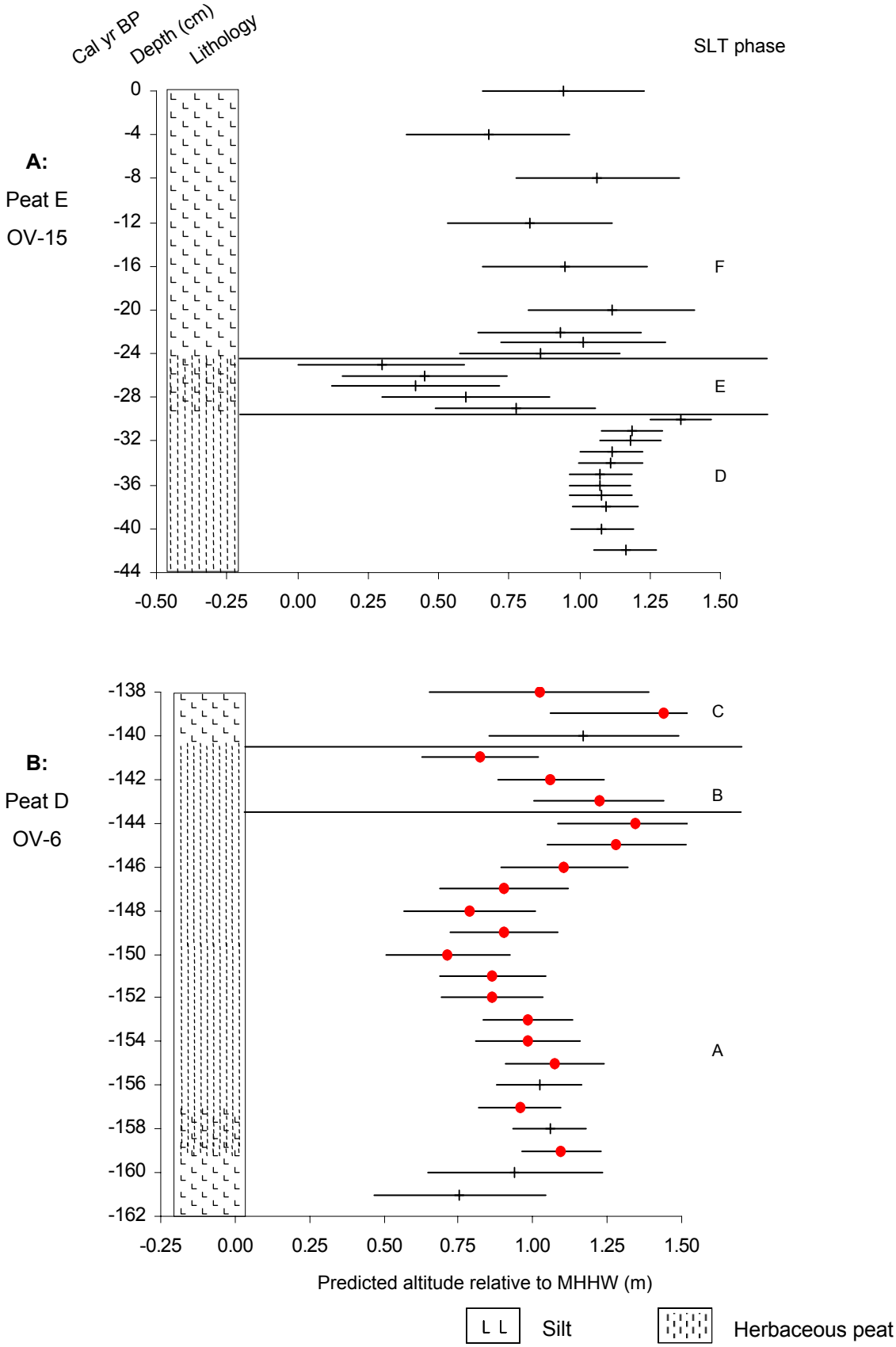

Figure 6.7
Reconstruction of relative sea-level change for Ocean View using the best combination of models (table 6.4). Samples in red have 'poor' modern analogues

A

B

C

Figure 6.8
Ocean View April 1st 2003
A: *Carex* marsh, with extensive frozen standing water and ice blocks
B: Melt out of sediment from ice block onto frozen waterlogged *Carex* marsh
C: Silt on surface of frozen waterlogged *Carex* marsh

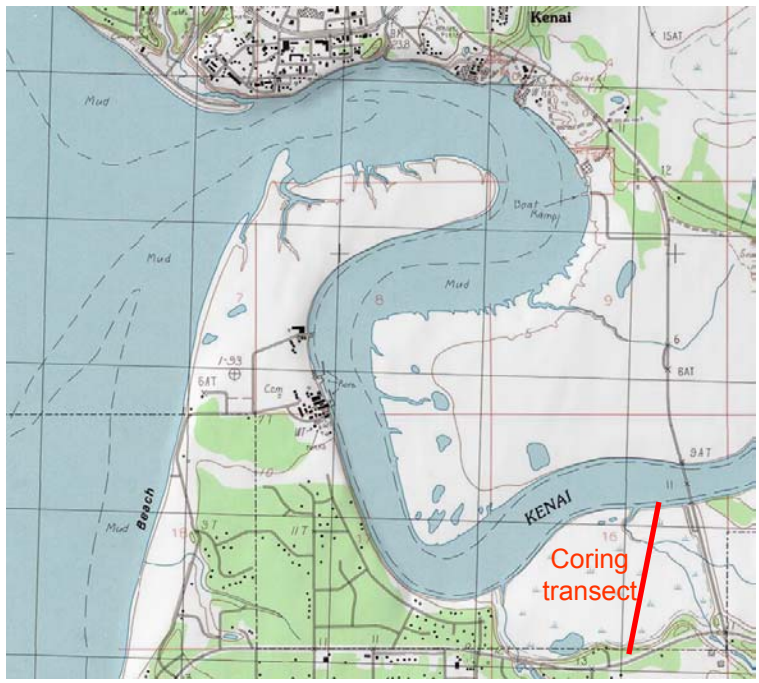

Map created with TOPO!™ © 2002 National Geographic Holdings (www.topo.com)

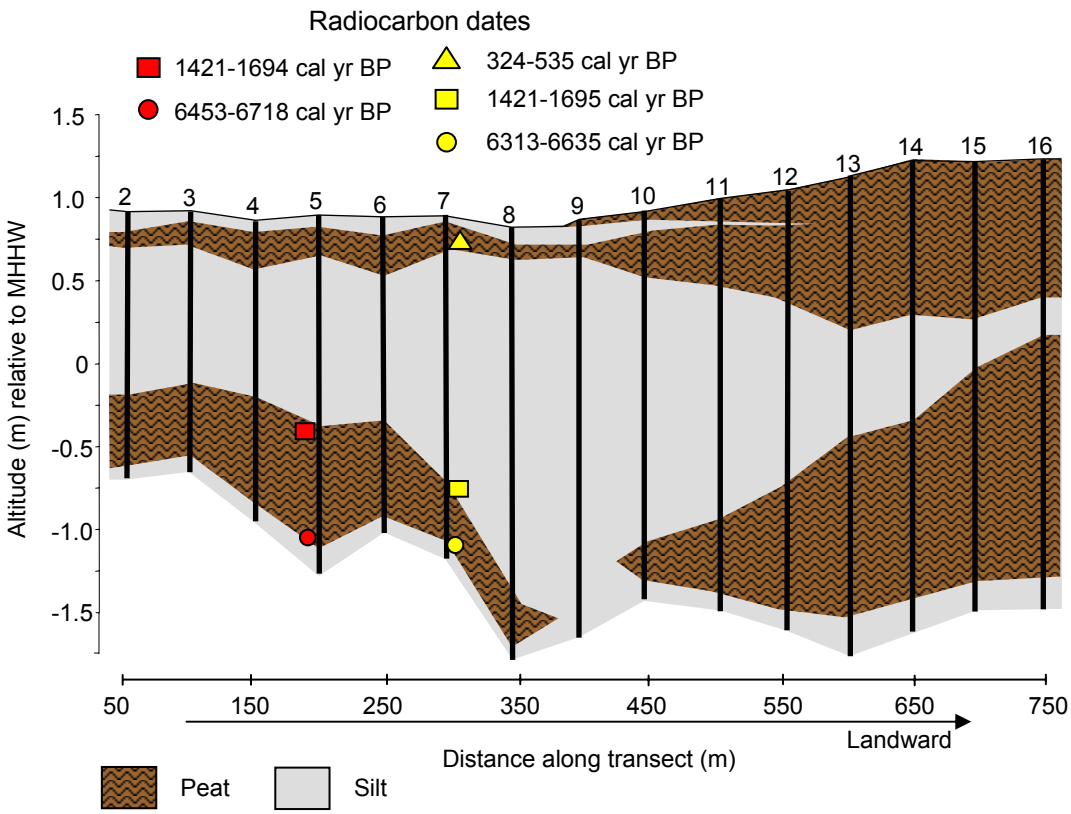

Figure 7.1
Location of coring transect and litho-stratigraphy at Kenai

Figure 7.2
Lithology of KE-7 showing the upper peat-silt boundary that represents co-seismic submergence during the 1964 earthquake. This sample was taken within 1 m of the monolith used for laboratory analyses, hence slightly different depth values

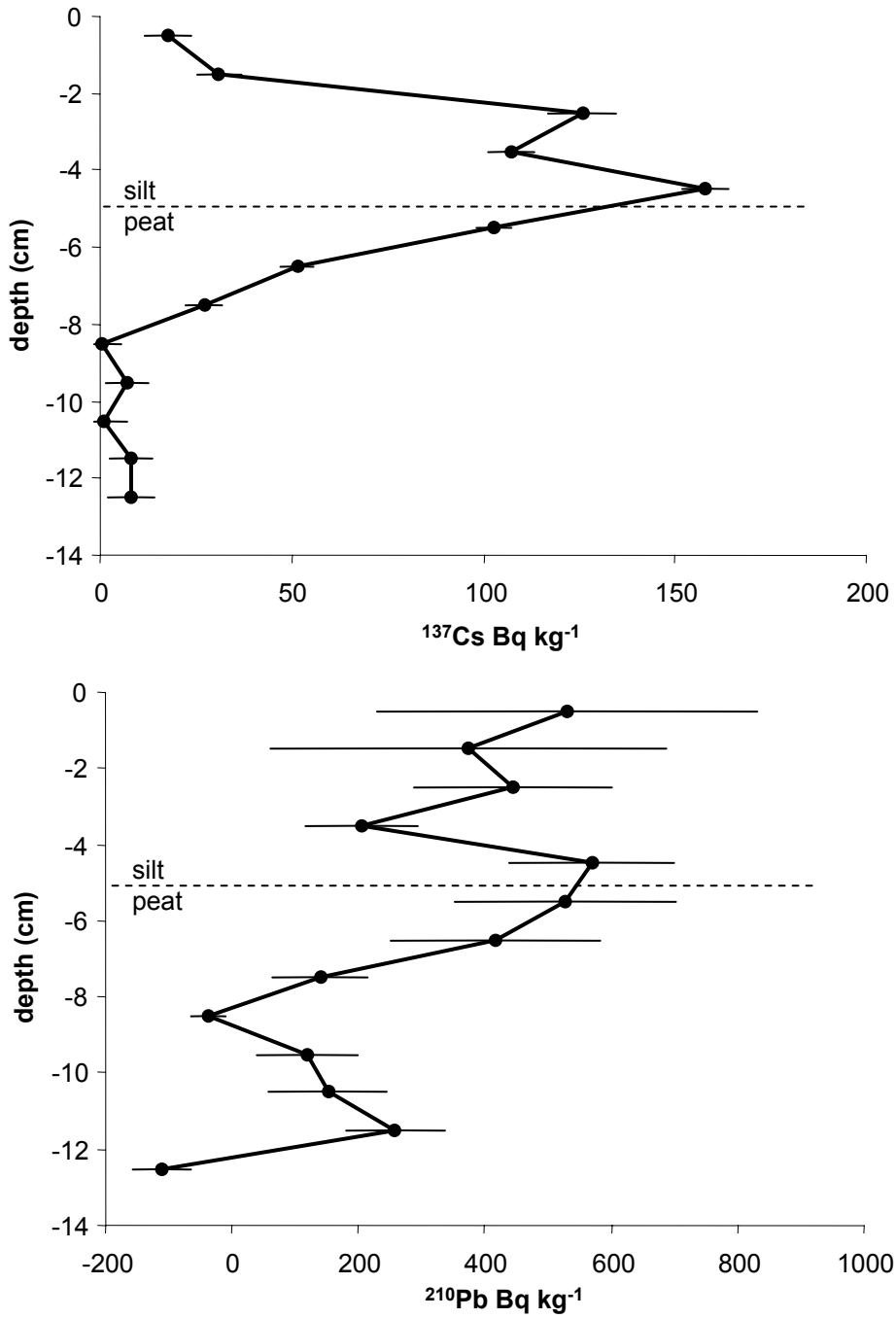

Figure 7.3
Radionuclide data for KE– 7. Minimum detectable limits are 5 Bq kg^{-1} ^{137}Cs and 20 Bq kg^{-1} ^{210}Pb

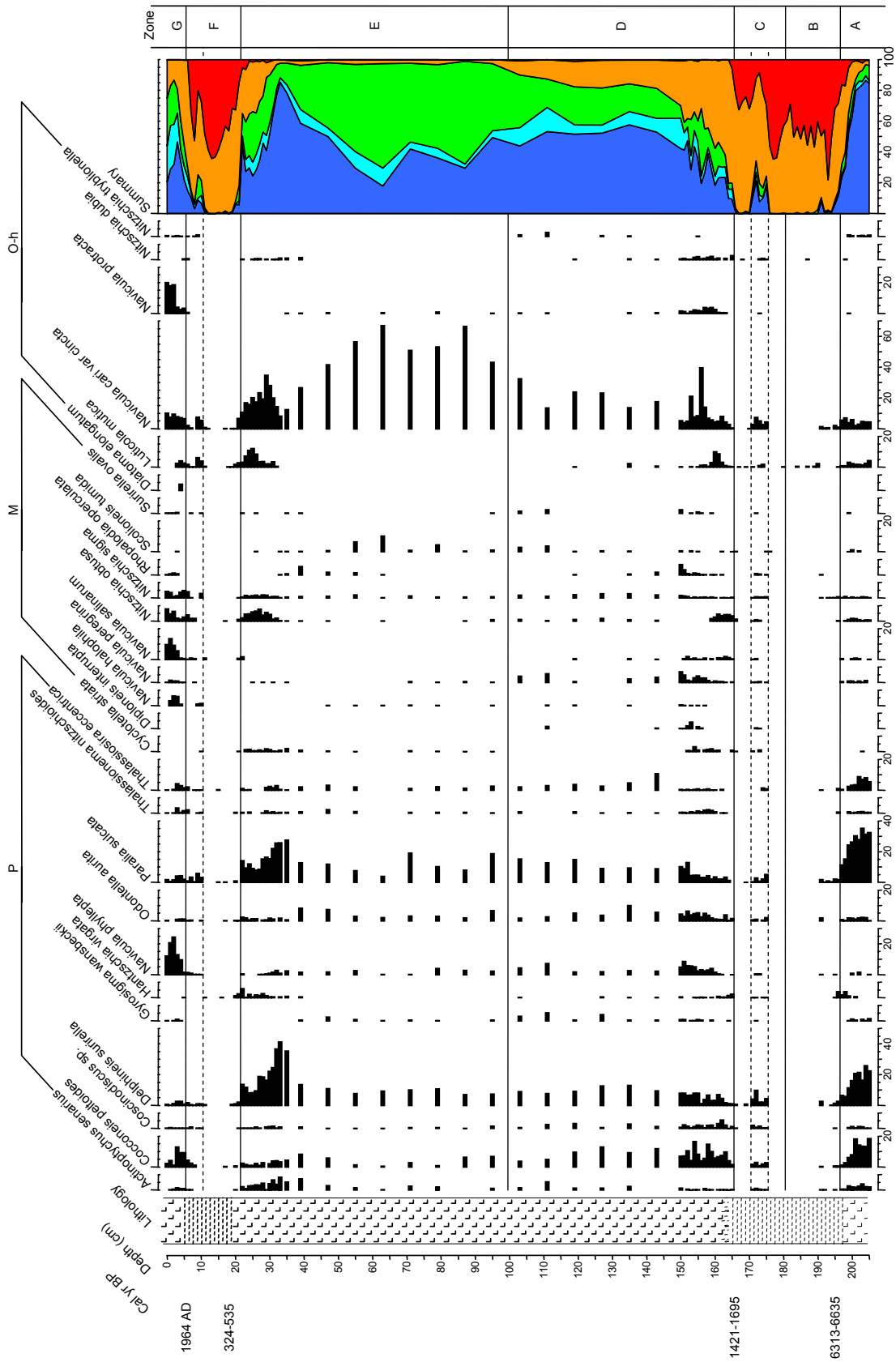

Figure 7.4a

KE-7 diatom data (>2% total diatom valves) showing polyhalobous (P), mesohalobous (M) and oligohalobous-halophile (O-h) salinity classes, ordered left to right in summary graph with oligohalobous-indifferent (O-i) and halophobous (H)

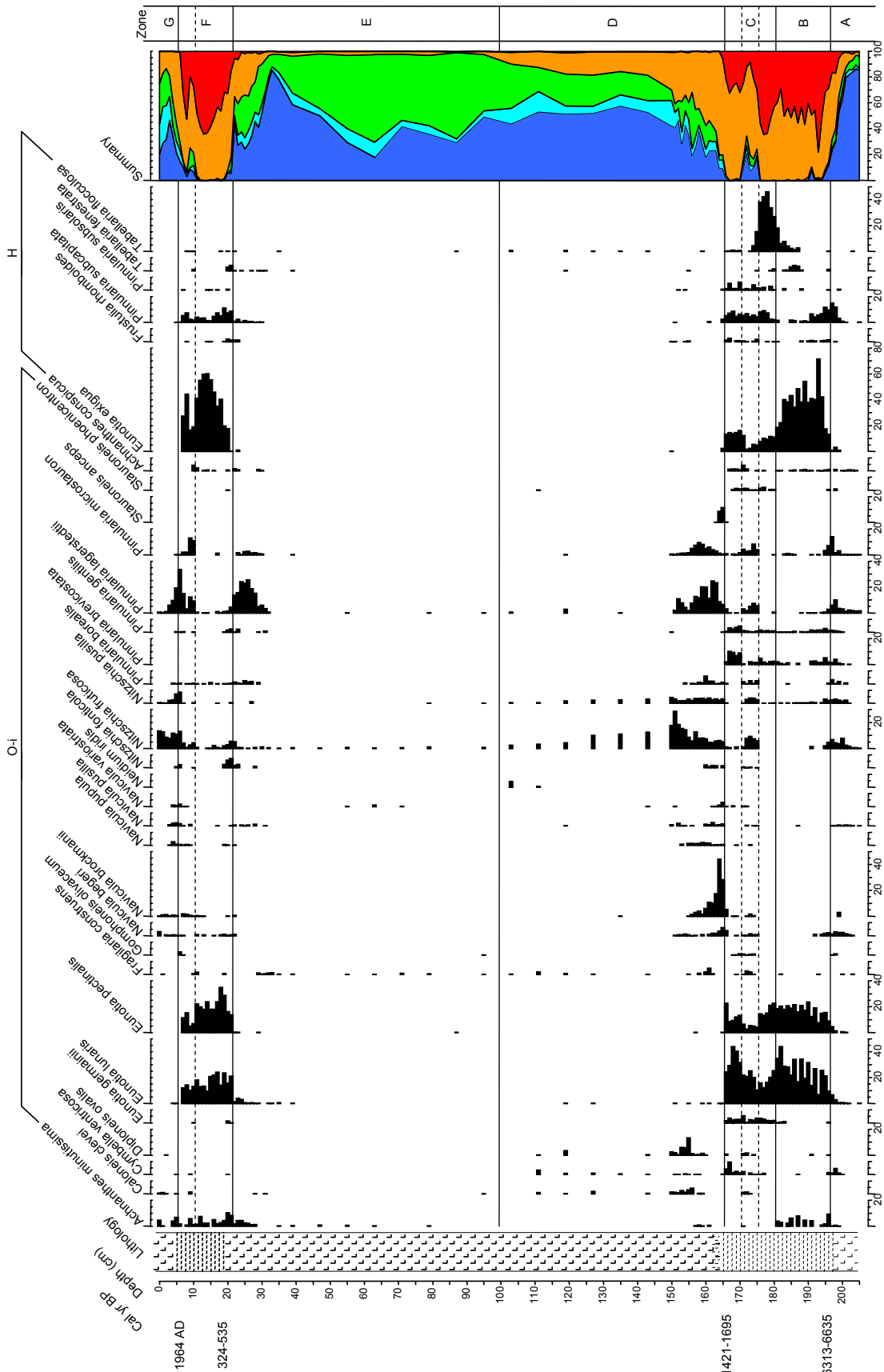

Figure 7.4b

KE-7 diatom data (>2% total diatom valves) showing oligohalobous-indifferent (O-i) and halophobous (H) salinity classes, ordered left to right in summary graph after polyhalobous (P), mesohalobous (M) and oligohalobous-halophile (O-h)

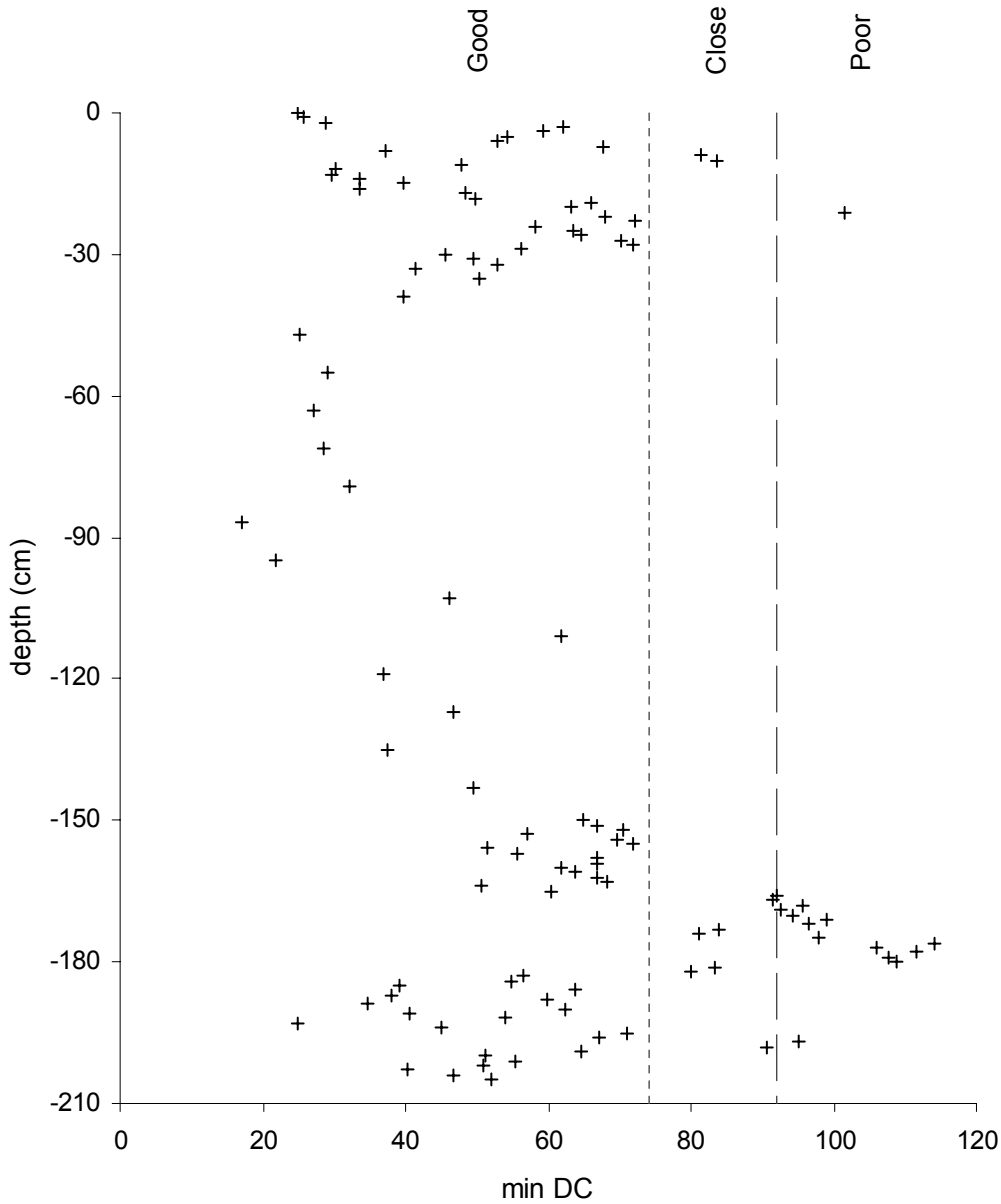

Figure 7.5
Minimum dissimilarity coefficient values from MAT for KE-7

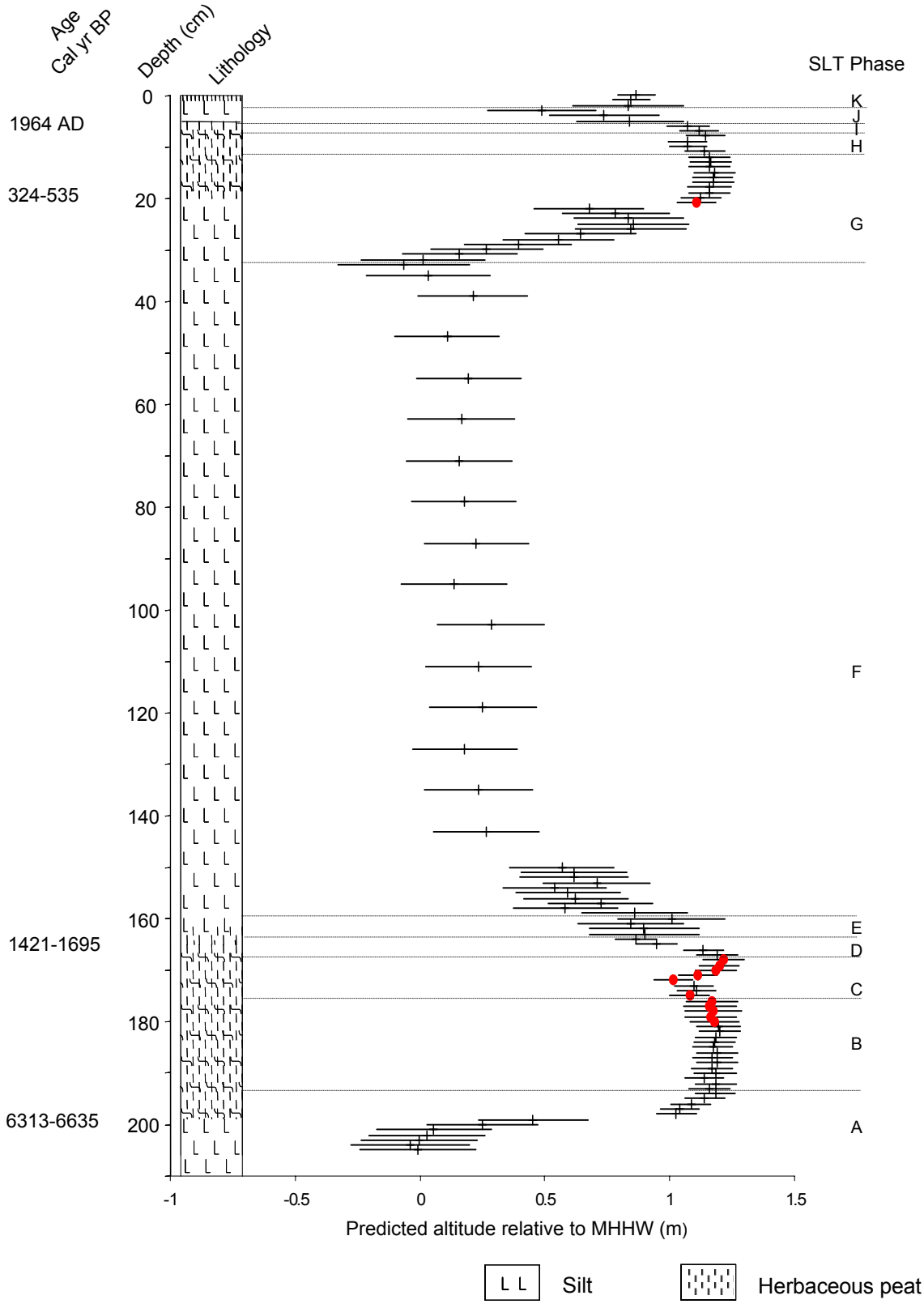

Figure 7.6
Reconstruction of relative sea-level change for KE-7 using the best combination of models (table 7.3). Samples in red have 'poor' modern analogues

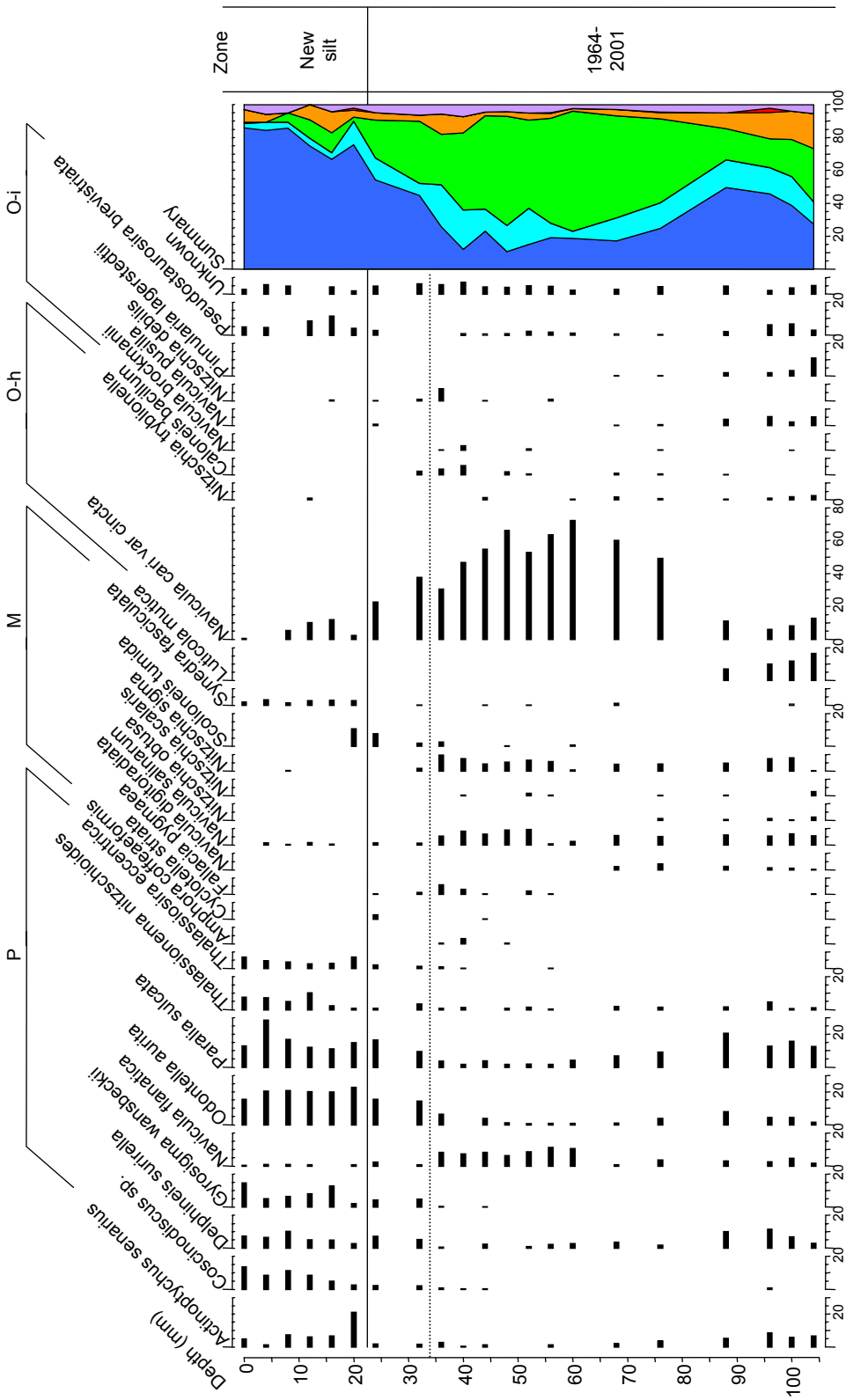

Figure 8.1
Diatom assemblages (>2%) through transplant test block. P: polyhalobous, M: mesohalobous, O-h: oligohalobous-halophile, O-i: oligohalobous-indifferent, H: halophobous, U: unknown diatom salinity groups ordered left to right in summary graph

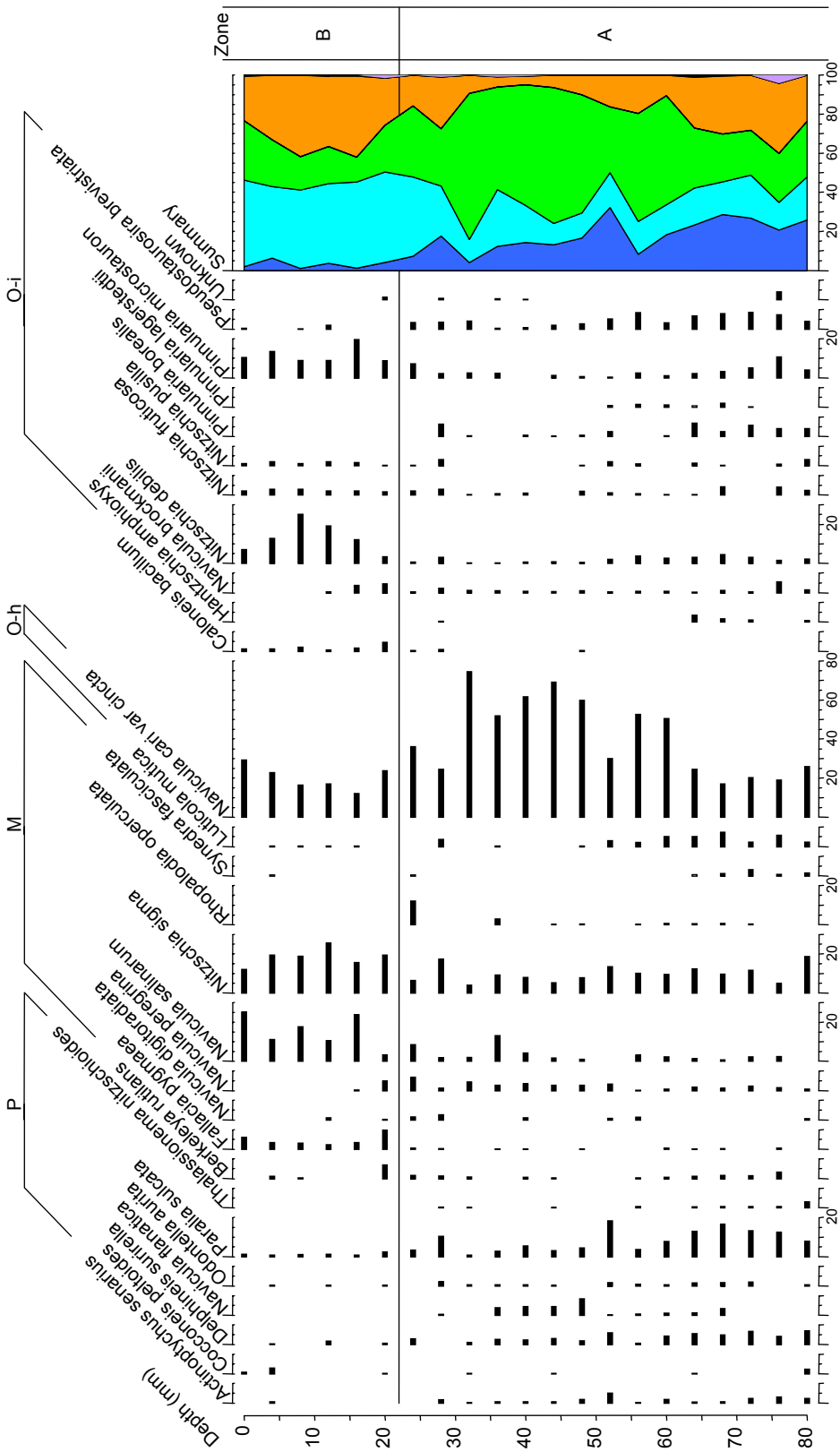

Figure 8.2
Diatom assemblages (>2%) through transplant control block. P: polyhalobous, M: mesohalobous, O-h: oligohalobous-halophile, O-i: oligohalobous-indifferent, H: halophobous, U: unknown diatom salinity groups ordered left to right in summary graph

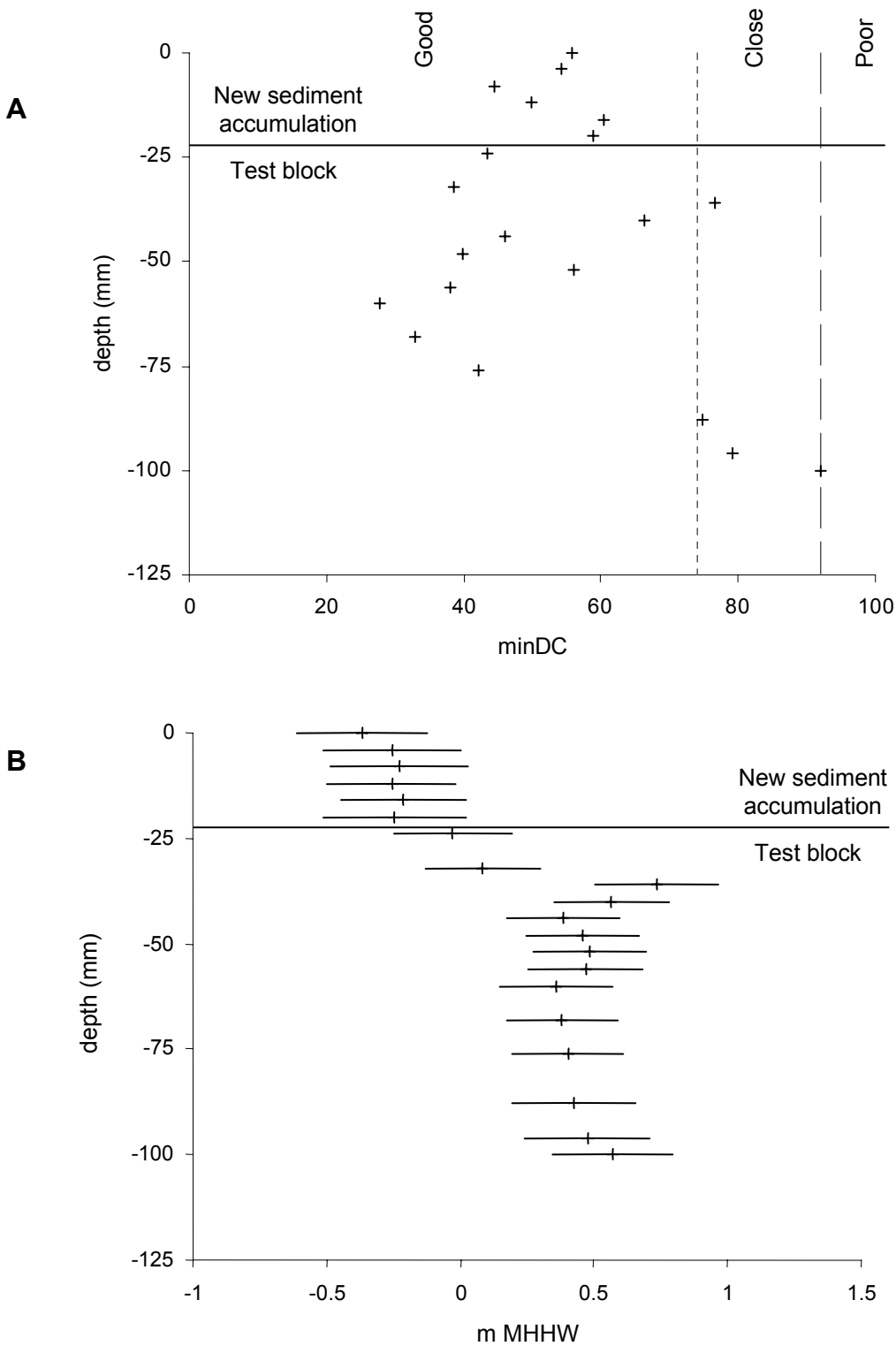

Figure 8.3
Minimum dissimilarity coefficient values from MAT (A) and quantitative reconstructions using the transfer function (B) through the transplant experiment

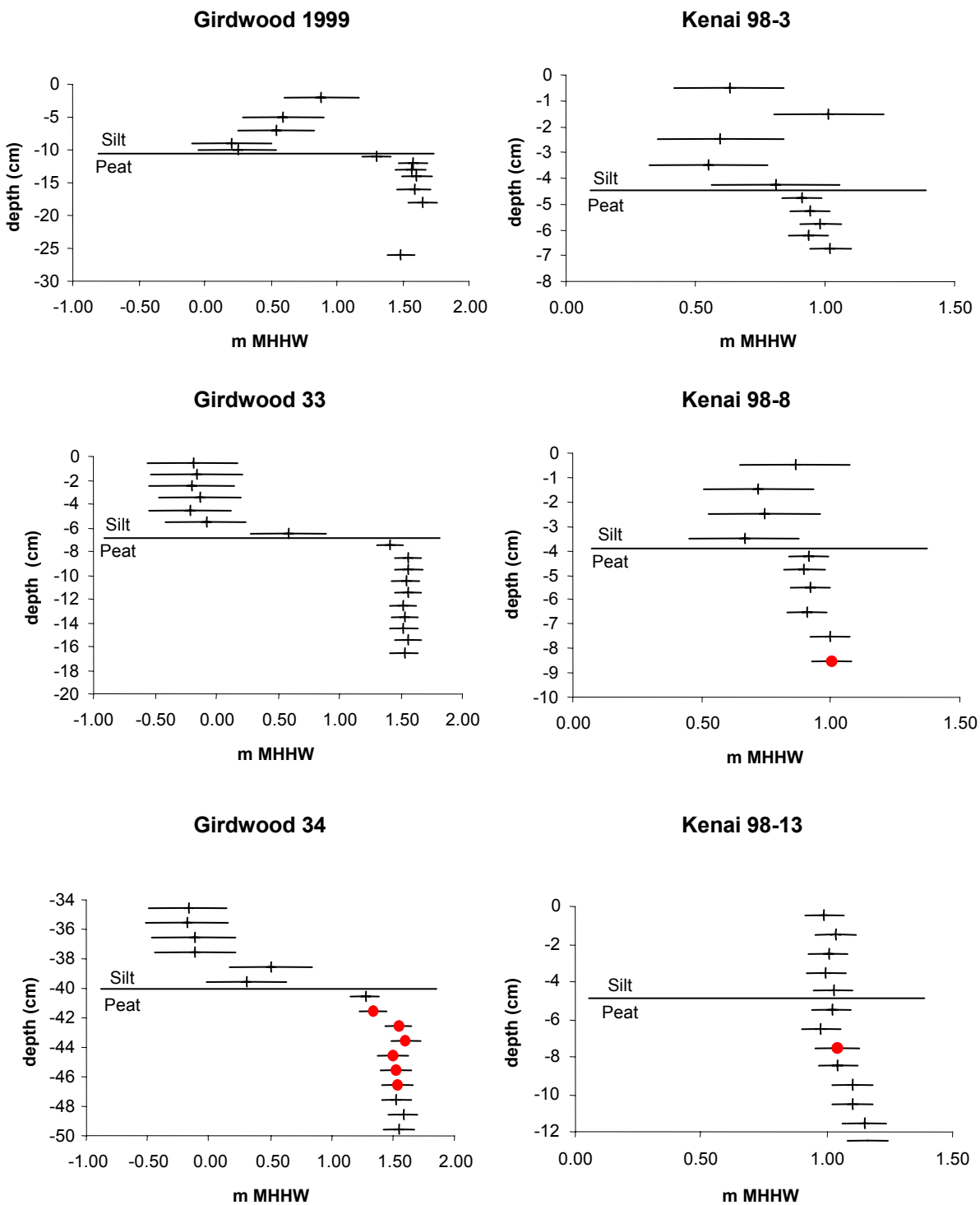

Figure 9.1
Reconstructions of relative sea-level / land-level change associated with the 1964 earthquake based on the diatom transfer function described in section 4 and fossil data reported by Shennan *et al*. (1999), for Girdwood 1999, and Zong *et al*. (2003) for the other sites. In each graph the horizontal line depicts the stratigraphic boundary that represents the 1964 earthquake. Solid circles indicate samples with poor modern analogues

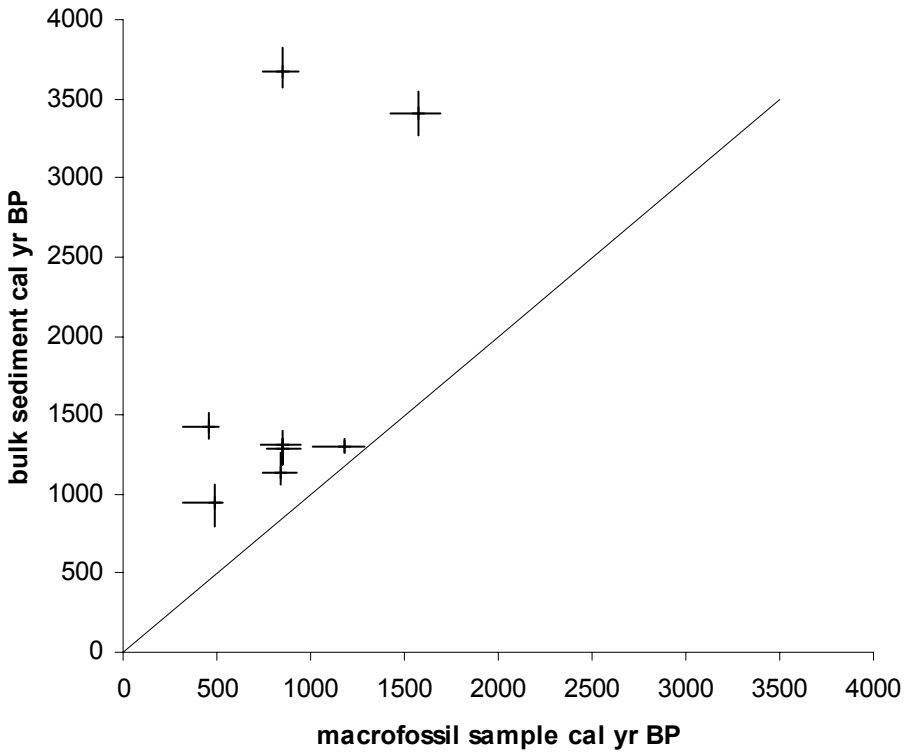

Figure 9.2
Comparison of AMS radiocarbon ages of bulk peat samples and *in situ* macrofossils extracted from the peat (data from Hamilton, 2003 and this project)

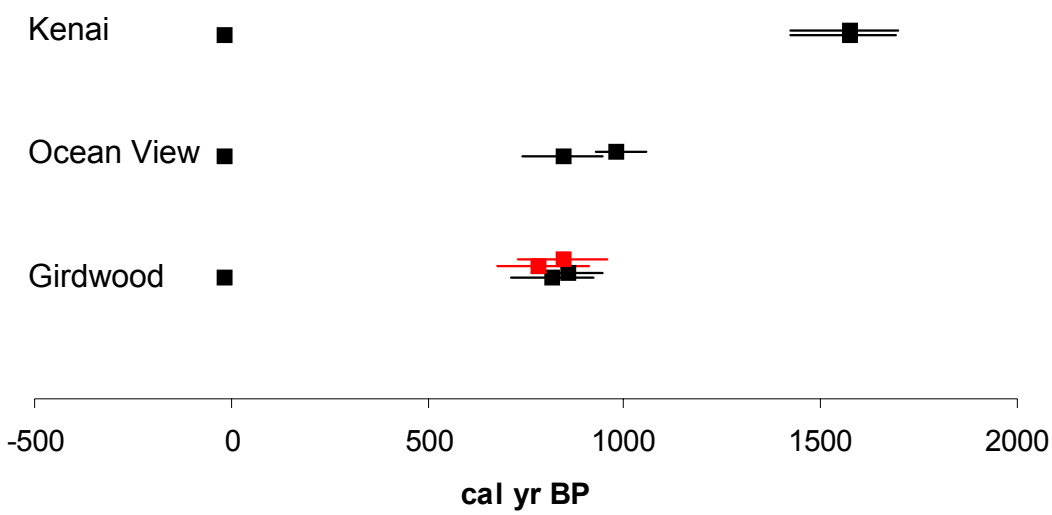

Figure 9.3
Ages of the last two co-seismic event recording co-seismic subsidence at Girdwood, Ocean View and Kenai. 1964 plots as -14 cal yr BP, zero equals 1950 AD. AMS radiocarbon ages on macrofossils from the top of peat layer are shown in black and conventional radiocarbon ages on wood from trees rooted in peat G at Girdwood (Combellick & Reger, 1994) in red. Recently received results date an older peat layer at Ocean View and Girdwood to 1350-1500 cal yr BP but diatom analysis has not been completed yet to determine if they represent co-seismic events